

# **Protein sorting to the apical membrane of epithelial cells**

## **DISSERTATION**

zur Erlangung des akademischen Grades

Doctor rerum naturalium

Der Fakultät für Mathematik und Naturwissenschaften

der Technischen Universität Dresden

vorgelegt von

**Sebastian Schuck**

Diplom-Biochemiker, geboren am 23. September 1974 in Hannover

Gutachter: Prof. Dr. Kai Simons, Max-Planck-Institute of Molecular Cell Biology  
and Genetics, Dresden  
Prof. Dr. Bernard Hoflack, Technische Universität Dresden  
Prof. Dr. Lukas Huber, Universität Innsbruck (Österreich)

Tag der Einreichung: 27.10.2004

Tag der Verteidigung: 20.12.2004

---

## **Declaration**

I herewith declare that I have produced this thesis without the prohibited assistance of third parties and without making use of aids other than those specified; notions taken over directly or indirectly from other sources have been identified as such. This thesis has not previously been presented in identical or similar form to any other German or foreign examination board.

The thesis work was conducted from March 2001 until October 2004 under the supervision of Prof. Dr. Kai Simons at the Max Planck Institute of Molecular Cell Biology and Genetics in Dresden.

Dresden, October 25, 2004

---

# Table of contents

<b>1. Summary</b> .....	<b>1</b>
<b>2. Introduction</b> .....	<b>4</b>
2.1. Properties of the apical and basolateral membrane .....	4
2.2. Mechanisms of polarised sorting .....	6
2.2.1. Sorting determinants .....	6
2.2.2. Sorting by receptor-mediated cargo capture .....	8
2.2.3. Lipid rafts as apical sorting platforms .....	9
2.2.4. Sorting by cargo recruitment into clustered rafts .....	10
2.2.5. Generation of transport carriers by raft clustering .....	16
2.3. Post-Golgi transport routes to the plasma membrane .....	17
2.3.1. Modes of sorting to the plasma membrane .....	18
2.3.2. Plasticity of polarised sorting .....	20
2.4. Implications of apical membrane biogenesis by raft clustering .....	22
2.5. Aim of this thesis .....	24
<b>3. Biochemical analysis of detergent-resistant membranes</b> .....	<b>25</b>
3.1. Protein content of DRMs .....	25
3.2. Lipid content of DRMs .....	32
3.3. Tools for manipulating DRM association .....	36
3.4. Conclusions .....	39
<b>4. Retrovirus-mediated RNA interference in epithelial cells</b> .....	<b>41</b>
4.1. Generation of knockdown cells by retrovirus-mediated RNAi .....	41
4.2. Properties of functional small interfering RNAs .....	45
4.3. Composition and stability of knockdown cell populations .....	48
4.4. Generation of double knockdowns .....	51
4.5. Conclusions .....	53

---

<b>5. Functional analysis of putative apical sorters</b> .....	<b>55</b>
5.1. Biochemical analysis of influenza virus hemagglutinin transport .....	55
5.2. A visual assay for surface transport .....	61
5.3. Rab10 as a putative regulator of membrane trafficking .....	68
5.4. Conclusions .....	70
<b>6. Discussion</b> .....	<b>72</b>
6.1. Detergents as tools for analysing membrane organisation and trafficking .....	72
6.2. Retroviral RNAi as a tool for gene inhibition in epithelial cell .....	76
6.3. Defining components of the apical sorting machinery .....	78
6.4. Future directions .....	81
<b>7. Materials and Methods</b> .....	<b>83</b>
7.1. Cell culture techniques .....	83
7.1.1. Cell culture .....	83
7.1.2. Metabolic labelling of MDCK and Jurkat cells .....	83
7.1.3. Cyclodextrin, saponin and sphingomyelinase treatment .....	84
7.2. Biochemical methods .....	84
7.2.1. Cell lysis .....	84
7.2.2. Detergent extraction and equilibrium density centrifugation .....	84
7.2.3. SDS polyacrylamid gel electrophoresis .....	85
7.2.4. Immunoblotting .....	86
7.2.5. Cell surface biotinylation .....	87
7.2.6. Lipid extraction .....	88
7.2.7. Mild alkaline hydrolysis of ester lipids .....	88
7.2.8. Cholesterol determination .....	89
7.2.9. Thin layer chromatography .....	89
7.2.10. Mass spectrometric analysis of phosphatidylcholine .....	89
7.3. Molecular biology methods .....	90
7.3.1. Cloning of retroviral RVH1 vectors .....	90
7.3.2. Cloning of adenoviral pAdeasy-RFP-rab10 vectors .....	90
7.3.3. Design of shRNAs and cloning into retroviral RVH1 vectors .....	91
7.3.4. RNA isolation and cDNA synthesis .....	92

---

7.3.5. Quantitative real time-PCR .....	92
7.3.6. Internal energy calculation .....	94
7.4. Virus techniques .....	95
7.4.1. Production of retroviruses .....	95
7.4.2. Retroviral transduction of MDCK cells .....	96
7.4.3. Generation and amplification of adenoviruses .....	96
7.5. Cell biology methods .....	97
7.5.1. Immunofluorescence .....	97
7.5.2. Transferrin uptake assay .....	98
7.5.3. Hemagglutinin transport assay .....	98
7.5.4. Surface transport of adenovirally expressed marker proteins .....	101
<b>8. References .....</b>	<b>102</b>
<b>9. Abbreviations .....</b>	<b>114</b>
<b>10. Appendix .....</b>	<b>117</b>
Appendix 1 - Quantification of DRM phosphatidylcholines .....	117
Appendix 2 - RNAi database .....	119
<b>11. Acknowledgements .....</b>	<b>121</b>

## 1. Summary

The structure and functions of lipid rafts and the mechanisms of intracellular membrane trafficking are major topics in current cell biological research. Rafts appear to play a key role in many cellular processes, including membrane transport to the cell surface. It has been proposed that rafts act as sorting platforms during biosynthetic transport, especially along the trafficking pathways that deliver proteins to the apical membrane of polarised cells. Based on this hypothesis, the aim of this work was to contribute to the mechanistic understanding of apical sorting in epithelial cells.

The study of how lipid rafts might be structured and how they might function in apical sorting has been hampered by the scarcity of techniques for their purification. Rafts are thought to be partially resistant to solubilisation by mild detergents, which has made the isolation of detergent-resistant membranes (DRMs) the primary method to characterise them biochemically. While a growing number of detergents is being used to prepare DRMs, it is not clear what can be inferred about the native structure of cell membranes from the composition of DRMs obtained with different detergents.

This issue was addressed by a biochemical analysis of DRMs prepared with a variety of mild detergents. The protein and lipid content of different DRMs from two cell lines, Madin-Darby canine kidney (MDCK) and Jurkat cells, was compared. It was shown that the detergents differed considerably in their ability to selectively solubilise membrane proteins and to enrich sphingolipids and cholesterol over glycerophospholipids, as well as saturated over unsaturated phosphatidylcholine. Moreover, cell type-dependent variations of the molecular characteristics of DRMs were observed. These results make it unlikely that different DRMs reflect the same underlying principle of membrane organisation. They do, however, indicate that besides Triton X-100 and CHAPS, the most commonly used detergents for studying membrane organisation, Brij 96 and Brij 98 may also be useful tools, for instance for the analysis of membrane trafficking in MDCK cells.

A second obstacle for a more detailed understanding of apical sorting is that the experimental evidence implicating certain proteins in this process has come from a number of disparate and sometimes inherently problematic approaches. It would therefore be helpful to re-examine the putative components of the apical sorting machinery in a single experimental system. The advent of RNA interference (RNAi) as a technique to specifically inhibit gene expression appears to make this possible. However, the application of RNAi to epithelial MDCK cells, which are the principal model system for polarised protein sorting, is limited by the poor transfectability of these cells.

To circumvent this problem, a retroviral system for RNAi in MDCK cells was established. Efficient suppression of thirteen genes putatively involved in membrane trafficking was achieved by retroviral co-expression of short hairpin RNAs and a selectable marker. The composition and stability of the resulting knockdown cell populations was characterised, and the usefulness of proposed guidelines for choosing RNAi target sequences was examined. Finally, it was shown that this system can be extended to simultaneously target two genes, giving rise to double knockdowns.

Retroviral RNAi was then applied to test the functional consequences of depleting proteins suggested to play a role in apical sorting. Surprisingly, none of the knockdowns analysed caused defects in surface delivery of influenza virus hemagglutinin, a commonly used marker protein for apical transport. Therefore, none of the proteins examined is absolutely required for transport to the apical membrane of MDCK cells.

Cells may adapt to the depletion of proteins involved in membrane trafficking by activating alternative pathways. This could be particularly relevant when experiments are performed after cells have been exposed to protein depletion by RNAi for several days. To avoid such adaptation, a visual transport assay was established. It is based on the adenoviral expression of fluorescent marker proteins whose surface transport can be followed microscopically as soon as RNAi has become effective. With this assay, it should now be possible to screen the set of thirteen knockdowns for defects in surface transport.

The visual transport assay can be used not only to assess the importance of proteins already implicated in polarised sorting, but can also be employed to evaluate new candidates. Making use of this assay, it was tested whether rab10 might be involved in plasma membrane transport. Expression of wild type or constitutively inactive rab10 did not significantly affect transport of the basolaterally targeted vesicular stomatitis virus glycoprotein, but expression of a constitutively active rab10 mutant blocked delivery of this marker protein to the cell surface. Thus, rab10 appears to regulate transport to the plasma membrane.

Taken together, this work has provided and evaluated a number of experimental tools for the study of membrane trafficking in epithelial cells. First, the biochemical analysis of DRMs highlighted that DRMs obtained with different detergents are unlikely to correspond to distinct types of membrane microdomains in cell membranes. It also indicated that some more recently introduced detergents could be useful for analysing the lipid environment of proteins in transit to the plasma membrane. Second, the retroviral RNAi system should be valuable for defining the function of proteins, not only in membrane transport, but also in processes like epithelial polarisation. Third, the visual assay for monitoring the surface transport of adenovirally expressed marker proteins should be suitable to detect defects in polarised sorting. The utility of this assay was demonstrated by preliminary observations suggesting that rab10 is regulator of post-Golgi trafficking.



## 2. Introduction

Most cell types generated by multicellular organisms are polarised. A characteristic feature of polarised cells is the division of their surface into functionally distinct membrane domains. This requires an intricate sorting machinery that delivers proteins and lipids to the right membrane domains. Hence, the sorting machinery is fundamental to the generation of polarity as well as its maintenance in the face of continuous plasma membrane turnover by endocytosis.

Epithelial cells provide a paradigm of cell polarisation. These cells have to perform seemingly contradictory functions. They constitute a protective barrier against the external environment, but also serve as exchange interfaces with the outside world. To fulfil these functions, epithelial cells have evolved characteristic apical and basolateral membrane domains. The basolateral membrane contacts neighbouring cells and the underlying tissue, whereas the apical membrane faces the lumen of an internal organ. The two membrane domains are separated by tight junctions, which help to prevent mixing of apical and basolateral membrane components and seal the epithelium (Tsukita et al., 2001).

In this chapter, the mechanisms of polarised sorting in epithelial cells are discussed, with particular focus on the biogenesis of the apical membrane and the role of lipid rafts in this process. Whereas parts of the machinery for basolateral transport have been uncovered, current knowledge about apical sorting has been much more difficult to integrate into a coherent picture. Still, the apical pathway plays a major role in the plasticity of epithelial tissues during differentiation and development (Lecuit and Pilot, 2003; Lubarsky and Krasnow, 2003). Therefore, insight into how sorting to the apical membrane works will contribute significantly to understanding cell polarisation and its role in tissue generation.

### 2.1. Properties of the apical and basolateral membrane

The apical membrane mediates most of the functions specific to epithelial cells, whereas the basolateral membrane shares many features of the plasma membrane of non-polarised cells. As the apical membrane of simple columnar epithelia is exposed to various

potentially harmful substances, it needs to be particularly robust. For example, the apical membrane of intestinal cells has to maintain its integrity despite contact with digestive enzymes and the acidic gastric contents. The apical membrane of hepatocytes, which encloses the bile canaliculi, has to be resistant to bile acid detergents, and the apical membrane of kidney cells has to withstand the osmotic pressure created by the high salt and urea concentrations in the kidney filtrate.

The unusual robustness of the apical membrane is in large part due to its special lipid composition. Compared to other cell membranes, in which unsaturated glycerophospholipids predominate, the apical membrane is strongly enriched in sphingolipids (Simons and van Meer, 1988). Together with cholesterol, these lipids have the propensity to form tightly packed membrane microdomains, called lipid rafts. Lipid rafts probably exist in the plasma membrane of practically any cell, in which they are present as small, highly dynamic liquid-ordered assemblies embedded in the surrounding liquid-disordered membrane (Kusumi et al., 2004; Simons and Vaz, 2004; but see Munro, 2003). Rafts have been estimated to cover approximately 30-40% of the plasma membrane of non-polarised cells, i.e. the dispersed raft microdomains constitute a minority phase within the continuous non-raft phase (Simons and Toomre, 2000; Prior et al., 2003). However, in the apical membrane of epithelial cells, the proportion of sphingolipids and cholesterol may be high enough for the liquid-ordered phase to form the majority phase. Thus, the apical membrane may be a continuous raft membrane with non-raft domains embedded in it (Verkade et al., 2000; Crane and Tamm, 2004). Sphingolipids are less abundant in the basolateral membrane, but rafts are clearly present also in this membrane domain, for instance in the form of caveolae (van Deurs et al., 2003).

Although the apical membrane is exceptionally sturdy, it is by no means only a rigid shield. Epithelial cells in the intestine and the kidney have a large capacity for absorption and secretion, which is mediated by transport proteins in the apical membrane. In addition, the apical membrane itself is turned over rapidly. Non-polarised cells, for example fibroblasts, endocytose up to two equivalents of their total surface area per hour (Mellman, 1996). The rate of endocytosis from the apical membrane of the well-characterised renal Madin-Darby canine kidney (MDCK) cell line depends on the cell strain (Bomsel et al., 1989; Naim et al., 1995), but the data show that epithelial cells are able to internalise and replace their entire apical membrane within hours.

Given this combination of protective and exchange functions, it is obvious that the composition of the apical membrane needs to be tightly controlled. Insertion of the wrong transport proteins into the apical membrane of kidney cells could destroy the steep ion gradients across the kidney epithelium, or lead to influx of toxic compounds like uric acid. Delivery of unsaturated glycerophospholipids to the apical membrane of hepatocytes might disturb its resistance to bile acid detergents. Given this need for strict exclusion of basolateral membrane components from the apical membrane, it is interesting that basolateral targeting is usually more accurate than apical targeting (Pfeiffer et al., 1985 and references therein). Thus, the physiological context of epithelial cells may place constraints on how much missorting can be tolerated and, therefore, on how polarised sorting to the plasma membrane can be organised.

## **2.2. Mechanisms of polarised sorting**

A polarised surface distribution of proteins and lipids can be achieved by targeted delivery or selective retention (Yeaman et al., 1999; Matter, 2000). Targeted delivery relies on the segregation of cargo molecules destined for different plasma membrane domains before they reach the cell surface. Selective retention works by trapping them once they arrive, for instance by anchoring to a domain-specific cytoskeletal scaffold. Proteins delivered to the wrong surface domain are removed by endocytosis and are then degraded or undergo another round of delivery. Targeted delivery and selective retention can be combined such that selective retention enhances the accuracy of intracellular sorting (Mays et al., 1995).

The basolateral as well as the apical pathway has been suspected to involve bulk flow, but it is now clear that neither is a general default pathway for the surface delivery of proteins. Instead, apical and basolateral sorting are both governed by sorting determinants embedded in the cargo proteins.

### *2.2.1. Sorting determinants*

The sorting information encoded in membrane proteins can reside in the cytoplasmic domain, the membrane anchor, or the extracellular domain (Table 2.1.).

Site	Determinant	Polarity	Examples
Cytoplasmic domain	Tyrosine-based motif	Basolateral	LDL receptor, transferrin receptor, vesicular stomatitis virus glycoprotein
	Dileucine motif	Basolateral	IgG Fc receptor, E-cadherin
	PDZ-binding motif	Apical/ Basolateral	CFTR (a), BGT-1 GABA transporter (bl), ERBB2 receptor tyrosine kinase (bl)
	Others	Apical/ Basolateral	H,K-ATPase $\alpha$ -subunit (a), megalin (a), GAT-2 GABA transporter (bl)
Membrane anchor	Transmembrane domain	Apical	influenza virus hemagglutinin and neuraminidase
	GPI-anchor	Apical	placental alkaline phosphatase, decay-accelerating factor, Thy-1
Extracellular domain	N-glycosylation	Apical	occludin (truncated version), FcLR (Fc receptor-LDL receptor chimera), GLYT2 glycine transporter
	O-glycosylation	Apical	neurotrophin receptor, sucrase isomaltase
	Oligomerisation?	Apical?	Kv1 potassium channel (neurons)

**Table 2.1.** Sorting determinants for apical or basolateral targeting of transmembrane proteins. a = apical, bl = basolateral.

Two classes of cytoplasmic domain determinants that mediate basolateral delivery consist of fairly well-defined amino acid sequence motifs, one based on a critical tyrosine, the other on a pair of leucines. They show a remarkable resemblance to endocytosis signals (Matter and Mellman, 1994). Several cytoplasmic domains known to determine apical or basolateral localisation contain PDZ-binding motifs. In addition, there is a growing list of cytoplasmic domain determinants involved in apical or basolateral transport that are unrelated at the amino acid sequence level (Altschuler et al., 2003; Muth and Caplan, 2003). The transmembrane domains of some viral proteins contain apical sorting determinants (Kundu et al., 1996; Lin et al., 1998). Membrane attachment by means of a glycosylphosphatidylinositol (GPI)-anchor usually confers localisation to the apical membrane (Brown et al., 1989; Lisanti et al., 1989), even though the GPI-anchor alone is not always sufficient for apical targeting (Brown and London, 1998; Benting et al., 1999a). Both N- and O-glycosylation have been implicated in directing proteins to the apical membrane (Scheiffele et al., 1995; Yeaman et al., 1997; Gut et al., 1998; Spodsborg

et al., 2001). On the other hand, there are also apical proteins that do not depend on glycosylation for proper targeting. Finally, oligomerisation of membrane proteins may be an important sorting determinant, particularly for apical trafficking. Direct evidence in epithelial cells is lacking so far, but the sorting of the voltage-gated potassium channel Kv1 into the axonal pathway of neurons, which is related to the apical pathway of epithelial cells (Horton and Ehlers, 2003), requires oligomerisation (Gu et al., 2003).

Overall, the known apical sorting determinants are more diverse and not as strict as prototypic basolateral determinants. Basolateral determinants seem to dominate over apical ones, as addition of a tyrosine-based or dileucine motif usually redirects apical proteins to the basolateral membrane. Such a hierarchy of sorting determinants could help to ensure stringent sorting of basolateral proteins away from the apical membrane. However, there are also examples of recessive basolateral determinants (Monlauzeur et al., 1995; Jacob et al., 1999; Ihrke et al., 2001), indicating that the hierarchy of sorting determinants is more complicated, or that the relative strength of sorting determinants may depend on the proteins they are present in.

### *2.2.2. Sorting by receptor-mediated cargo capture*

Certain cytoplasmic domain determinants are recognised by specific sorting receptors. Best characterised are the adaptor protein (AP) complexes, which sort proteins along many intracellular trafficking routes (Robinson, 2004). Several tyrosine-based motifs interact with the epithelia-specific  $\mu$ 1B subunit of the AP-1 adaptor complex, and this interaction is crucial for the basolateral sorting of the LDL receptor and the transferrin receptor (Folsch et al., 1999; Sugimoto et al., 2002). Other adaptors implicated in the recognition of basolateral determinants are the AP-3 and AP-4 complexes (Nishimura et al., 2002; Simmen et al., 2002).

How the binding of adaptor complexes to cargo proteins is coupled to the machinery responsible for the formation and movement of transport carriers is not understood. The ability of the AP-1 complex to bind clathrin makes an involvement of clathrin-coated vesicles in basolateral transport plausible, but direct evidence has been difficult to obtain. Adaptor complexes can also bind to motor proteins, which then move cargo containers towards the cell periphery. This has been demonstrated in non-polarised cells, in which the

AP-1 complex and the kinesin family member KIF13A interact (Nakagawa et al., 2000), and also in neurons, where a multisubunit adaptor complex facilitates dendritic transport by binding to KIF17 (Setou et al., 2000). Alternatively, motor proteins themselves may serve as receptors for cytoplasmic domain determinants, as is the case for the dynein-mediated apical transport of rhodopsin (Tai et al., 2001). In any event, receptor-mediated cargo capture by specific protein-protein interactions provides a very stringent mechanism for the inclusion of proteins into transport carriers.

Whether cytoplasmic PDZ-domain-binding motifs are recognised by sorting receptors or mediate selective retention at the target membrane is not clear. In the case of the cystic fibrosis transmembrane conductance regulator (CFTR), a PDZ-domain-binding motif seems to be responsible for its selective apical retention after initial transport to both membrane domains (Swiatecka-Urban et al., 2002). The PDZ protein NHERF links CFTR to the actin network beneath the apical membrane (Short et al., 1998), and NHERF probably plays this scaffolding role for various apical proteins (Shenolikar and Weinman, 2001; Altschuler et al., 2003). Similarly, the epithelial GABA transporter BGT-1 and the receptor tyrosine kinase ErbB-2 have PDZ-domain-binding motifs that mediate basolateral retention by interacting with the PDZ protein LIN-7 (Perego et al., 1999; Shelly et al., 2003). However, there are reports arguing that the PDZ-domain-binding motif is dispensable for the apical targeting of CFTR (Benharouga et al., 2003; Ostedgaard et al., 2003), and basolateral targeting of BGT-1 and ErbB-2 still occurs when the motifs are deleted. Localisation of these proteins therefore appears to involve a combination of targeting and retention mechanisms.

### *2.2.3. Lipid rafts as apical sorting platforms*

Sorting receptors that engage in direct protein-protein interactions with apical sorting determinants in membrane anchors or extracellular domains have not been identified. Instead, the sorting of many apical proteins may be governed by lipid-lipid and lipid-protein interactions. The enrichment of sphingolipids in the apical membrane, together with their propensity to associate with cholesterol to form lipid rafts, has led to the concept that rafts preferentially traffic to the apical membrane after intracellular assembly. Since certain proteins associate with rafts during apical transport, rafts could act as apical sorting platforms (Simons and Ikonen, 1997).

Support for this hypothesis has come from two types of experiment. First, apical sorting is particularly sensitive to depletion of cholesterol and sphingolipids (Mays et al., 1995; Keller and Simons, 1998; Hansen et al., 2000; Lipardi et al., 2000). However, this is only indirect evidence, because depletion of these raft lipids could also affect apical trafficking in a more general way. Second, certain apically targeted proteins such as the GPI-anchored placental alkaline phosphatase (PLAP) and influenza virus hemagglutinin, but not typical basolateral proteins enter rafts before they reach the cell surface (Skibbens et al., 1989; Brown and Rose, 1992). Apical sorting of these proteins thus correlates with a dramatic change in their lipid environment during surface transport, but whether this change is required for accurate targeting is unclear. In addition, in these experiments rafts were defined as detergent-resistant membranes (DRMs), i.e. membranes that resisted solubilisation with mild detergents such as Triton X-100. Although useful, detergent resistance is a rather crude criterion to determine raft association (London and Brown, 2000). Indeed, several endogenous apical proteins in MDCK cells are fully detergent soluble, and some DRM-associated proteins still reach the apical membrane when rendered detergent-soluble by mutation or cholesterol depletion (Lin et al., 1998; Lipardi et al., 2000). Detergent extraction probably disrupts weak interactions of proteins with raft domains, but these interactions might nonetheless be important for sorting (Shvartsman et al., 2003). Thus, a lack of suitable methods has made it difficult to obtain conclusive evidence for or against sorting by raft association.

#### *2.2.4. Sorting by cargo recruitment into clustered rafts*

Substantial progress has, however, been made in understanding the ability of individual rafts to selectively cluster into large domains. Based on what is known about this clustering process, a more comprehensive model of the role of rafts in polarised sorting can be proposed (Figure 2.1.). To introduce this model, the clustering of rafts at the cell surface is examined first. It is then explained how raft clustering might be utilised for sorting. Next, it is discussed how the known apical sorting determinants fit into this picture and what kind of protein machinery could mediate raft clustering. Last, it is argued that different raft clusters can be produced, which might explain why raft components are also transported to the basolateral membrane.

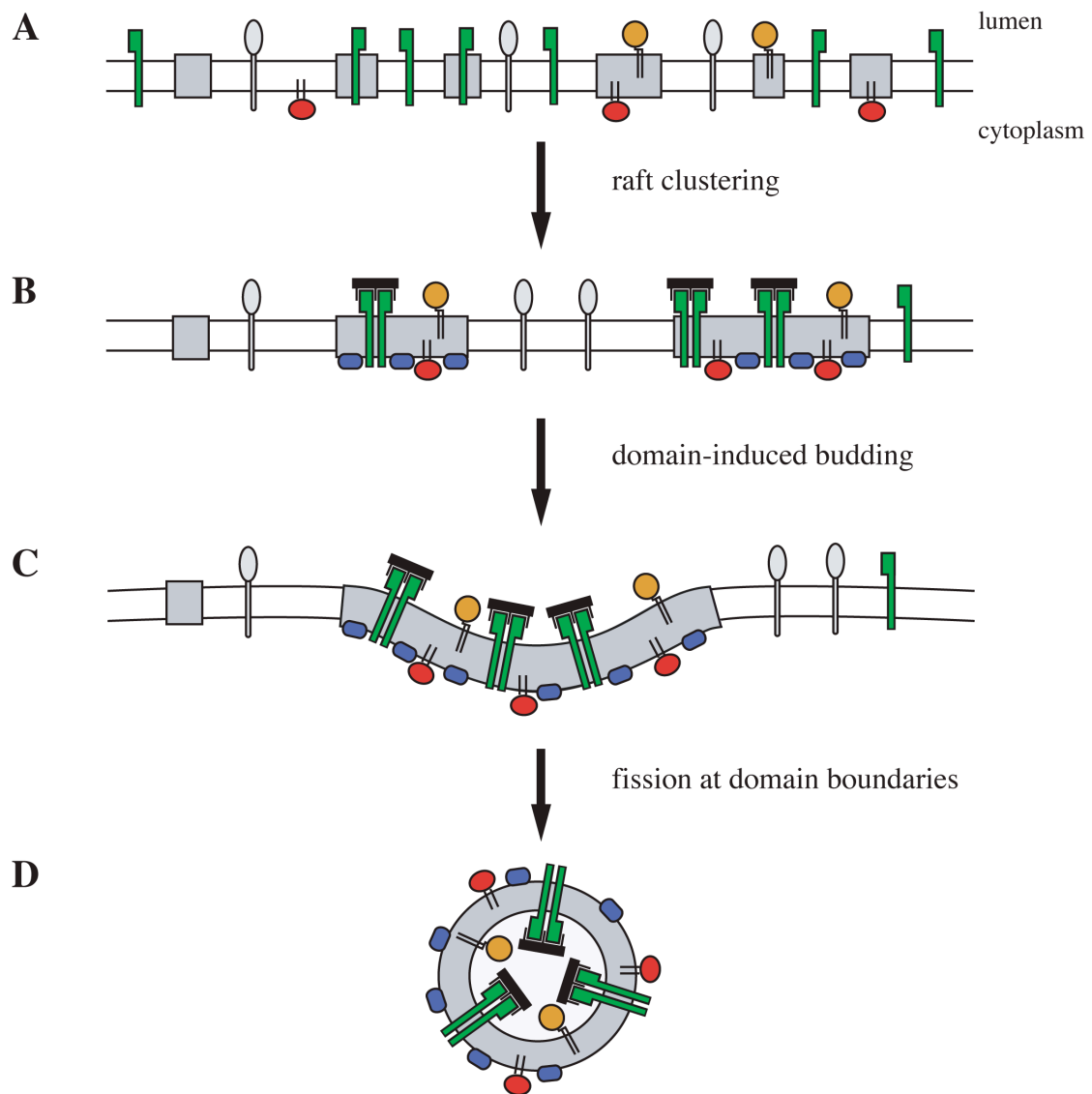


**Figure 2.1.** Raft clustering and domain-induced budding. Before clustering, proteins associate with rafts (grey) to various extents. A GPI-anchored protein (golden) resides exclusively in rafts, a doubly-acylated protein (red) is mainly in rafts, a transmembrane protein (green) is mainly outside rafts, while another transmembrane protein (light grey) is excluded from rafts (A). Clustering is induced, in this example by the binding of a multimeric cytoplasmic protein of the annexin type (blue) to the cytoplasmic face of rafts. The strongly raft-associated GPI-anchored and the doubly acylated protein partition into clustered rafts. The weakly raft-associated transmembrane protein is driven into clustered rafts by crosslinking, which is mediated by a divalent interaction partner, for example a lectin (black). Note that the recruitment of the weakly raft-associated transmembrane protein into clustered rafts is not complete, nor are all rafts clustered. For simplicity, only one type of raft cluster, i.e. the differential clustering of rafts into separate domains with different constituents is not depicted (B). Growth of the clustered raft domain beyond a critical size induces budding (C). Finally, a transport carrier that consists exclusively of raft components pinches off from the parent membrane by fission at the domain boundaries (D).



The size and stability of rafts in the unperturbed state is controversial, but there is a growing consensus that individual rafts can be induced to form large, stable clusters (Kusumi et al., 2004; Simons and Vaz, 2004). Raft clustering can be initiated by the oligomerisation of raft components. At the cell surface, clustering can be brought about artificially by antibody crosslinking, but it also occurs naturally, for example when interactions between the T cell antigen receptor and MHC-peptide complexes on antigen-presenting cells trigger the clustering of rafts during formation of the immunological synapse (Harder and Engelhardt, 2004). As a consequence of raft clustering, raft association of proteins and lipids that have an affinity for liquid-ordered domains is stabilised, whereas non-raft components are excluded. For example, antibody crosslinking of the GPI-anchored PLAP or the apical transmembrane protein gp114 at the plasma membrane of MDCK cells strengthens their raft association, as judged by increased detergent resistance (Harder et al., 1998; Verkade et al., 2000). This presumably happens because oligomerisation by crosslinking multiplies the tendency of these proteins to associate with raft domains. In thermodynamic terms, the partitioning coefficient of oligomers between the raft and the non-raft phase is given by the product of the partitioning coefficients of the monomers they are composed of. This leads to an exponential increase in raft affinity as oligomer size increases (Simons and Vaz, 2004).

Importantly, antibody crosslinking of PLAP leads to co-clustering of the doubly acylated raft protein Fyn, a peripheral membrane protein that resides on the opposite side of the membrane. Thus, the crosslinking of one raft protein moves whole lipid microdomains together in both membrane leaflets (Harder et al., 1998; Prior et al., 2003). The same is true for raft lipids, as shown by crosslinking of the glycosphingolipid GM1 with the pentameric cholera toxin, which leads to co-clustering with various raft proteins (Janes et al., 1999). This presumably occurs because lipids and proteins within raft microdomains associate tightly enough to allow these domains to behave as stable entities (Pralle et al., 2000). In contrast to raft components, non-raft proteins, such as the transferrin receptor, are excluded from clustered rafts, even when crosslinked (Harder et al., 1998; Janes et al., 1999). These examples show that the clustering of individual rafts reinforces the segregation of the raft and the non-raft phase and sharpens the distribution of membrane components between the two phases. Thus, raft clustering is a mechanism for the selective recruitment of proteins and lipids that have an affinity for liquid-ordered domains, as well as the efficient exclusion of non-raft proteins.

Extrapolating from these effects of raft clustering, it can be envisaged that the clustering of lipid rafts can be used as a sorting mechanism to recruit certain cargo proteins while excluding others. Stabilisation of rafts should attract proteins and lipids that have a strong affinity for ordered domains. Indeed, clustered rafts might exhibit an even greater degree of lipid ordering than individual rafts, thus providing a preferable environment for these molecules. Recruitment into clustered rafts could be assisted by additional interactions in the case of weakly raft-associated proteins. Crosslinking by a multivalent interaction partner outside rafts could augment their raft affinity. Also, they could bind to other proteins that drag them into clustered rafts. There, they could become entrapped by further modifications that strengthen their raft association, such as palmitoylation, oligomerisation or a conformational change (Bagnat et al., 2001; Cherukuri et al., 2004). This recruitment may not be complete so that certain proteins and lipids that have raft affinity might still partially localise to non-raft membranes or non-clustered rafts. Nevertheless, clustering should create membrane patches consisting of a highly selected group of molecules whose trafficking fates are connected.

Certain apical sorting determinants are able to facilitate raft association, especially when rafts are clustered. First, GPI-anchored proteins generally associate with lipid rafts based on the favourable packing of the GPI anchor into liquid-ordered domains. However, GPI anchors are structurally diverse, so this might not be true for all GPI-linked proteins (Benting et al., 1999b; Mayor and Riezman, 2004). Interestingly, raft association of GPI-anchored proteins might need to be stabilised by oligomerisation for them to be sorted apically (Paladino et al., in press). Second, transmembrane domains known to act as apical sorting determinants also mediate raft association (Scheiffele et al., 1997; Barman and Nayak, 2000). The principles underlying the association of transmembrane proteins with rafts are poorly understood. One element is binding to raft lipids and, possibly, conformational changes induced by specific protein-lipid interactions (Simons and Vaz, 2004). Another factor may be the length of the transmembrane domain (TMD). It has been proposed that the targeting of transmembrane proteins to different cell membranes is based on TMD length (Bretscher and Munro, 1993). Long TMDs could have a preference for raft membranes, whereas proteins that have short TMDs might be excluded. Indeed, owing to the ordering of lipid side chains, raft membranes are probably thicker than non-raft membranes. In addition, they have different elastic properties, e.g. they are more difficult to bend or compress. Recently, a theoretical study showed that these elastic properties,

rather than membrane thickness, provide the primary driving force for the exclusion of proteins with short TMDs from cholesterol-enriched membranes (Lundbaek et al., 2003). If clustering were to increase the lipid order of rafts and make them even less elastic, raft clustering would potentiate the effect of TMD length on the raft association of transmembrane proteins. Third, oligomerisation should amplify the affinity of proteins for rafts by the same mechanism as antibody crosslinking does. This could explain why oligomerisation might be an important determinant for raft-mediated apical sorting.

Whether there is a connection between glycosylation as an apical sorting determinant and lipid rafts as apical sorting platforms, has not yet been established. The role of glycosylation in sorting implies the existence of lectins that influence the trafficking of their binding partners. If such lectins were raft-associated, they could mediate raft entry of glycoproteins. Additionally, multivalent lectins could be employed to crosslink glycoproteins, thereby amplifying their raft affinity. The lectin VIP36 has been proposed to sort glycoproteins to the apical membrane of MDCK cells (Hara-Kuge et al., 2002), but may actually function in the early secretory pathway (Füllekrug et al., 1999). Known raft-associated lectins are DC-SIGN, which is found at the plasma membrane of dendritic cells (Cambi et al., 2004), and ZG16p, which has been proposed to play a role in regulated secretion in pancreatic cells (Schmidt et al., 2001). It is not known if related proteins are present in epithelial cells. Finally, members of the galectin family are interesting candidates for lectins involved in raft recruitment (see below).

How might raft clustering be induced? From what is known about the clustering process, any oligomerisation of raft components could be sufficient. Several proteins might promote raft clustering, although the available evidence is circumstantial. One type of "clustering agent" might be represented by VIP17/MAL and the closely related MAL2. Both are tightly raft-associated integral membrane proteins and play a role in apical targeting (Puertollano et al., 1999; Cheong et al., 1999; de Marco et al., 2002). Moreover, VIP17/MAL can form oligomers, which might be utilised for to cluster rafts at the site(s) at which sorting takes place. Similarly, caveolins, flotillins and stomatin are raft-associated membrane proteins that form oligomers (Monier et al., 1995; Snyers et al., 1999; Neumann-Giesen et al., 2004). Caveolins clearly have the ability to cluster rafts, acting as scaffolds for caveolae (van Deurs et al., 2003). It has been proposed that caveolin-1 is required for transport of GPI-anchored proteins to the plasma membrane

(Sotgia et al., 2002), but evidence speaks against a major role of caveolin-1 in polarised sorting in MDCK cells (Manninen, A., Füllekrug, J. and Simons, K., unpublished).

Raft clustering may be promoted in a slightly different way by annexin 13b and annexin 2, cytosolic proteins that facilitate apical transport in MDCK cells (Lafont et al., 1998; Jacob et al., 2004). Both are unusual annexins because they preferentially associate with cholesterol-rich membranes (Lafont et al., 1998; Rescher and Gerke, 2004). Again, they could act as membrane organisers through their ability to oligomerise, since some annexins, including annexin 2, form large, two-dimensional ordered arrays (Oling et al., 2001). Little is known about the cytoplasmic side of rafts, but it might contain enough cholesterol to serve as a preferred docking site for annexin 13b and annexin 2. Although rafts are primarily thought of as assemblies in the exoplasmic membrane leaflet, there clearly is leaflet coupling such that raft domains on the exoplasmic side are matched by raft domains on the cytoplasmic side (Harder et al., 1998; Korlach et al., 1999; Prior et al., 2003). Thus, clustering of raft lipids on the cytoplasmic side by annexin oligomers should cluster raft components in the exoplasmic leaflet.

Lectins of the galectin family might be involved in driving glycolipids and glycoproteins into clustered rafts. Galectins are usually multivalent owing to self-association and can organise glycoproteins into large, regular arrays (Brewer et al., 2002). Galectin-4 tightly associates with rafts on the outside of the brush border membrane of intestinal cells and stabilises raft domains (Braccia et al., 2003). Recent studies implicate galectin-4 in apical sorting in enterocytes (Delacour, D., Gouyer, V., Manninen, A., Simons, K. and Huet, G., unpublished). Galectins are secreted from cells by a non-classical mechanism that bypasses the Golgi complex. How they could enter the secretory pathway is therefore unclear. However, they might be reinternalised by endocytosis and thus gain access to intracellular sorting sites.

Finally, it is important to realise that rafts can be clustered differentially. For example, migrating T lymphocytes are able to set up separate raft domains that have distinct compositions at the leading edge and the uropod (Gomez-Mouton et al., 2001). Likewise, the mating projection in yeast is a specialised membrane domain that might arise by raft clustering, but raft proteins are also found elsewhere in the plasma membrane (Bagnat and Simons, 2002). The immunological synapse formed by activated T cells is viewed as a raft

cluster but nevertheless excludes raft proteins that have no function in immune signalling (Harder and Kuhn, 2000; Bunnell et al., 2002). In all these processes the actin cytoskeleton plays a key role. However, even when raft components are clustered artificially, selective co-clustering of raft components is still observed (Wilson et al., 2004). Hence, differential raft clustering appears to be a general principle.

In the context of sorting, raft clustering might be employed to specify either apical or basolateral delivery. In MDCK cells, raft proteins such as caveolin-1 and 2 are also found at the basolateral membrane. Possibly, rafts can be differentially clustered in the membrane(s) where apical and basolateral cargo is segregated, such that a subset of rafts is diverted to the basolateral membrane. Thus, the function of rafts as sorting platforms may not be restricted to the apical pathway.

#### *2.2.5. Generation of transport carriers by raft clustering*

Raft clustering could also provide a mechanism for the generation of transport carriers. If phases with different properties coexist in the same membrane, as in the case of liquid-ordered microdomains in a membrane mainly in the liquid-disordered phase, there is line tension at the phase boundaries. Line tension is the two-dimensional equivalent of surface tension and arises from the immiscibility of membrane components that prefer different phases. The energetic cost of line tension can be reduced by decreasing the contact between phases, i.e. by decreasing the boundary length of domains that constitute the minority phase. This is achieved most effectively when domains that are part of the minority phase bud out of the majority phase and eventually detach from the parent membrane. Line tension-driven budding is opposed by the energy required to bend the membrane of the incipient bud. Importantly, the balance between line tension and bending energy depends on the size of the membrane domain in the minority phase. The line tension increases with increasing domain size, whereas the bending energy is independent of the domain size. Small domains give rise to buds that have higher degrees of curvature than large buds, but the energy to deform the membrane into a sphere is the same. As a result, a growing domain within a membrane will reach a critical size beyond which budding becomes energetically favourable (Lipowsky, 1993; Lipowsky, 2002). This mechanism, termed domain-induced budding, was originally postulated on theoretical grounds but has recently received experimental support from studies of model membranes

(Baumgart et al., 2003). As predicted, domains in the minority phase were observed to bud out of the surrounding membrane, with fission occurring at the phase boundaries.

In cell membranes, individual rafts usually form a dispersed minority phase within a continuous non-raft phase (Simons and Toomre, 2000; Prior et al., 2003). Therefore, clustering of small rafts into large domains should induce budding, followed by fission at the domain boundaries and the generation of vesicles strongly enriched in raft components (Fig. 1C and D). However, the factors governing the budding size of clustered raft domains are likely to be more complex in cell membranes. The line tension between raft and non-raft membranes could be modulated by surfactancy effects of lipids as well as proteins at the domain interfaces (Simons and Vaz, 2004). The spontaneous curvature of raft domains that results from lipid asymmetry between the two membrane leaflets could play a part in controlling the budding process (Huttner and Zimmerberg, 2001). Moreover, budding must be regulated in cells by proteins and probably also supported by traction forces generated by molecular motors, and scission of the bud neck could be assisted by proteins such as dynamin (Kreitzer et al., 2000).

### **2.3. Post-Golgi transport routes to the plasma membrane**

Apical and basolateral proteins traverse the Golgi together until they reach the trans-Golgi network (TGN). There, they are segregated from Golgi proteins, from proteins trafficking to endosomes, and sometimes from each other, giving rise to a complicated intracellular trafficking map (Figure 2.2.). Cargo sorting may not be confined to a single station along a given pathway, but may take place sequentially. It is therefore difficult to assign sorting events to specific cellular locations. The enormous morphological and molecular complexity of the post-Golgi membrane system, together with the rapid and extensive exchange of molecules within this system by means of membrane trafficking, makes the definition of distinct compartments problematic. Therefore, the “compartment vocabulary” in the following discussion will be restricted to the terms TGN, early endosomes, recycling endosomes and late endosomes, even though the cellular reality is much more complicated than these terms disclose. Moreover, these simplifying terms are not meant to describe independent entities, but only the more identifiable elements of a highly interconnected system. This interconnectivity makes it unlikely that cargo molecules that

have different destinations are segregated from each other in a single step. Despite these difficulties, a few basic ways of cargo delivery can be distinguished.

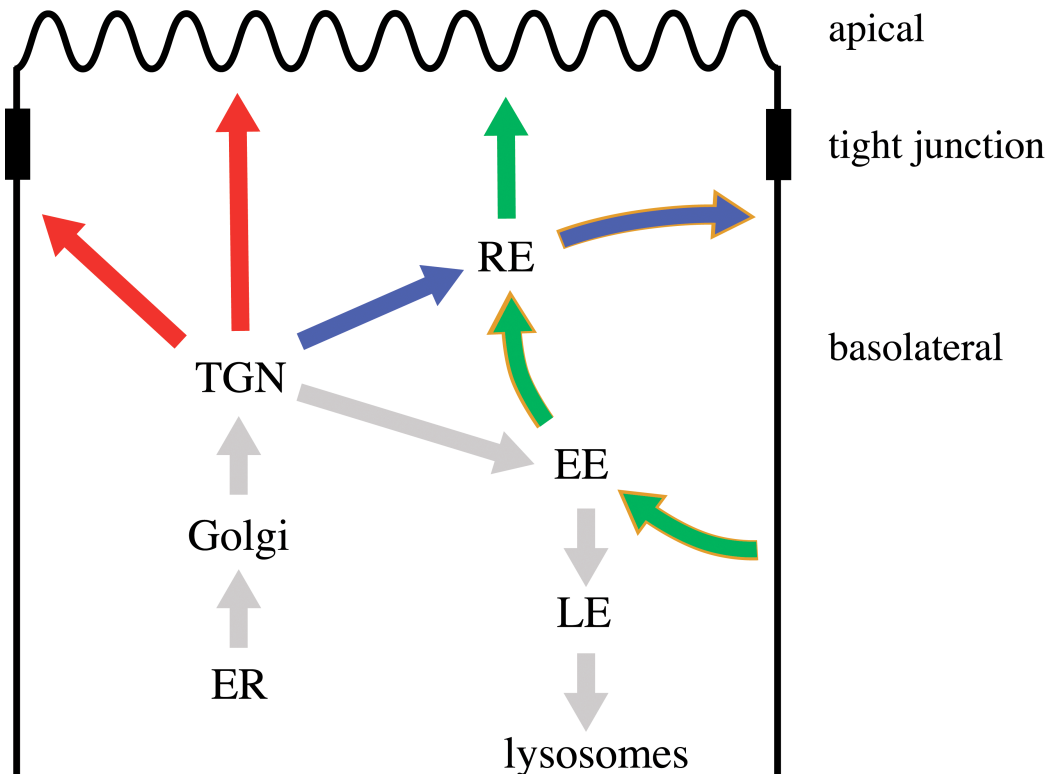


**Figure 2.2.** Trafficking pathways in polarised epithelial cells. After passage through the early secretory pathway, cargo can be transported from the TGN directly to the apical or basolateral membrane (red). Basolateral cargo can also reach the plasma membrane via endosomes (blue). Following initial transport to the basolateral membrane, apical cargo can reach the apical membrane via the transcytotic route (green), which passes through early and recycling endosomes. The arrows marked with a golden lining together constitute the basolateral recycling pathway. The apical recycling pathway and the apical-to-basolateral transcytotic pathway are omitted for clarity. EE = early endosomes, ER = endoplasmic reticulum, LE = late endosomes, RE = recycling endosomes.

### 2.3.1. Modes of sorting to the plasma membrane

In some epithelial cells, such as MDCK cells, the TGN appears to be a major site for sorting apical from basolateral biosynthetic cargo. Raft association of apical proteins, as well as the packaging of sphingolipids and cholesterol into transport carriers destined for

the plasma membrane, also takes place in the TGN. The TGN therefore probably is a compartment in which sorting based on raft clustering operates. In the TGN of endocrine and exocrine cells, raft clustering may mediate not only constitutive sorting to the plasma membrane, but also formation of immature secretory granules (Thiele and Huttner, 1998; Schmidt et al., 2001). This again underscores that the clustering of rafts does not lead to a random aggregation of raft components.

Transport carriers often arise from the TGN as large tubules (Hirschberg et al., 1998), which then undergo fission and fusion (Toomre et al., 1999). Segregation of apical and basolateral cargo might continue after transport containers have left the TGN, so that mixed carriers mature into apical carriers through removal of basolateral proteins (Musch, 2004). This would be analogous to the maturation of immature secretory granules into dense core granules. TGN-derived apical and basolateral transport carriers can then directly fuse with their respective target plasma membrane domain (Keller et al., 2001).

However, TGN-derived carriers can also intersect with other trafficking routes before their cargo is delivered to the surface. Basolateral proteins such as the transferrin receptor, the asialoglycoprotein receptor and vesicular stomatitis glycoprotein (VSV-G) can pass through endosomes before they reach the cell surface (Futter et al., 1995; Leitinger et al., 1995; Ang et al., in press). Given the similarity between certain basolateral sorting determinants and endocytosis signals, basolateral cargo and molecules endocytosed from the plasma membrane might meet in an endosomal compartment, probably in recycling endosomes. From there, basolateral cargo could move to the basolateral membrane together with molecules that are being recycled (Matter and Mellman, 1994; Traub and Apodaca, 2003). A similar endosomal stop-over has not been observed for apical cargo, except for mutants of the normally basolateral polymeric immunoglobulin receptor and VSV-G (Orzech et al., 2000; Ang et al., in press). This, however, may simply reflect a sorting defect along the basolateral route. These mutants might first travel from the TGN to recycling endosomes like their wild-type counterparts, but then fail to find their way to the basolateral membrane. They could subsequently leak into the pathway from recycling endosomes to the apical membrane that is normally used for apical recycling and transcytosis.



In some epithelial cells, such as hepatocytes, most apical cargo is first delivered to the basolateral membrane, followed by transcytosis (Bastaki et al., 2002). This could be achieved by selective endocytosis of apical proteins or, more likely, sorting after endocytosis so that basolateral proteins are recycled whereas apical proteins are transcytosed. The transcytotic route has been suggested to involve another transport intermediate, the apical recycling endosome (Brown et al., 2000; Mostov et al., 2000). However, it is not clear whether this intermediate really is a distinct compartment or a part of recycling endosomes (Sheff et al., 1999; Hoekstra et al., 2004).

These three modes of apical sorting (direct sorting from the TGN, sorting via endosomes and indirect sorting via the basolateral membrane) probably operate simultaneously in all polarised cell types but are used to different extents. Hepatocytes favour the transcytotic route, but also sort apical proteins directly (Kipp and Arias, 2000). Similarly, direct delivery is preferred in MDCK cells (Matlin and Simons, 1984; Misek et al., 1984), but transcytotic sorting may nevertheless be used. Polishchuk et al. have recently claimed that GPI-anchored proteins are sorted to the apical surface of MDCK cells along the transcytotic pathway (Polishchuk et al., 2004). However, their observations contradict several previous studies (Brown et al., 1989; Lisanti et al., 1989; Keller et al., 2001). Thus, it remains to be seen whether they can be substantiated.

The underlying sorting mechanisms in the TGN and in endosomes are probably similar. Basolateral cytoplasmic domain determinants are likely to be recognised by similar sorting receptors (Folsch et al., 2003) and raft clustering might be reused to govern the trafficking of endocytosed molecules. The sorting machinery might also be reused. For instance, the closely related proteins VIP17/MAL and MAL2 have been proposed to participate in apical sorting at the TGN and in endosomes, respectively (Puertollano et al., 1999; Cheong et al., 1999; de Marco et al., 2002). Similarly, rab11, in addition to its function in recycling endosomes, has been suggested to regulate exit of basolateral cargo from the TGN (Chen et al., 1998).

### *2.3.2. Plasticity of polarised sorting*

The evidence discussed so far indicates that the cellular repertoire of basic sorting mechanisms is small compared to the multitude of sorting determinants. This raises the

question why such an abundance of sorting determinants might have evolved and why some proteins contain several sorting determinants, which sometimes even oppose each other.

It has been argued that the large variety of sorting determinants is crucial to endow polarised sorting with plasticity. The same protein may need to be differentially localised in different epithelial cell types whose plasma membrane domains are otherwise very similar. Kidney cells target a  $\text{Na}^+/\text{K}^+/\text{Cl}^-$  cotransporter to the apical membrane and a chloride channel to the basolateral membrane in order to absorb sodium chloride, whereas the distribution of the same two proteins is reversed in NaCl-secreting intestinal cells (Muth and Caplan, 2003). Similarly, alpha- and beta-intercalated cells, two cell types of the kidney collecting duct, need to have opposite distributions of a proton ATPase and a  $\text{Cl}^-/\text{HCO}_3^-$  exchanger, as the former absorb bicarbonate while the latter secrete it (Al-Awqati, 2003). Unless different variants of such proteins can be generated, for instance by alternative splicing, the parts of the sorting machinery responsible for their transport need to be adaptable. Such specific alterations would be impossible if only a single sorting determinant existed for the targeting to a particular plasma membrane domain, since changes in how the sorting machinery interprets this determinant would affect the trafficking of many proteins (Muth and Caplan, 2003).

The seemingly futile presence of multiple sorting determinants in the same protein can be rationalised in two ways. First, combining several weak determinants with identical polarity may be used to enhance the fidelity of sorting. Second, the simultaneous presence of opposing determinants may be utilised to switch proteins between plasma membrane domains. This is illustrated by the well-studied example of pIgR trafficking in MDCK cells. The pIgR contains a dominant basolateral determinant that dictates delivery to the basolateral membrane. However, upon ligand binding this determinant is inactivated, unmasking a recessive determinant that then guides the ligand-bound receptor to the apical membrane along the transcytotic route (Mostov et al., 2000). The function of having multiple trafficking routes to the same membrane domain could likewise be to allow for plasticity of polarised sorting. These transport routes could provide sorting modules that can be reprogrammed independently of each other, perhaps to be used by functionally related cargo proteins.

## 2.4. Implications of apical membrane biogenesis by raft clustering

The hypothesis that basolateral sorting is mainly based on specific cargo capture by sorting receptors, whereas apical sorting relies on cargo recruitment into raft domains, could explain why basolateral proteins are sorted more accurately. Receptor-mediated cargo capture is a stringent mechanism for the inclusion of a particular set of proteins into transport carriers, but may not exclude other proteins very effectively. Hence, apical proteins could become part of basolateral transport containers simply by accident. On the other hand, cargo recruitment into clustered rafts may not be absolute, because it ultimately relies on differential affinities for different lipid environments. However, raft clustering followed by domain-induced budding is a mechanism well suited to stringently exclude non-raft proteins.

A more fundamental reason for this mechanistic organisation of epithelial exocytosis is that apical sorting must ensure the special lipid composition of the apical membrane responsible for its robustness. A raft-based sorting mechanism, in which selective lipid-lipid associations provide the driving force for sorting and the formation of transport containers, may be best suited for this purpose. Sorting based on specific protein-protein interactions, by contrast, may not exert much control over which lipids are included into the transport containers. The basolateral membrane contains a sizeable fraction of raft lipids that could simply have been delivered by default.

Another feature of sorting by recruitment into clustered rafts is that cargo can be transported by substoichiometric interactions with the machinery responsible for moving transport containers. When molecular motors bind to adaptors that directly interact with cargo proteins, a single motor protein controls the transport only of those proteins it captures via the adaptor. In contrast, a motor protein that associate with a raft domain could potentially move all lipids and proteins present in that domain. Apical transport involves kinesin motors (Kreitzer et al., 2000). So far, the only kinesin known to bind membranes by protein-lipid recognition is KIF1A (Klopfenstein and Vale, 2004), but there may be more. An interesting candidate is KIFC3, which has been proposed to associate with rafts and mediate the apical transport of raft proteins (Noda et al., 2001). Movement of transport containers is followed by fusion with the target membrane. Again, raft association of only a few proteins that mediate fusion may be sufficient to govern the

targeting of whole raft domains. Indeed, syntaxin-3 and TI-VAMP, two components of the apical fusion machinery (Galli et al., 1998; Low et al., 1998), associate with rafts (Lafont et al., 1999). Hence, KIFC3, syntaxin-3 and TI-VAMP could act as molecular guideposts to ensure the economical, co-ordinated targeting of apical cargo.

Apical membrane biogenesis during tube formation by epithelial cells could be another process in which raft clustering plays a key role. Tube formation occurs in a number of ways, all of which involve the generation of a new apical membrane (Lubarsky and Krasnow, 2003). For instance, MDCK cells as well as epithelial cells of the *Caenorhabditis elegans* gut and *Drosophila* heart can depolarise and form a cord consisting of two layers of cells (Figure 2.3.). In this unpolarised state, apical membrane components are deposited in an intracellular vacuolar apical compartment (VAC), which may be a specialised endosome (Vega-Salas et al., 1987; Low et al., 2000). Once the cord is established, the cells repolarise and form a new apical membrane at the site where the two cell layers face each other, thus generating a tube lumen. They achieve this by exocytosing the entire VAC (Vega-Salas et al., 1988).

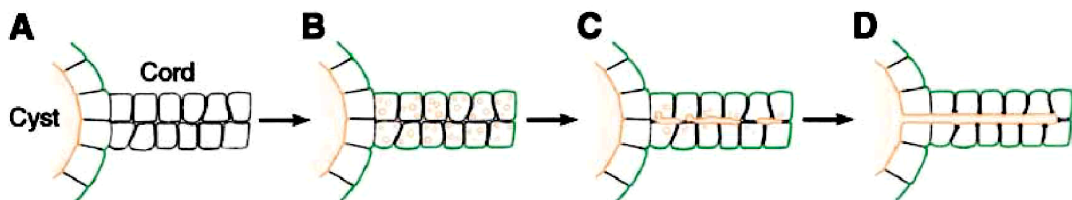


**Figure 2.3.** MDCK cell tube formation. Polarised cells in an MDCK cell cyst migrate out from the cyst and form a long multicellular cord (shown in longitudinal section). During their migration, apicobasal polarity is lost (A). After an external cue triggers repolarisation, cell surfaces in contact with the extracellular matrix accumulate basal markers (green). Cytoplasmic vesicles carrying apical membrane components (orange circles) target the developing apical (luminal) surfaces (B). The apical vesicles fuse, creating pockets of lumen at the apical surface (C). Continued delivery of apical vesicles expands the lumen pockets until they merge and form a complete lumen connecting to the cyst cavity (D). From Lubarsky and Krasnow, 2003.

Similarly, newly formed *Drosophila* tracheal tubes are expanded in a two-step process that involves the cytoplasmic accumulation of vesicles containing apical membrane components and their subsequent fusion with the apical membrane, thereby increasing its area (Beitel and Krasnow, 2000; Lubarsky and Krasnow, 2003). Raft clustering clearly is a

mechanism suited to bring about the collective transport of large sets of molecules. Because only a few "guidepost" proteins may be necessary to make whole patches of membrane moveable, raft clustering could be used to deliver blocks of prospective apical membrane to a new destination.

## **2.5. Aim of this thesis**

The general aim of this thesis was to contribute to the molecular analysis of apical sorting in epithelial cells. Progress towards elucidating the mechanisms underlying this process will likely come from a better understanding of the properties of lipid rafts, and from the characterisation of the protein parts of the apical sorting machinery. Both issues have been addressed in this work, as outlined below.

The biochemical analysis of lipid rafts primarily relies on the isolation of DRMs with mild detergents. It is thought that sphingolipid-cholesterol rafts are able to resist detergent solubilisation due to their tight lipid packing. Hence, DRM association of a protein is taken to indicate a strong interaction with highly ordered membrane microdomains. DRMs are most commonly prepared with Triton X-100 and CHAPS, but other detergents have also been used. However, it is unclear how the composition of different DRMs correlates with the organisation of lipid microdomains in cell membranes. It has even been proposed that different detergents might be used to differentiate between microdomain subtypes. To help clarify these points and evaluate the usefulness of different detergents for the study of processes like membrane trafficking, a systematic analysis of the protein and lipid content of DRMs obtained with various mild detergents was undertaken.

A number of proteins have been implicated in apical transport. However, the available experimental evidence is weak in most cases. This can partially be attributed to the lack of a general method for interfering with the function of proteins. The discovery of RNA interference and its application as a powerful tool for specific protein depletion has dramatically changed this situation. It is now possible to suppress the synthesis and thus activity of essentially any protein without a need for specialised reagents such as function-blocking antibodies. Therefore, it was attempted to generate so called "knockdowns" for all proteins putatively involved in apical sorting in MDCK cells, followed by an analysis of the resulting phenotypes with regard to possible defects in membrane trafficking.

### 3. Biochemical analysis of detergent-resistant membranes

The goal of this chapter was to comprehensively compare the protein and lipid content of detergent-resistant membranes (DRMs) obtained with different detergents. All detergents previously used for the isolation of DRMs were tested, namely Triton X-100 (referred to as Triton; Brown and Rose, 1992), CHAPS (Kurzchalia et al., 1992), Brij 58 (Bohuslav et al., 1993), Brij 96 (Madore et al., 1999), Lubrol WX (referred to as Lubrol; Röper et al., 2000), and Brij 98 (Drevot et al., 2002). In addition, Tween 20 (referred to as Tween) was included in the analysis, a very mild detergent known to solubilise cell membranes very inefficiently (Helenius and Simons, 1975). Two cell lines, MDCK and human T cell leukemia (Jurkat) cells, were used in order to test whether the characteristics of DRMs and the effectiveness of particular detergents varied between cell types. Finally, reagents to manipulate the DRM association of proteins were evaluated.

#### 3.1. Protein content of DRMs

First, suitable conditions for extraction were established for each detergent. Provided the detergent concentration is above the critical micelle concentration, the effectiveness of membrane solubilisation is determined by the molar ratio of detergent to membrane lipid (Helenius and Simons, 1975; Ostermeyer et al., 1999). To test different ratios, homogenate was prepared from MDCK cells metabolically labelled with  $^{35}\text{S}$ -methionine, and a fixed amount of cellular material (corresponding to 1 mg of total protein), was extracted with varying concentrations of detergent (expressed as per cent weight per volume). DRMs were separated from detergent-soluble material by equilibrium density centrifugation, also known as flotation, on sucrose step gradients. Equal aliquots of the floating material were solubilised with 0.1% SDS, and the radioactivity of  $^{35}\text{S}$ -labelled proteins was measured by liquid scintillation counting (Table 3.1.).

	Tween	Brij 58	Lubrol	Brij 98	Brij 96	Triton	CHAPS
0.5%	n.d.	1	1	n.d.	1	n.d.	n.d.
1%	1	0.93	0.95	1	0.89	1	1
2%	0.99	0.85	0.93	0.76	0.65	1.07	n.d.
4%	0.99	n.d.	n.d.	0.67	n.d.	3.04	0.29
6%	n.d.	n.d.	n.d.	n.d.	n.d.	n.d.	0.27

**Table 3.1.** Protein amounts of DRMs from MDCK cells. Homogenate from  $^{35}\text{S}$ -labelled MDCK cells was extracted with varying concentrations of Tween 20, Brij 58, Lubrol WX, Brij 98, Brij 96, Triton X-100 or CHAPS. DRMs were prepared by flotation on sucrose step gradients, and equal aliquots of the floating fractions were analysed by liquid scintillation counting. The amount of radioactivity in the floating fraction obtained with the lowest detergent concentration was set to one in each case. n.d. = not determined. All detergent concentrations are in % (w/v).

In the case of Tween, Brij 58 and Lubrol, the amount of DRM protein was approximately equal with all detergent concentrations. For Brij 98 and Brij 96, a decrease in DRM protein occurred with increasing detergent concentration, indicating that the maximum solubilisation possible with these detergents was not reached, even with the highest concentrations used. For CHAPS, a substantial reduction in DRM protein was observed when raising the detergent concentration from 1% to 4%. Triton, on the other hand, showed a similar extent of solubilisation at 1% and 2%, but the amount of floating material was increased at 4%.

For subsequent experiments, Tween and Brij 58 were used at a concentration of 1%, Lubrol at 0.5%, and CHAPS at 4%, as these conditions seemed to correspond to detergent to membrane ratios sufficient for the maximum solubilisation possible with these detergents. The concentrations for Brij 58 and Lubrol are identical to earlier studies (Montixi et al., 1998; Röper et al., 2000). CHAPS has previously been applied at a concentration of 1.25% (20 mM). This concentration seems insufficient for maximum solubilisation of the amount of cell membranes used here. For Brij 98 and Brij 96, respective concentrations of 1% and 0.5% were chosen, as has been done before (Drevot et al., 2002; Madore et al., 1999). These concentrations do not achieve maximum solubilisation, but higher concentrations proved problematic due to the resulting higher amounts of detergent in the DRMs, which interfered with the analysis of DRM lipids (see

section 3.2.). The increase of DRM protein at high Triton concentrations may reflect that, under certain conditions, Triton can promote the formation of DRMs (Heerklotz, 2002). To avoid this complication, Triton was applied at 1%, the commonly used concentration.

For an analysis of the total DRM content, homogenate from MDCK and Jurkat cells metabolically labelled with  $^{35}\text{S}$ -methionine was extracted with the different detergents under the conditions established above, and DRMs were isolated by equilibrium density centrifugation. For comparison, total cell membranes (TCMs) were prepared using the same procedure, except that detergent was omitted. Equal aliquots of TCMs and the various DRMs were analysed by SDS-PAGE (Figure 3.1.).

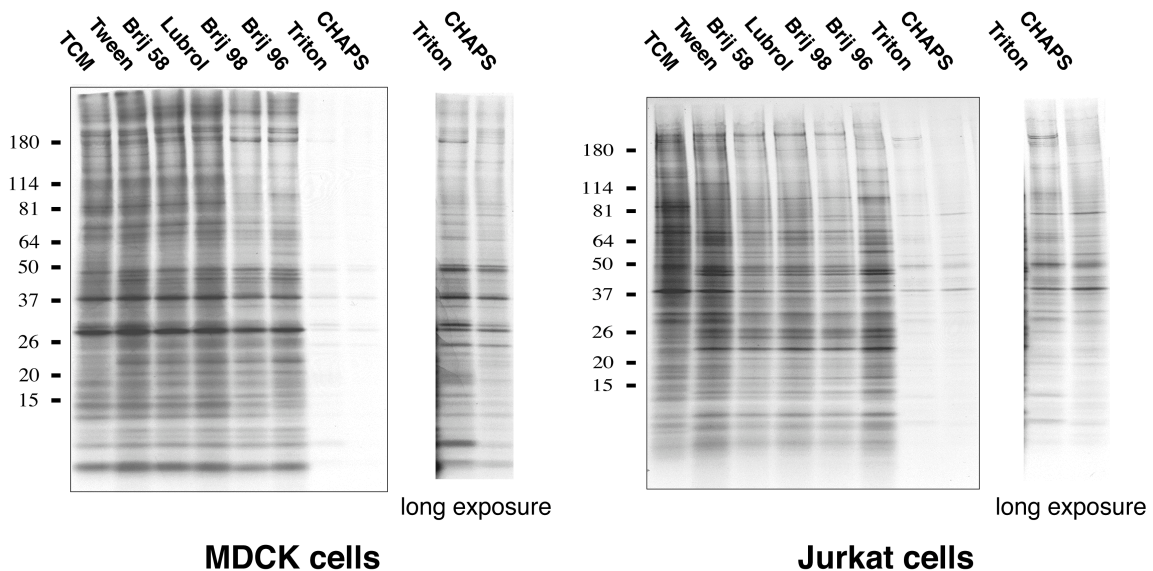


**Figure 3.1.** Protein content of DRMs from MDCK and Jurkat cells. Homogenate from  $^{35}\text{S}$ -labelled MDCK or Jurkat cells was either not extracted or extracted with 1% Tween 20, 1% Brij 58, 0.5% Lubrol WX, 1% Brij 98, 0.5% Brij 96, 1% Triton X-100 or 4% CHAPS. Total cell membranes (TCMs) and DRMs were prepared by flotation on sucrose step gradients. Equal aliquots of the floating fractions were separated by SDS-PAGE on 8-16% gels. Proteins were revealed by autoradiography.

In MDCK cells, TCMs and the DRMs prepared with Tween, Brij 58 and Lubrol seemed remarkably similar, both in the amount and the identity of the proteins they contained. DRMs obtained with Brij 98 and Brij 96 contained less protein, but only with Triton and CHAPS was the majority of the TCM protein solubilised. A similar trend was observed



when comparing TCMs and DRMs from Jurkat cells, even though in this case Brij 98 and Brij 58 solubilised proteins more efficiently than Brij 96. These results indicate that the various detergents differ significantly in their ability to solubilise proteins. In addition, the comparison of DRMs from MDCK and Jurkat cells shows that the effectiveness of a given detergent may be cell type-dependent.

However, the comparison of the total protein content of different DRMs may be obscured by mixing proteins from different subcellular locations and by contamination with, for example, cytoskeletal proteins. To avoid these potential problems, the analysis was restricted to plasma membrane proteins. MDCK cells were surface biotinylated, extracted with the various detergents or not, and DRMs as well as total cell membranes (TCMs) were prepared by flotation as before (Figure 3.2.).

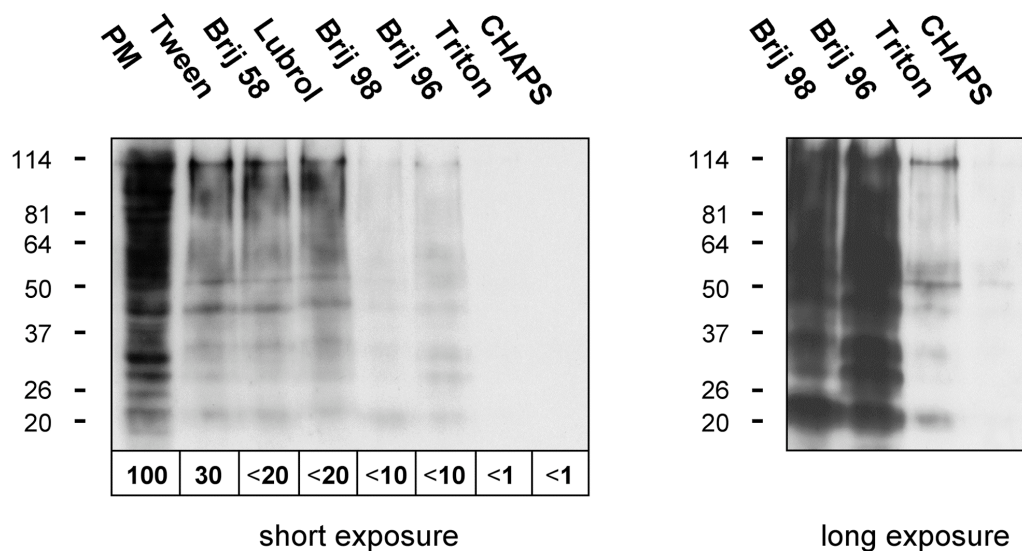


**Figure 3.2.** Protein content of plasma membrane DRMs from MDCK cells. Surface biotinylated MDCK cells were extracted with 1% Tween 20, 1% Brij 58, 0.5% Lubrol WX, 1% Brij 98, 0.5% Brij 96, 1% Triton X-100 or 4% CHAPS. DRMs were prepared by flotation on sucrose step gradients. Equivalent aliquots of the starting material before detergent treatment, which contained the total plasma membrane protein (= PM), and the various DRMs were analysed by Western blotting using peroxidase-conjugated extravidin to reveal biotinylated proteins. Two exposures of the same membrane are shown. The amounts of biotinylated protein were quantified, setting PM to 100% (panel below short exposure).

All detergents solubilised a substantial fraction of the biotinylated plasma membrane protein, indicating that simple DRM preparations as in Figure 3.1. contain substantial amounts of contaminating non-membrane proteins, as has also been revealed by proteomic analyses of DRMs (von Haller et al., 2001; Nebl et al., 2002; Foster et al., 2003). Even Tween reduced the amount of biotinylated protein recovered in the floating fraction, presumably by solubilising proteins which are bound to the outside of MDCK cells, like galectins. However, the different DRMs again contained very different amounts of protein. For instance, Tween, Brij 58 and Lubrol produced DRMs containing over ten-fold more protein than DRMs prepared with Triton or CHAPS. Hence, Triton and CHAPS were the most selective detergents in that they allowed only relatively few proteins to remain associated with lipids.

To investigate the differences between detergents in more detail, detergent resistance of particular marker proteins was evaluated using MDCK-PLAP cells. Cell homogenate, or detergent extracts prepared with Lubrol, Brij 96 or Triton, were floated on linear sucrose gradients. The distribution of the tetraspan protein VIP17/MAL, GPI-anchored PLAP, caveolin-1, stomatin, the doubly acylated Src-like kinase Yes, transferrin receptor (TfR), the sialoglycoprotein gp114, calnexin and rab-5 was analysed by immunoblotting (Figure 3.3.).

Flotation without detergent treatment demonstrated membrane association of the above proteins (Figure 3.3. top left). Lubrol largely solubilised calnexin and rab-5, as reflected by their retention in the high-density fractions, whereas the other proteins were predominantly detergent-resistant (Figure 3.3., top right). Brij 96 additionally solubilised gp114, most of the TfR and about 50% of Yes (Figure 3.3., bottom left), while Triton solubilised rab-5, calnexin, gp114, TfR and most of Yes (Figure 3.3., bottom right). Hence, DRM association of these marker proteins confirms the graded selectivity of the detergents observed by analysis of the plasma membrane DRM protein content.

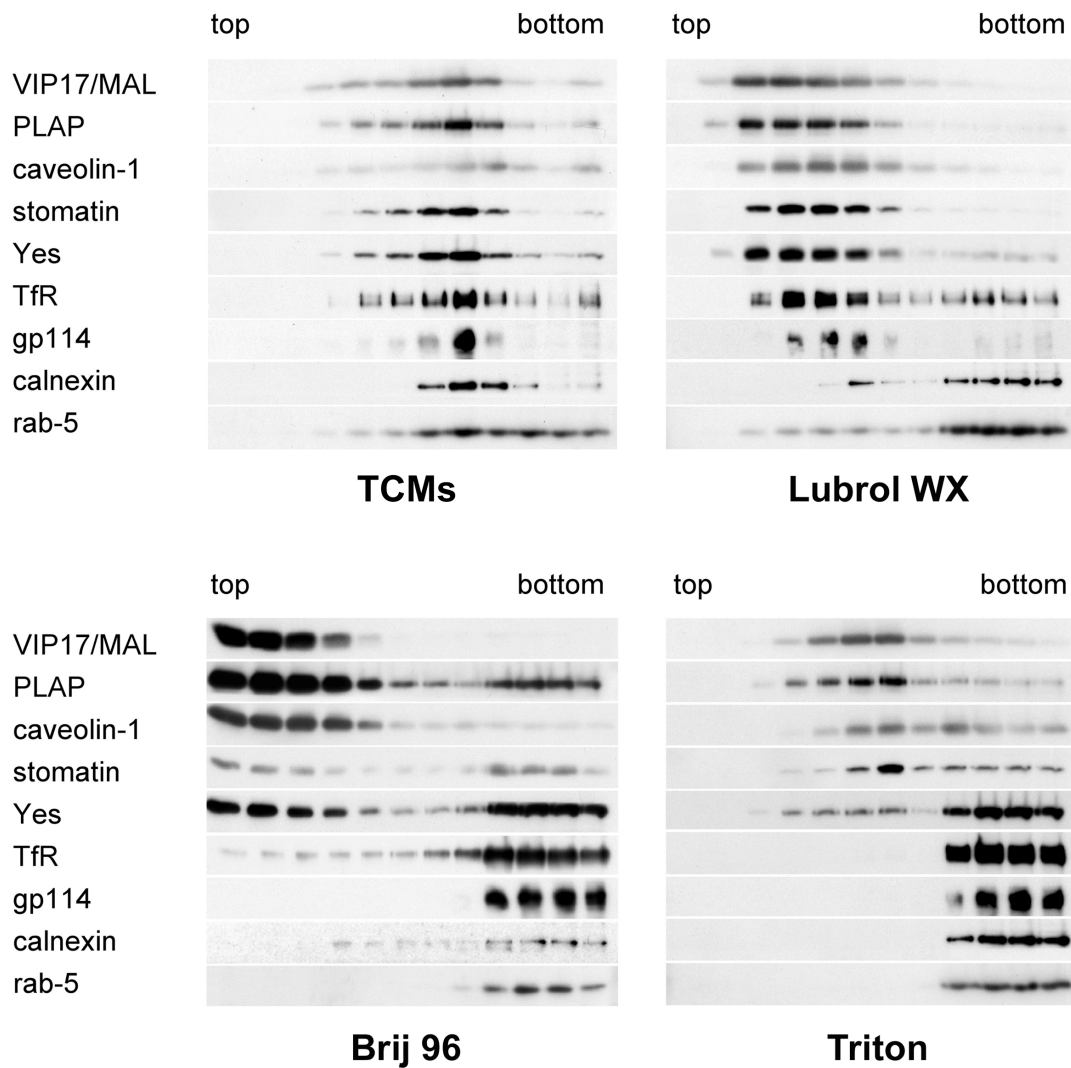


**Figure 3.3.** DRM association of marker proteins from MDCK cells. MDCK-PLAP cell homogenate was not extracted, or extracted with 0.5% Lubrol WX, 0.5% Brij 96 or 1% Triton X-100, and floated on linear sucrose gradients. 12 fractions were collected from the top, the last four fractions of which contained the detergent-soluble material. The distribution of marker proteins was analysed by immunoblotting. The light fractions from the top of the gradients are on the left, the heavy bottom fractions on the right.

The results with Triton agree with earlier observations (Puertollano et al., 1999; Brown and Rose, 1992; Snyers et al., 1999; Lafont et al., 1998). Regarding Lubrol, calnexin had previously been found to be partly insoluble (Röper et al., 2000), consistent with the results shown here. In contrast, the TfR, which largely resisted extraction with Lubrol, had been reported to be Lubrol-soluble in MDCK cells (Röper et al., 2000).

To clarify this contradiction, the experimental conditions used by Röper et al. were reproduced as accurately as possible, but the majority of the TfR remained Lubrol-insoluble (data not shown). Next, the antibodies used for detection of the TfR were compared. In the experiments shown in Figure 3.3., a monoclonal antibody raised against the human transferrin receptor from Zymed was used, whereas Röper et al. applied a mouse antibody from Serotec raised against the rat TfR. Both the Zymed and the Serotec antibody were tested by immunoblotting with MDCK and rat liver lysate (Figure 3.4.).

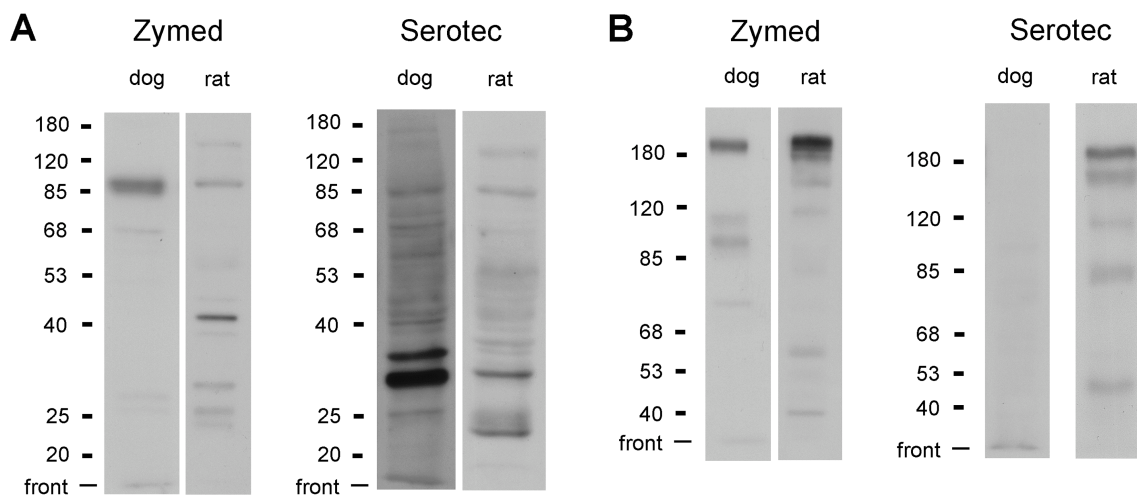


**Figure 3.4.** Recognition of the dog and rat transferrin receptor by different antibodies. MDCK (dog) and rat liver lysate (rat) were separated by SDS-PAGE on a 10% gel under reducing conditions (**A**) or on a 7.5% gel under non-reducing conditions (**B**). The membranes were probed with the mouse anti-human transferrin receptor antibody from Zymed (left panels) or the mouse anti-rat transferrin receptor antibody from Serotec (right panels). In some cases, different exposures from the same membrane are shown next to each other.

Under reducing SDS-PAGE conditions, the major band revealed by the Zymed antibody in MDCK lysate corresponded to a molecular weight of about 85 kDa (Figure 3.4. A, left). This is in agreement with the molecular weight of the canine TfR (87 kDa for the unmodified polypeptide according to the SwissProt database). A protein of about 85 kDa was also detected in rat liver lysate, but the major band appeared at about 40 kDa. Under non-reducing SDS-PAGE conditions, the Zymed antibody recognised a protein with an apparent molecular weight of 180 kDa in both dog and rat cell lysate (Figure 3.4. B, left), consistent with the known dimerisation of the TfR by means of a disulfide bond (Jing and

Trowbridge, 1987). On the other hand, the major band revealed by the Serotec antibody under reducing conditions in dog cell lysate corresponded to a molecular weight of less than 40 kDa, and only a minor band appeared at 85 kDa (Figure 3.4. A, right). In addition, no band appeared at 180 kDa with MDCK cell lysate under non-reducing conditions (Figure 3.4. B, right). With rat liver lysate bands were seen at 85 kDa and 180 kDa under reducing and non-reducing conditions, respectively, even though several cross-reacting bands were present. Hence, the Zymed antibody recognises the dog as well as the rat TfR receptor, whereas the Serotec antibody only recognises the rat TfR. The band observed with the Serotec antibody in MDCK lysates under reducing conditions probably is the result of antibody crossreactivity. Röper et al. failed to notice that the major band revealed by the Serotec antibody in MDCK cell lysate appears at less than 40 kDa because they routinely used 7.5% SDS-PAGE gels in their study (Denis Corbeil, personal communication). Instead, they presumably mistook the crossreacting minor band at 85 kDa for the TfR. Therefore, it appears that the contradiction between the results shown in Figure 3.3. and those of Röper et al. can be explained by the different antibodies used.

Overall, the analysis of the protein content of DRMs from MDCK cells shows that the detergents differ considerably in their ability to enrich strongly lipid-associated proteins, i.e. they differ in their 'DRM selectivities'. Triton and CHAPS are very selective as they allow only a small group of membrane proteins to stay lipid-associated, whereas detergents like Tween, Brij 58 and Lubrol are much less selective.

### **3.2. Lipid content of DRMs**

To analyse the lipid content of DRMs, MDCK and Jurkat cells were used to either label all lipids with  $^{14}\text{C}$ , or phospholipids with  $^{32}\text{P}$ . TCMs and DRMs were obtained by flotation on sucrose step gradients. Lipids were extracted and resolved by thin-layer chromatography (Figure 3.5.).

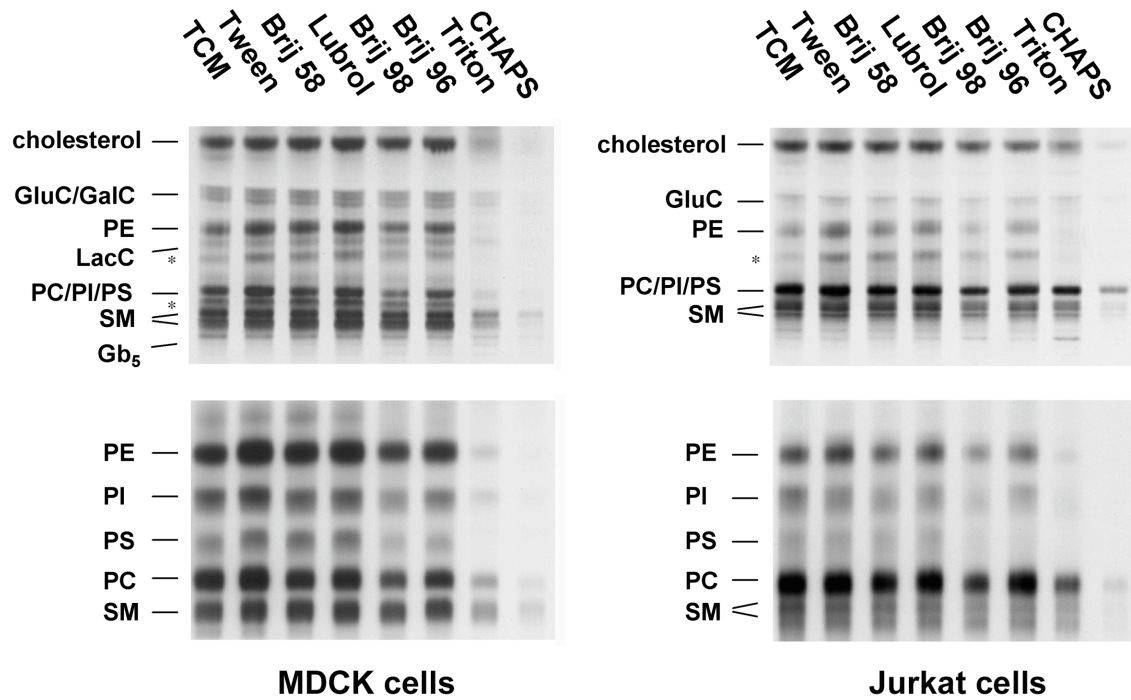


**Figure 3.5.** Lipid content of DRMs from MDCK and Jurkat cells. Lipids from total cell membranes (TCMs) and DRMs from  $^{14}\text{C}$ - or  $^{32}\text{P}$ -labelled MDCK and Jurkat cells were analysed by TLC (top panels:  $^{14}\text{C}$ -labelled lipids, bottom panels:  $^{32}\text{P}$ -labelled lipids). GluC/GalC/LacC = glucosyl/galactosyl/lactosyl ceramide, SM = sphingomyelin, Gb<sub>5</sub> = pentosylglucoside, PE = phosphatidylethanolamine, PC = phosphatidylcholine, PI = phosphatidylinositol, PS = phosphatidylserine. Asterisks denote lipids not identified by co-migration with lipid standards.

As observed for the protein content of DRMs, the amounts of lipid present in the DRMs varied considerably between detergents. To show qualitative changes in the lipid composition of DRMs compared to TCMs, lipids were grouped into sphingolipids, cholesterol and glycerophospholipids. Sphingolipid to glycerophospholipid and cholesterol to glycerophospholipid ratios were calculated. The fold changes of these ratios relative to the TCMs are depicted in Fig. 3.6.

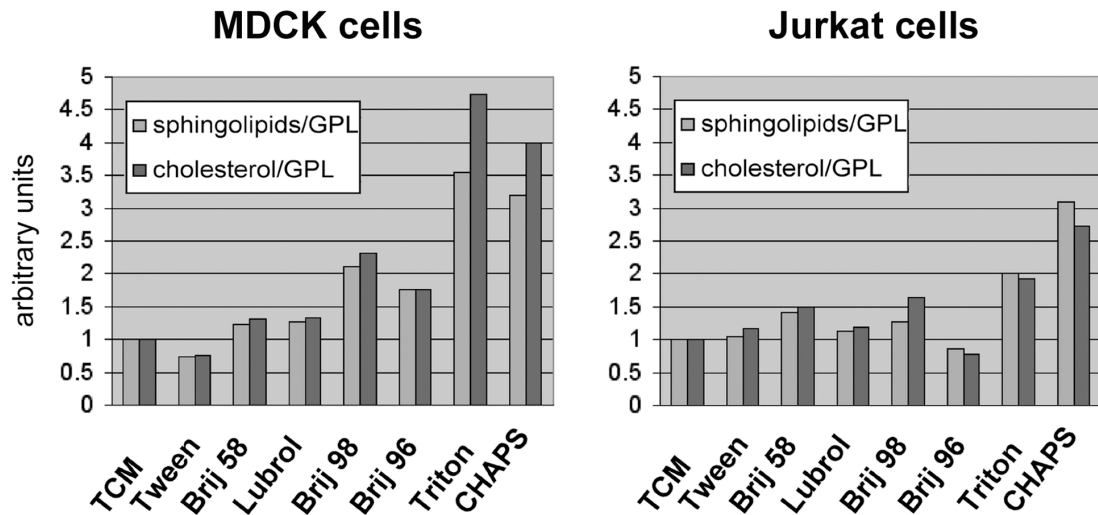


**Figure 3.6.** Lipid content of DRMs from MDCK and Jurkat cells. Lipids from the TLC plates shown in Figure 3.5. were quantified and grouped into sphingolipids (GalC + GluC + LacC + SM + Gb<sub>5</sub> for MDCK cells, GluC + SM for Jurkat cells, intensities taken from <sup>14</sup>C-labelled lipids), cholesterol and glycerophospholipids (PE + PI + PS + PC, intensities taken from <sup>32</sup>P-labelled lipids). Sphingolipid to glycerophospholipid and cholesterol to glycerophospholipid ratios relative to the ratios for TCMs are shown. GPL = glycerophospholipids.

Compared to TCMs, DRMs from MDCK cells prepared with Triton and CHAPS showed a clear enrichment of sphingolipids and cholesterol over glycerophospholipids. The other detergents enriched these lipids less strongly. Nevertheless, their capacity for enrichment correlated with the DRM specificity with regard to proteins, such that Brij 98 and Brij 96 caused a more pronounced enrichment of sphingolipids and cholesterol than Tween, Brij 58 and Lubrol. The same trend was observed for Jurkat cells, but notable differences existed. Contrary to MDCK cells, Brij 98 and Brij 58 enriched sphingolipids and cholesterol to a similar extent, whereas Brij 96 did not.

The behaviours of Brij 58, Brij 96 and Brij 98 in MDCK and Jurkat cells again illustrate that the effect of a given detergent may vary between cell types. Moreover, the enrichment of sphingolipids and cholesterol was overall less pronounced in Jurkat than in MDCK cells, showing that the lipid composition of DRMs prepared with a particular detergent can be cell type-dependent.

Next, the fatty acid substitution pattern of glycerophospholipids in different DRMs was analysed. Lipids from the floating fractions of MDCK and Jurkat cells were prepared as before, and phosphatidylcholine (PC), the major glycerophospholipid, was analysed by mass spectrometry. Seventeen PC species, differing in the total number of carbon atoms and/or the number of double bonds in the fatty acid moieties, were detected. For each species, its percent fraction of the total PC was calculated. In addition, the relative concentration of each species was determined to allow comparison of the amounts present in different DRMs (see Appendix 1). PC species were then grouped according to the degree of saturation of their fatty acids (Figure 3.7.).

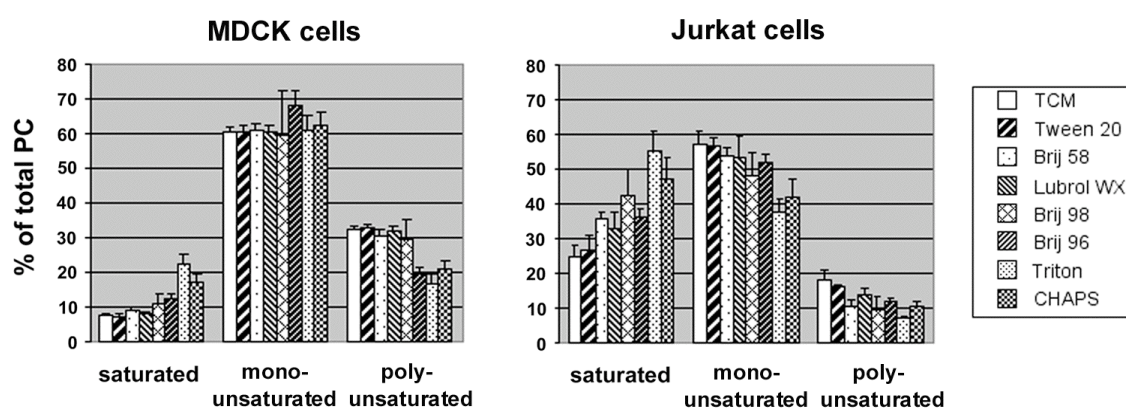


**Figure 3.7.** Saturation profile of phosphatidylcholines (PCs) in DRMs from MDCK and Jurkat cells. TCMs and DRMs were obtained as before, lipids were extracted and PC was analysed by mass spectrometry. Percent fractions of each PC species were determined and grouped into saturated (30:0, 31:0, 32:0, 34:0), mono-unsaturated (31:1, 32:1, 33:1, 34:1, 36:1) and polyunsaturated (32:2, 33:2, 34:2, 35:2, 36:3, 36:2, 38:3) PC species (in x:y, x indicates the total number of carbon atoms of the fatty acid side chains, y indicates the number of double bonds). Error bars represent standard deviations of three measurements of the same samples.

In MDCK cells, about 60% of the total cell membrane PC was mono-unsaturated, less than 10% was fully saturated, and about 30% possessed more than one double bond. With increasing detergent strength, increasing enrichment of saturated PCs at the expense of polyunsaturated PCs was observed. A similar trend was found for Jurkat cells, which additionally showed depletion of mono-unsaturated PCs with increasing solubilisation efficiency of the detergents.



Interestingly, PCs from Jurkat cells contained a larger fraction of saturated PCs (25% of the total cell membrane PC compared to less than 10% in MDCK cells). This could explain the less pronounced enrichment of sphingolipids and cholesterol in DRMs from these cells. Saturated glycerophospholipids preferentially partition into the liquid-ordered phase, so that liquid-ordered domains in Jurkat cell membranes may contain a comparatively high proportion of glycerophospholipids. As a result, enrichment of these domains by DRM isolation does not cause the marked depletion of glycerophospholipids characteristic of MDCK cells. These results again underscore differences between DRMs from different cell types.

Taken together, the lipid analysis showed quantitative, as well as qualitative differences between DRMs prepared with different detergents. DRM selectivities of the detergents, as defined by their ability to enrich a subset of proteins during DRM preparation, correlated well with their ability to enrich sphingolipids and cholesterol over glycerophospholipids and saturated over unsaturated glycerophospholipids. Thus, the term ‘DRM selectivity’ can be extended to comprise characteristic changes in the lipid composition of DRMs. Trends were similar in MDCK and Jurkat cells, but significant cell type-dependent differences regarding the composition of DRM lipids were observed.

### **3.3. Tools for manipulating DRM association**

Finally, tools to manipulate the DRM association of proteins were evaluated. Methyl-beta-cyclodextrin (referred to as cyclodextrin) extracts cholesterol from membranes and disrupts domains whose integrity depends on cholesterol (Simons and Toomre, 2000; Dietrich et al., 2001). Live MDCK-PLAP cells were either left untreated, or treated with 10 mM cyclodextrin for 30 or 60 minutes. These treatments did not affect cell integrity or viability as shown by Trypan Blue exclusion and continued cell growth when cyclodextrin was replaced by normal culture medium. Cell homogenates were prepared, and used for cholesterol determination, as well as for Triton extraction followed by flotation on linear sucrose gradients. Figure 3.8. shows the distribution of VIP17/MAL and PLAP in these gradients.

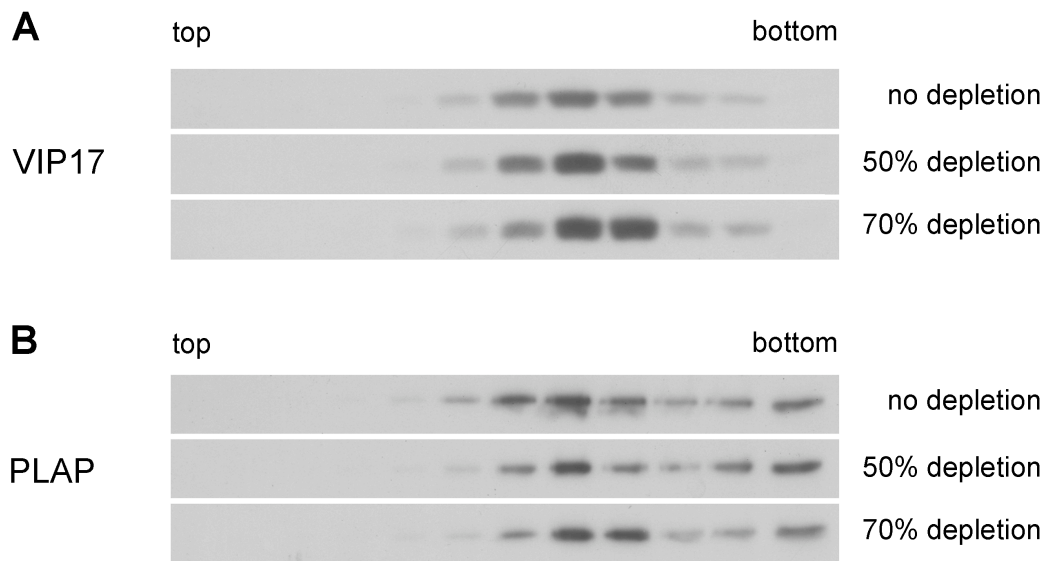


**Figure 3.8.** Manipulation of DRM association by cholesterol depletion from live MDCK cells. MDCK-PLAP cells were left untreated or treated with 10 mM methyl-beta-cyclodextrin for 30 or 60 min, resulting in a reduction of cellular cholesterol levels by 50% or 70% respectively. Cell homogenates were extracted with 1% Triton X-100 and floated on 12 ml linear sucrose gradients. 11 fractions of 0.75 ml were collected from the top. The remaining 3.75 ml, which contained the Triton-soluble material, constituted fraction 12. Equivalent aliquots from each fraction were used to analyse the distribution of VIP17 (**A**) and PLAP (**B**) by immunoblotting. The light fractions from the top of the gradients are on the left, the heavy bottom fractions on the right.

Without cholesterol depletion, VIP17/MAL is entirely Triton resistant, as before (Figure 3.8. A). No immunoreactivity can be detected in the bottom fraction, which contains the detergent soluble material in this experiment. Surprisingly, depleting total cellular cholesterol by 50% or even 70% failed to render VIP17/MAL sensitive to solubilisation with Triton. Only a slight shift in the distribution of VIP17/MAL towards higher density occurred, which probably reflects an increased density of the cholesterol-depleted DRMs. Similarly, cholesterol depletion did not increase the Triton-soluble fraction of PLAP, but shifted PLAP towards slightly higher density (Figure 3.8. B).

One potential reason for why the cholesterol depletion of live cells failed to render proteins like VIP17/MAL and PLAP detergent-soluble is that the pool of cholesterol responsible for their insolubility may be protected from cyclodextrin extraction. Hence,

the overall depletion of cellular cholesterol may not apply to the immediate membrane environment of VIP17/MAL and PLAP. In addition, living MDCK cells may be able to maintain detergent-resistant domains under conditions of severe cholesterol depletion by redistributing the remaining cholesterol.

As a result of these observations, cell homogenate instead of live cells was tested as a starting material for cholesterol depletion experiments, because all cell membranes should be equally accessible to cyclodextrin once the cells have been mechanically disrupted. In addition, cyclodextrin was combined with saponin or sphingomyelinase (SMase) treatment. Saponin complexes cholesterol and is thought to sequester it away from other interactions, whereas sphingomyelinase (SMase) converts sphingomyelin to ceramide, and might thus disturb the organisation of sphingomyelin-rich membranes.

MDCK-PLAP cells were left untreated, or treated with saponin or SMase. Cells were homogenised, and the homogenates were mock-treated or treated with 10 mM cyclodextrin for 30 minutes. Lipid analysis of TCMs prepared from these homogenates showed that SMase degraded approximately 30% of the sphingomyelin, while cyclodextrin depleted cholesterol by 50%. Saponin did not extract any lipid, as expected. In addition, flotation of the homogenates on Optiprep step gradients confirmed that none of the treatments alone, i.e. without subsequent Triton extraction, disrupted membrane association of gp114, PLAP, Yes, caveolin-1 or VIP17/MAL, except for cyclodextrin, which solubilised a minor portion of Yes (data not shown). Homogenates after saponin, SMase and/or cyclodextrin treatment were extracted with Triton, soluble and insoluble material were separated by flotation on Optiprep step gradients, and the distribution of gp114, PLAP, Yes, caveolin-1 and VIP17/MAL was analysed by immunoblotting (Figure 3.9.).

Cyclodextrin treatment of cell homogenate significantly reduced DRM association of PLAP, Yes, caveolin-1 and VIP17/MAL. Saponin had similar effects, confirming that the DRM association of various proteins depends on the availability of cholesterol. SMase treatment on its own did not reduce DRM association of the above proteins, but it augmented the effects of cyclodextrin, suggesting that resistance to Triton extraction is also disturbed by the conversion of sphingomyelin to ceramide. No synergy was observed between saponin and cyclodextrin, or between saponin and SMase (data not shown).

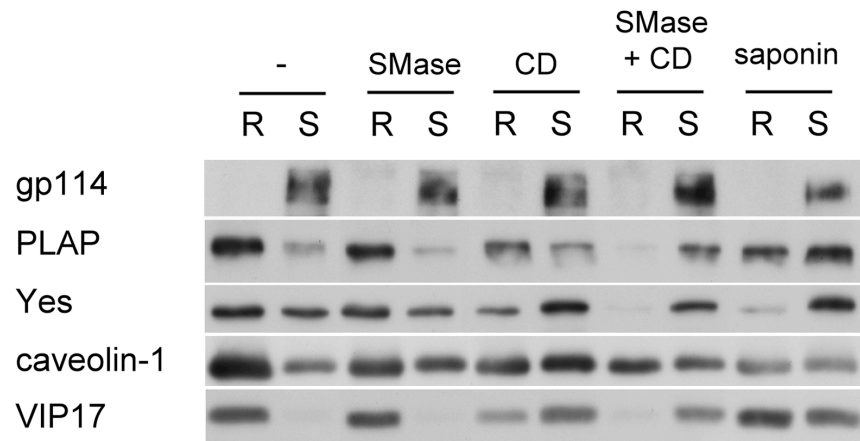


**Figure 3.9.** Manipulation of DRM association. MDCK cells were left untreated or treated with sphingomyelinase (SMase), methyl- $\beta$ -cyclodextrin (CD), saponin, or first SMase and then CD. After extraction with 1% Triton X-100 and flotation on Optiprep step gradients, two fractions containing the detergent-resistant (R = resistant) and detergent-soluble (S = soluble) material were collected and analysed by immunoblotting. Note that Triton on its own solubilised less than 50% of Yes, whereas in Figure 3.3. more than half of Yes was Triton-soluble. This can probably be explained by the fact that here the detergent-to-protein mass ratio was 5:1, but about 10:1 in the experiment shown in Figure 3.3.

### 3.4. Conclusions

The findings presented in this chapter demonstrate that DRMs prepared with a variety of mild detergents show considerable quantitative, as well as qualitative differences in their protein and lipid content. First, the amount of proteins and lipids recovered in the DRM fractions differed dramatically between detergents. Second, the detergents differentially solubilised a set of marker proteins. Third, the detergents differed in their ability to enrich cholesterol and sphingolipids over glycerophospholipids, and saturated over unsaturated phosphatidylcholine. Hence, the DRM selectivities of the detergents, as defined by their ability to enrich a subset of membrane proteins, cholesterol, sphingolipids, and saturated phosphatidylcholine, varied widely. These observations make it unlikely that the biophysical basis for how biological membranes resist different detergents is the same.

In addition, significant cell type-dependent variations in the composition of DRMs and in the DRM selectivities of some detergents were observed. In MDCK cells, the approximate

order of DRM selectivity was CHAPS  $\approx$  Triton  $>$  Brij 98  $\approx$  Brij 96  $>$  Lubrol  $\approx$  Brij 58  $>$  Tween. In Jurkat cells, it was CHAPS  $\approx$  Triton  $>$  Brij 98  $\approx$  Brij 58  $>$  Lubrol  $\approx$  Brij 96  $>$  Tween. This argues that results obtained with a particular detergent can not be easily transferred from one cell type to another.

Finally, the results show that cyclodextrin and saponin can be useful tools to test whether the DRM association of a proteins depend on cholesterol. Effective cyclodextrin treatment may, however, sometimes require cell disruption before cholesterol depletion. The effects of SMase treatment are probably more complicated, as discussed in chapter 6.

## 4. Retrovirus-mediated RNA interference in epithelial cells

RNA interference (RNAi), a naturally occurring mechanism of eukaryotic gene regulation, can be utilised as an experimental tool to inhibit the expression of genes by specific mRNA ablation (Dykxhoorn et al., 2003). This is achieved by introducing small interfering RNAs (siRNAs) into cells, most commonly by transient transfection of chemically synthesised siRNAs (Elbashir et al., 2001). Alternatively, cells can be transfected with expression plasmids that lead to the production of short hairpin RNAs (shRNAs) (Paddison et al., 2002; Brummelkamp et al., 2002). These shRNAs are then processed into siRNAs by the cellular RNAi machinery. The applicability of RNAi MDCK cells is limited by the poor transfectability of these cells. Therefore, a retroviral system was chosen for the delivery of shRNA expression plasmids into MDCK cells. The initial goal was to generate so called “knockdown“ cells for all genes putatively involved in apical sorting.

### 4.1. Generation of knockdown cells by retrovirus-mediated RNAi

A retroviral vector was constructed that allows stable co-expression of an shRNA and a selectable marker in MDCK cells. This vector, called RVH1-puro, was based on the previously described RVH1 (Barton and Medzhitov, 2002). It harbours the H1 promoter, which drives the expression of shRNAs, and a puromycin resistance gene controlled by the CMV promoter.

The set of target mRNAs consisted of 13 transcripts. Between one and six so called target sequences were selected per transcript, giving rise to a total of 37 target sequences (see Appendix 2). Corresponding shRNAs were designed as described (Brummelkamp et al., 2001; see also Figure 7.2.), and introduced into RVH1-puro. Retroviruses pseudotyped with the vesicular stomatitis virus envelope glycoprotein for enhanced virus stability and efficient infection of MDCK cells were produced, and typically yielded transduction rates of about 70%. Following puromycin selection to eliminate non-transduced cells, the RNAi-mediated depletion of target mRNAs was measured by quantitative RT-PCR. With the best target sequence for each gene, mRNA reductions in the range of 70-95% were

achieved (Table 4.1.). These results were highly reproducible as indicated by the standard deviations calculated from at least three independent experiments in each case.

Target gene	mRNA reduction
rab11b	96 ± 1 %
rab8a	93 ± 4 %
VIP17	92 ± 2 %
annexin 13	91 ± 2 %
caveolin-1	90 ± 3 %
TI-VAMP	90 ± 4 %
MAL2	88 ± 3 %
annexin 2	81 ± 4 %
VIP36	81 ± 5 %
rab11a	77 ± 6 %
annexin 13b	74 ± 4 %
KIFC3	73 ± 4 %
syntaxin-3	71 ± 2 %

**Table 4.1.** RNAi-mediated reduction of target gene mRNA levels. Target gene mRNA levels were determined by quantitative RT-PCR. Levels in knockdown cells are given as percent mRNA reduction relative to the levels in control cells transduced with empty RVH1-puro. Standard deviations are from at least three independent experiments in each case. Note that annexin 13a cannot be targeted individually as annexin 13b comprises the entire annexin 13a sequence. The annexin 13 knockdown therefore affects both isoforms.

Immunoblotting showed that the reduced mRNA levels of caveolin-1, VIP17, annexin 13, TI-VAMP, and annexin 2 corresponded to strong and specific reductions of the target protein levels, while the empty RVH1-puro had no effect (Figure 4.1.). Specific reductions were also observed in VIP36, annexin 13b, as well as syntaxin-3 knockdown cells (data not shown, see also Figure 4.2.). For lack of antibodies it was not possible to analyse the protein levels of MAL2 and KIFC3, whereas in the case of rab8a/b and rab11a/b the available antibodies recognised both isoforms. However, it is likely that the mRNA depletion translated into a corresponding reduction of the protein levels also for these genes.

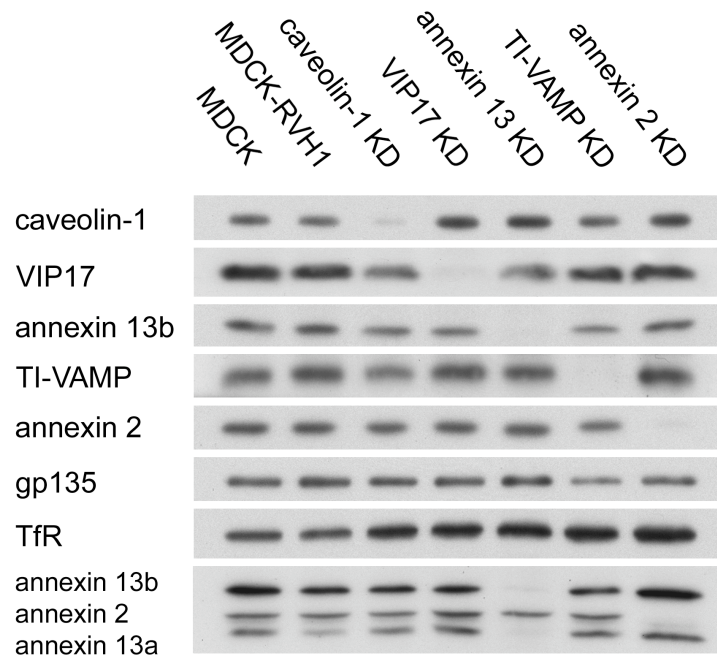


**Figure 4.1.** RNAi-mediated reduction of target gene protein levels. Equal amounts of protein from MDCK cells, MDCK cells transduced with empty RVH1-puro (MDCK-RVH1) and knockdown (KD) cells were analysed by immunoblotting. gp135 and transferrin receptor (TfR) were used as controls. Note that the annexin 13-2 antibody recognises annexin 13a, annexin 13b and annexin 2 (bottom panel), and that both annexin 13a and b are depleted in annexin 13 knockdown cells.

To assess how well mRNA and protein depletion correlated, the reduced protein levels of caveolin-1, TI-VAMP, annexin 2, annexin 13b and syntaxin-3 in more detail by immunoblotting using serial dilutions. Lysate from control cells was diluted five- or ten-fold and compared to lysates from knockdown cells, thus obtaining a rough estimate for target protein depletion (Figure 4.2.). The protein levels of the target genes were depleted at least as strongly as their mRNA levels, except for caveolin-1, where the protein was reduced by about 80% compared to an mRNA reduction of 90%. In the case of caveolin-1, which forms the characteristic striated coat on the cytoplasmic surface of caveolae, this could result from a very stable pool of the protein.



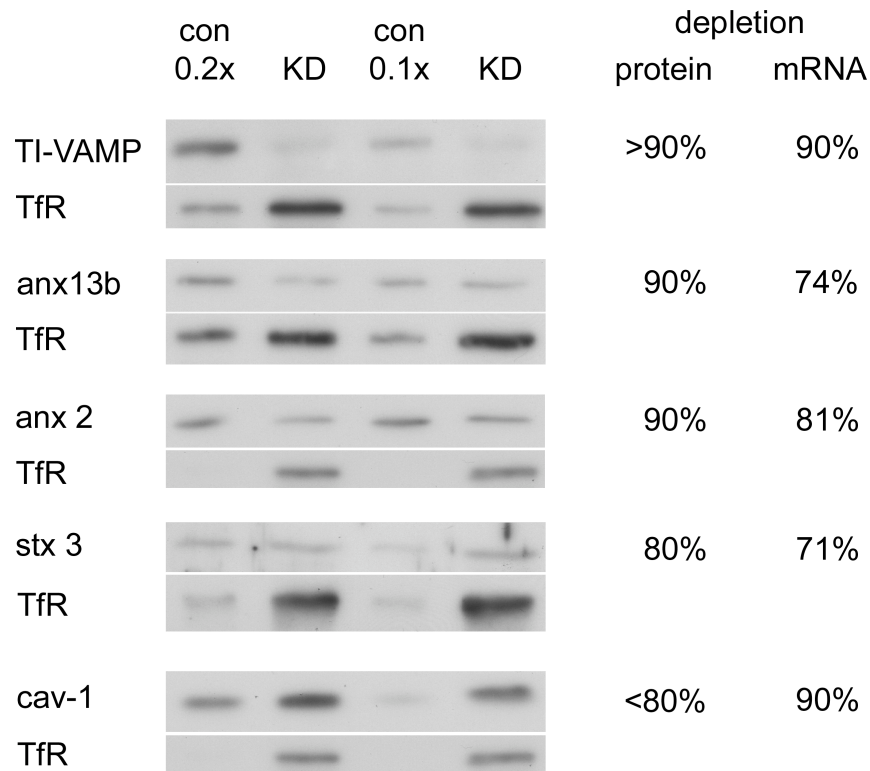


**Figure 4.2.** Quantification of RNAi-mediated reduction of target gene protein levels in TI-VAMP, annexin 13b, annexin 2, syntaxin 3 and caveolin-1 knockdown cells. Protein from knockdown cells (KD) and five times or ten times lower amounts of protein from control cells transduced with empty RVH1-puro (con 0.2x and con 0.1x) were analysed by immunoblotting. Transferrin receptor (TfR) was used as loading control. The approximate percent depletion of target gene protein levels are shown on the right, together with the depletion of target gene mRNA levels (taken from Table 4.1.).

Raising the retrovirus titer might improve depletion of a target mRNA, because increasing the number of integration events leads to stronger shRNA expression and, subsequently, to higher intracellular siRNA concentrations. To test to what extent target mRNA depletion can be augmented in this way, different viruses with knockdown efficiencies ranging from 55-95% (see Appendix 2) were concentrated by pelleting. No significant loss of infectivity was caused by the pelleting procedure alone, as virus resuspended in the original volume performed as well as untreated virus (data not shown). Substantially improved knockdowns could be obtained with concentrated virus (Figure 4.3.).

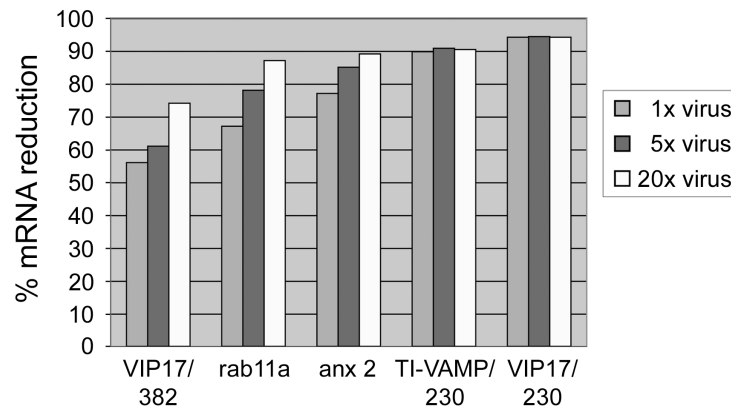


**Figure 4.3.** Improvement of knockdowns by increasing virus titers. Five viruses expressing different shRNAs (VIP17/382, rab11a, anx2, TI-VAMP/230, and VIP17/230; anx 2 = annexin 2) were pelleted by centrifugation and resuspended in 1x, 0.2x, or 0.05x the original volume, resulting in 1x, 5x, or 20x the original virus concentration. Percent mRNA reductions relative to the levels in control cells transduced with empty RVH1-puro were measured as in Table 4.1.

This enhancement was most pronounced for viruses achieving weak or intermediate knockdowns, whereas higher titers did not improve the knockdown in the case of viruses that yielded mRNA reductions of >90% already without concentrating. This indicates that removal of the remaining mRNA is prevented by factors other than insufficient levels of shRNA expression. Nevertheless, these results show that increasing the virus titer can often be used to improve knockdowns.

#### 4.2. Properties of functional small interfering RNAs

The above data indicate that the retroviral RNAi system is able to strongly and specifically inhibit gene expression. However, to date no well-defined rules have been published for the selection of efficient target sequences, making this step an obstacle to routine application of RNAi in mammalian cells. The set of 37 target sequences is relatively small, making it difficult to derive selection guidelines from it. Yet, the data set can be used to test previous suggestions for the selection of target sequences, such as the proposal that the free energy profiles of siRNAs are predictive of their efficiencies (Khvorova et al., 2003). Therefore, the siRNA duplexes that presumably arise from Dicer-mediated processing of the expressed shRNAs were subjected to the same kind of analysis carried

out by Khvorova and co-workers (see Figure 4.5. for a schematic representation of shRNA processing). siRNAs were grouped in two categories, functional siRNAs (>70% mRNA reduction, n = 21) and non-functional siRNAs (<70% reduction, n = 16). The average energy profiles of functional and non-functional siRNAs were calculated starting from the 5' antisense end of the duplexes. Figure 4.4. shows that non-functional siRNAs have a more stable 5' antisense end than functional siRNAs. In addition, non-functional siRNAs are more stable in the central region between position 10 and 13. These results are consistent with earlier findings (Khvorova et al., 2003; Aza-Blanc et al., 2003).

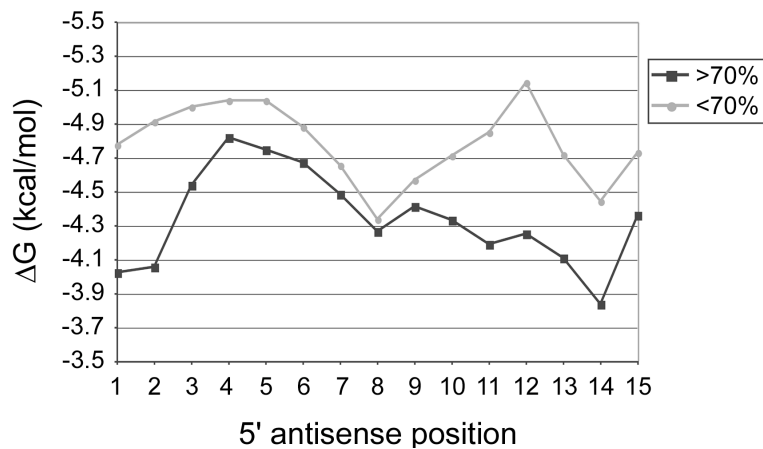


**Figure 4.4.** Internal energy profiles of functional versus non-functional siRNAs. Pentamer hybridisation energies were calculated along the length of the siRNA duplexes starting from the 5' end of the antisense strands. The average pentamer hybridisation energies ( $\Delta G$ ) for the first 15 positions of functional siRNAs (>70% mRNA reduction) and non-functional siRNAs (<70% mRNA reduction) are shown.

Next, the relative stabilities of the two ends of siRNA duplexes were compared. In the case of non-functional siRNAs, the two ends were of nearly equal duplex stability ( $\Delta G = 0.17$  kcal/mol). Functional siRNAs on the other hand had less stable 5' antisense ends ( $\Delta G = 0.7$  kcal/mol). This is in agreement with the idea that a less stable 5' antisense end leads to preferential incorporation of the antisense strand into the RNA-induced silencing complex (RISC) and hence to efficient mRNA degradation (Khvorova et al., 2003; Schwarz et al., 2003).

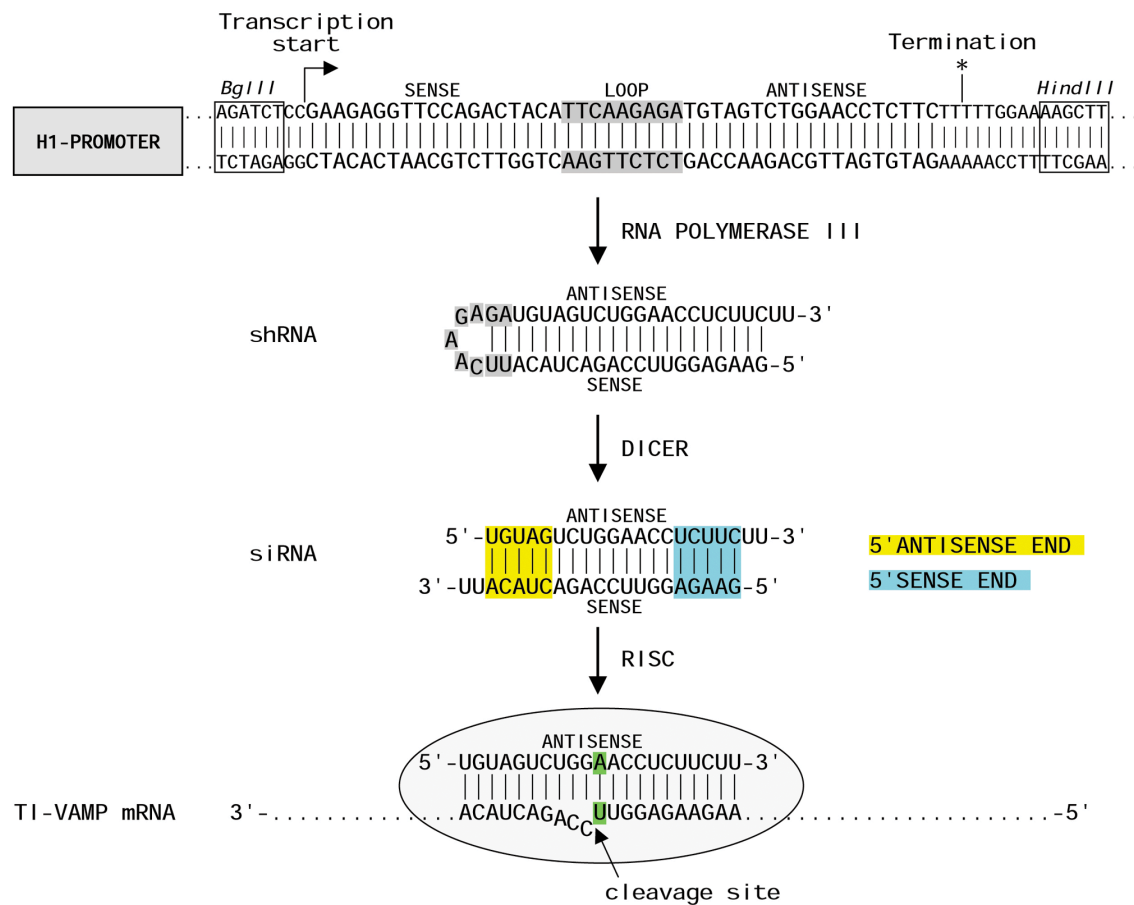


**Figure 4.5.** Expression of shRNAs, processing into siRNAs, and mRNA cleavage. shRNAs consist of the target sequence in sense orientation, a short loop, and the target sequence in antisense orientation. Expression of shRNAs (TI-VAMP/230 in this example) is driven by the H1 promoter, which is an RNA polymerase III promoter. It has a well-defined start of transcription (arrow) and a termination signal consisting of five consecutive thymidines. Transcription is terminated after the second thymidine (asterisk). Complementary regions within the transcript fold the molecule back onto itself thereby forming a hairpin structure. The resulting shRNA serves as a substrate for Dicer and is processed into an siRNA. One of the siRNA strands becomes incorporated into the RNA-induced silencing complex (RISC), while the other strand is degraded. The stabilities of the 5' antisense end (yellow) and the 5' sense end (blue) of an siRNA influence the strand selection, so that the strand with the less stable 5' end preferentially enters the mRNA degradation pathway. Only RISCs containing the antisense strand are functional in target mRNA ablation. The RISC cleaves target mRNAs between the nucleotides complementary to nucleotide 10 and 11 downstream of the 5' end of the antisense strand. An adenosine at position 11 (green) of the antisense strand favours efficient cleavage.

Finally, the frequency with which each of the four nucleotides occurred at each position of functional and non-functional siRNAs was analysed. Adenosine was clearly over-represented at position 11 of the antisense strand of functional siRNAs, as it occurred in 52% of the functional compared to 31% of the non-functional siRNAs. Strikingly, all seven siRNAs that achieved mRNA reductions of 90% or more had an adenosine at position 11 of the antisense strand. As mRNA cleavage invariably takes place between the nucleotides complementary to position 10 and 11 of the antisense strand (Elbashir et al., 2001), it appears that the RISC preferentially cleaves mRNA 3' of a uridine (see Figure 4.5. for a schematic representation of shRNA processing and mRNA cleavage). The fact that these trends manifest themselves so clearly even in this small data set indicates that the efficiency of siRNAs strongly depends on the characteristic features of functional siRNAs described above.

### 4.3. Composition and stability of knockdown cell populations

Both mRNA and protein levels provide a measure for the average knockdown, but they do not indicate how the residual protein is distributed in a population of knockdown cells. Therefore, the distribution of the residual caveolin-1 protein in knockdown cells was examined using immunofluorescence (Figure 4.6.).

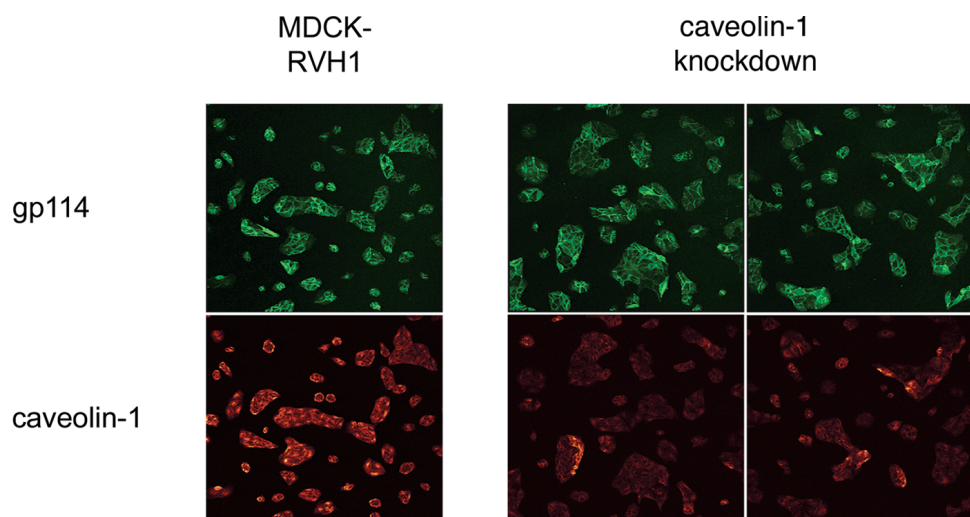


**Figure 4.6.** Distribution of residual protein in a knockdown cell population. Caveolin-1 and the plasma membrane protein gp114 were visualised by immunofluorescence in caveolin-1 knockdown cells and control cells transduced with empty RVH1-puro (MDCK-RVH1). Magnification was 20x. Identical settings were used for control and knockdown cells.

There was a strong overall reduction in the caveolin-1 signal in knockdown cells compared to control cells, while the expression of the plasma membrane protein gp114 was unaffected. However, the expression of caveolin-1 in knockdown cells was quite heterogeneous and occasionally as strong as in control cells. Using a virus directed against caveolin-1 in which the puromycin resistance gene was replaced by GFP showed that the correlation between the extent of caveolin-1 depletion and GFP expression is not strict (Figure 4.7.).

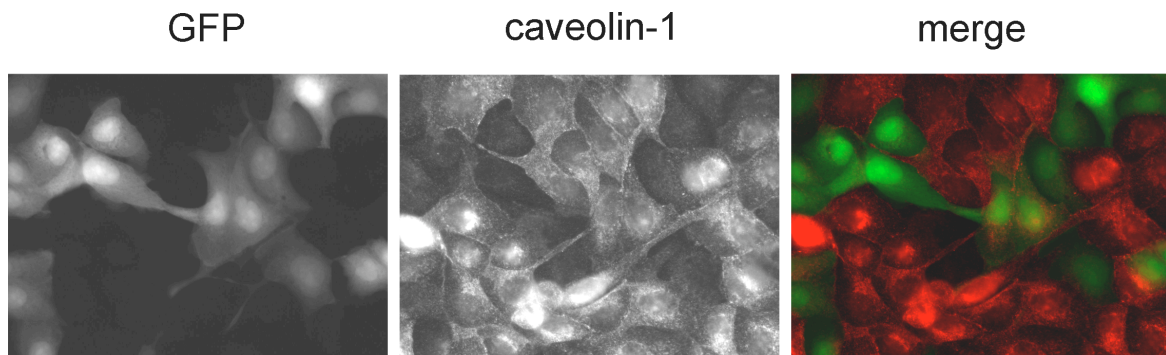


**Figure 4.7.** Correlation between knockdown efficiency and marker expression. MDCK cells transduced with RVH1-GFP/cav-1, which targets the caveolin-1 mRNA and encodes cytoplasmic GFP, were analysed by caveolin-1 immunofluorescence (middle panel). Transduced cells can be identified by GFP expression (left panel). Magnification was 100x. Note that GFP expression and depletion of caveolin-1 correlate incompletely, as obvious from a pair of cells in the centre of the image, which are GFP-positive, but retain nearly wild-type levels of caveolin-1.

This finding indicates that the activities of the H1 and the CMV promoter of RVH1-puro, which drive expression of the shRNAs and the puromycin resistance gene, are not linked very tightly, despite their immediate neighbourhood. This lack of tight coupling would explain why a small number of puromycin-resistant cells retain substantial expression of the targeted protein. In addition, mutations in the shRNA expression cassette, which might occur during reverse transcription of the retroviral genome by the error-prone viral reverse transcriptase, could contribute to this phenomenon.

If RNAi-mediated depletion of a protein caused a growth disadvantage, cells with low levels of that protein would gradually be eliminated from a heterogeneous cell population, thus limiting the time during which experiments can be performed. To test the stability of

knockdowns within populations of retrovirus-transduced cells, time-course experiments were performed. The mRNA levels of VIP17, caveolin-1, rab11a and VIP36 were followed in continuously dividing knockdown cell populations for over three weeks after infection (Figure 4.8.).

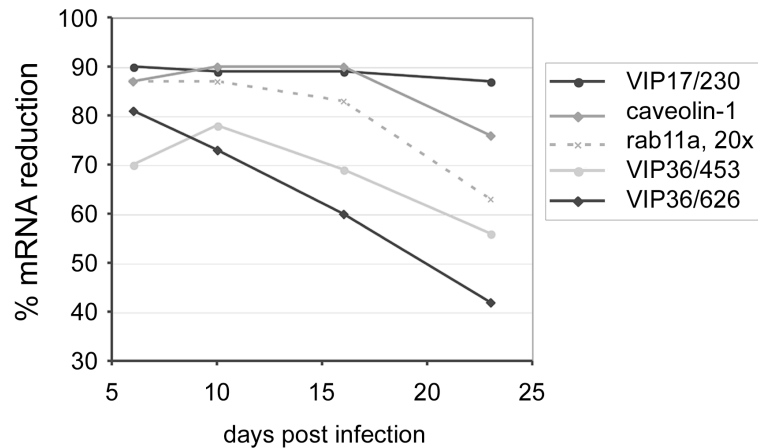


**Figure 4.8.** Stability of target gene mRNA reductions in knockdown cell populations. MDCK cells were transduced with different viruses (VIP17/230, caveolin-1, rab11a, VIP36/453, and VIP36/626). Target gene mRNA levels were monitored between day 6 and day 23 post infection. Percent mRNA reductions relative to the levels in control cells transduced with empty RVH1-puro were measured as in Table 4.1. Note that the rab11a virus was concentrated twenty-fold prior to infection.

In all cases the mRNA reduction decayed over time. Reselecting with puromycin did not restore the knockdowns (data not shown), ruling out that this decline is due to cells that have lost or inactivated the integrated retroviral construct. These results demonstrate that the knockdowns are not stable within a population of transduced cells. Instead, they slowly decay over time in a manner that may correlate with the severity of the growth disadvantage caused by the knockdown. However, no major changes occurred within the first ten days after the end of the initial selection, especially in the case of very strong knockdowns.

#### 4.4. Generation of double knockdowns

To make simultaneous depletion of two proteins possible, a second retroviral vector was created, RVH1-hygro, which confers hygromycin instead of puromycin resistance. Viruses produced with this vector achieved the same knockdown efficiencies as RVH1-puro viruses, as verified for rab11a, VIP17 and VIP36 (data not shown). Next, a procedure for sequential transduction of MDCK cells with an RVH1-puro and an RVH1-hygro virus was established. In this way the expression of two different proteins can be reduced to levels identical to those observed in the single knockdowns, as exemplified by the VIP17/annexin 13 and the rab11a/rab11b double knockdown (Figure 4.9).

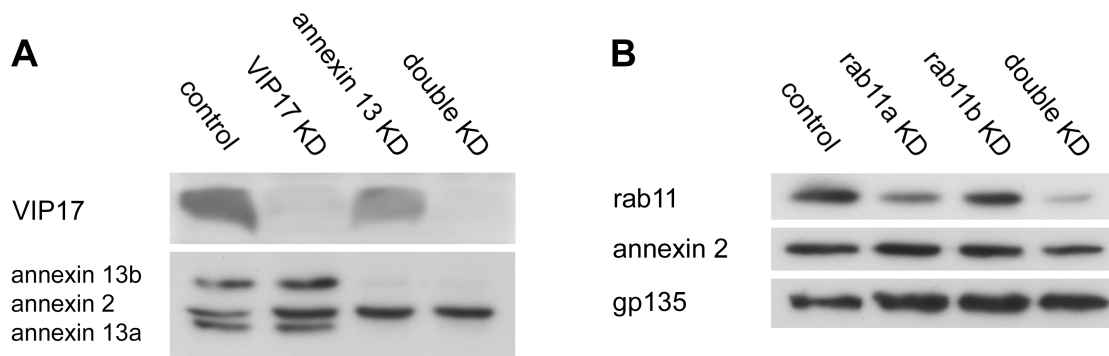


**Figure 4.9.** RNAi-mediated reduction of target gene protein levels in single and double knockdown cells. Equal amounts of protein from MDCK cells transduced with empty RVH1-puro as well as empty RVH1-hygro (control), single and double knockdown (KD) cells were analysed by immunoblotting. Annexin 2 was used as control for the VIP17/annexin 13 knockdown (A), and annexin 2 as well as gp135 were used as controls for the rab11a/rab11b knockdown (B). Note that rab11a appears to be the major rab11 isoform in MDCK cells.

To investigate whether single and double knockdowns generated with the retroviral RNAi system could be useful for the study of membrane trafficking, the endocytosis of transferrin in cells with reduced levels of rab11a and rab11b was tested. First, control and rab11a/b double knockdown cells were labelled with Alexa-transferrin and analysed by fluorescence microscopy using identical settings in both cases. Figure 4.10. shows several particularly striking examples for a reduced transferrin uptake by rab11a/b-depleted cells.



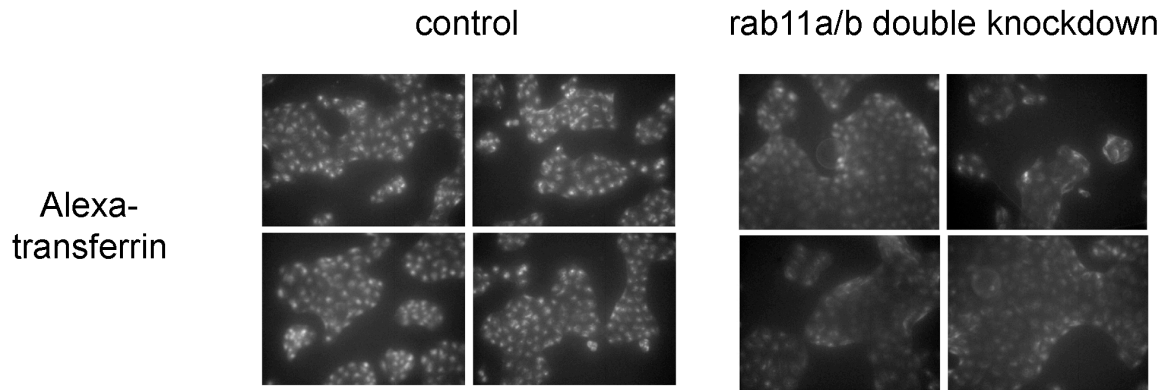


**Figure 4.10.** Transferrin uptake in control and rab11a/b double knockdown cells. Cells transduced with empty RVH1-puro as well as empty RVH1-hygro (control) and rab11a/b double knockdown cells were grown on coverslips, allowed to endocytose Alexa-transferrin at 37°C for 10 min, fixed, and analysed by fluorescence microscopy. Magnification was 20x. Identical settings were used for control and knockdown cells.

An attempt was made to obtain a rough estimate for the RNAi-induced reduction in transferrin uptake. For this, fluorescence images were acquired from cells labelled with Alexa-transferrin in such a way that peripheral regions of cell islands were excluded, as they showed a much higher transferrin uptake than central regions (see Figure 4.10.). Identical settings were applied to control, single and double knockdown cells, and the total fluorescence of these images was quantified (Figure 4.11.).

Depleting the levels of rab11a or rab11b individually reduced transferrin uptake by approximately 15% and 10%, respectively. These effects were additive, as simultaneously knocking down rab11a and rab11b yielded a reduction of about 25%, indicating at least partially overlapping functions of the two rab11 isoforms. Even though this microscopy-based assay does not measure endocytosis very accurately, the results show that inhibiting rab11 expression leads to a reduced transferrin uptake in MDCK cells. This finding could be due to a defect in the recycling of endocytosed transferrin receptor, in line with the role of rab11 in the regulation of trafficking through recycling endosomes (Ullrich et al., 1996; Ren et al., 1998).

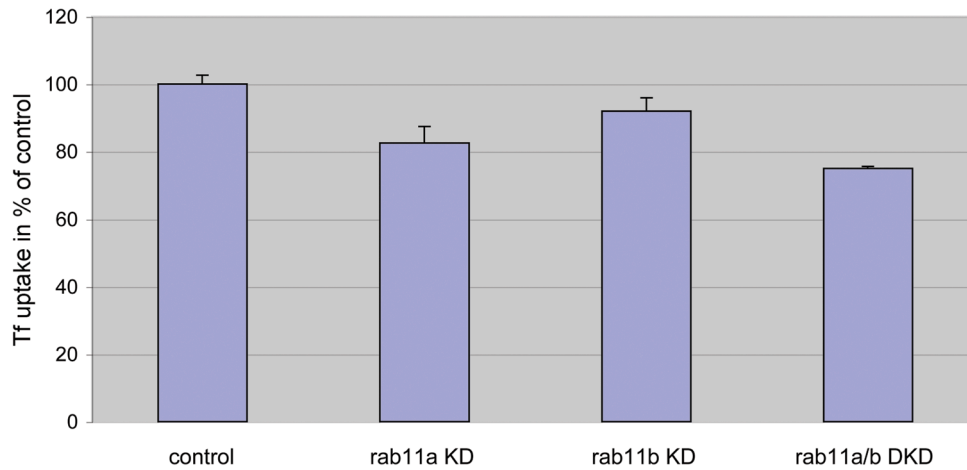


**Figure 4.11.** Quantification of transferrin uptake in control, rab11a, rab11b and rab11a/b knockdown cells. Uptake experiments were performed as in Figure 4.10. Fluorescence images were acquired with a magnification of 40x, excluding cells at the periphery of cell islands and applying identical microscope settings for all images. The average fluorescence from triplicate coverslips was determined for each condition, and expressed as % of control. KD = knockdown, DKD = double knockdown.

#### 4.5. Conclusions

In this chapter, an RNAi system that combines retroviral transduction with selectable markers to generate single and double knockdowns in mammalian cells was established. Knockdowns were generated for 13 genes proposed to play a role in apical membrane transport in MDCK cells. Previously suggested guidelines for the selection of target sequences were confirmed, and it was found that incorporating an adenosine in position 11 of the antisense strand of siRNAs appears to favour efficient target mRNA cleavage. In addition, the characterisation of the retrovirus-transduced knockdown cell populations with regard to composition and stability indicated that there is a time window of about 10-15 days during which target protein depletion is maximal (see chapter 6 for further discussion).

This system was employed because MDCK cells are difficult to transfect. However, the principal advantages of the retroviral system, namely the virtually unlimited host range, the high transduction rates, the speed and ease with which a population of knockdown

cells can be generated, and the sustained expression of shRNAs should make retroviruses a generally applicable and convenient tool for gene silencing.

Using transferrin uptake in rab11-depleted MDCK cells as a test case, it was shown that the retroviral RNAi system has the capacity to produce phenotypes related to membrane trafficking events. Therefore, the knockdown cells generated by retrovirus-mediated RNAi may allow a functional analysis of genes putatively involved in transport to the apical membrane of MDCK cells.

## 5. Functional analysis of putative apical sorters

The goal of this chapter was to find an assay suitable for screening the knockdowns described in the previous chapter for possible defects in apical sorting. Different kinds of assays are employed to study biosynthetic transport to the plasma membrane. In many cases, so called marker proteins are introduced into cells with the help of viruses, who allow these proteins to be expressed at high levels and thus make their detection relatively straightforward. The trafficking of virally expressed marker proteins is then monitored by biochemical means or by microscopy.

### 5.1. Biochemical analysis of influenza virus hemagglutinin transport

A commonly used marker protein for apical transport is the influenza virus hemagglutinin (HA), whose appearance on the cell surface of polarised MDCK cells can be followed by the well-established HA transport assay (Matlin and Simons, 1984). This assay relies on the expression of a furin-resistant HA variant, which reaches the plasma membrane without undergoing proteolytic processing. HA that has arrived at the cell surface can be cleaved by trypsin and thus be distinguished from intracellular HA (see section 7.5.3. for details). The first knockdown to be analysed by this assay was that of VIP17/MAL (referred to as VIP17), since the role of VIP17 in apical transport is well documented (Puertollano et al., 1999; Cheong et al., 1999; Martin-Belmonte et al., 2000).

MDCK cells were transduced with empty RVH1-puro virus or retrovirus directed against VIP17, selected with puromycin, and grown on permeable filter supports for three days. Control as well as knockdown cells underwent normal epithelial polarisation, as judged by the polarised distribution of the plasma membrane proteins gp135, gp114 and E-cadherin (data not shown). Cells were infected with influenza virus encoding furin-resistant HA, host protein shut-off was allowed to occur, and newly synthesised viral proteins were pulse-labelled with <sup>35</sup>S-methionine. Proteins were either immediately chased to the plasma membrane, or first accumulated in the TGN by incubation at 19.5°C and then released. At the end of the chase, HA at the apical membrane was cleaved by trypsin, cell lysates were

separated by SDS-PAGE, and radioactive viral proteins were revealed by autoradiography (Figure 5.1.).

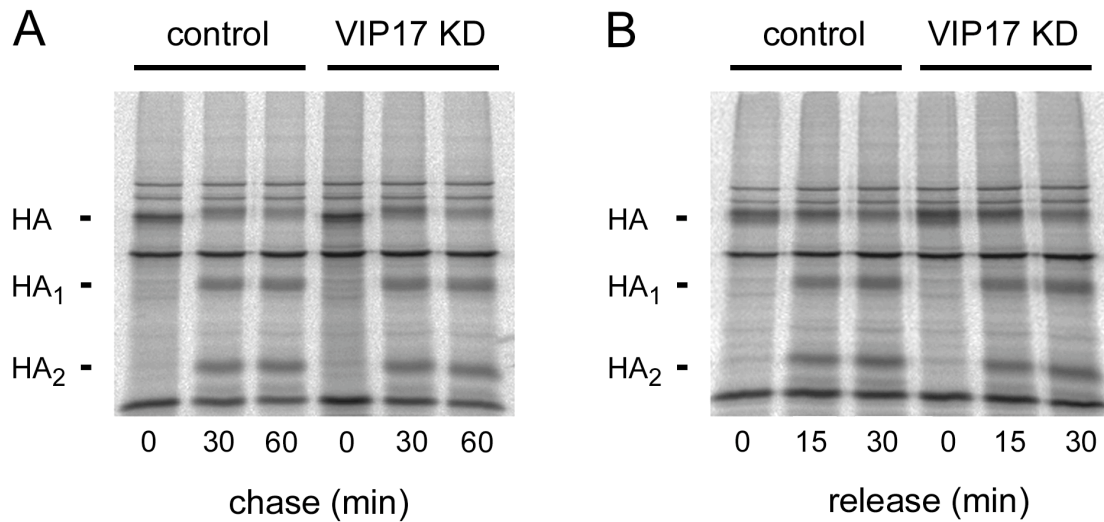


**Figure 5.1.** Influenza virus hemagglutinin transport assay in control and VIP17 knockdown cells. Filter-grown control cells transduced with empty RVH1-puro and VIP17 knockdown cells were infected with influenza virus for 1 h. After a 4 h incubation at 37°C to allow host protein synthesis shut-off, newly synthesised viral proteins were pulse-labelled with <sup>35</sup>S-methionine for 8 min. Proteins were either immediately chased to the cell surface at 37°C for 0, 30, or 60 min (A), or first accumulated in the TGN by incubation at 19.5°C and then released to the cell surface at 37°C for 0, 15 or 30 min (B). Hemagglutinin that had reached the apical membrane was cleaved by trypsin treatment from the apical side, cell lysates were prepared and separated by SDS-PAGE, and radioactive proteins were revealed by autoradiography. The positions of uncleaved HA, and the two cleavage products, HA<sub>1</sub> and HA<sub>2</sub>, are indicated.

When HA was chased to the cell surface directly after pulse labelling, a slight shift of full-length HA towards higher molecular weight occurred (Figure 5.1. A). This shift is consistent with the known N-glycosylation of HA in the Golgi complex (Matlin and Simons, 1984). In contrast, when HA was first accumulated in the TGN, the low molecular weight form of HA was absent (Figure 5.1. B), indicating that the labelled HA had reached the TGN and become fully glycosylated during the incubation at 19.5°C. Hence, the assay can be used to measure apical HA transport from the endoplasmic reticulum (ER) or from the TGN (Figure 5.1. A and B, respectively).

The apical transport index, expressed as % apically transported HA, was calculated for each time point (Figure 5.2.). HA was transported to the apical surface of control and VIP17 knockdown cells with equal efficiency, regardless of whether or not HA had been accumulated in the TGN.

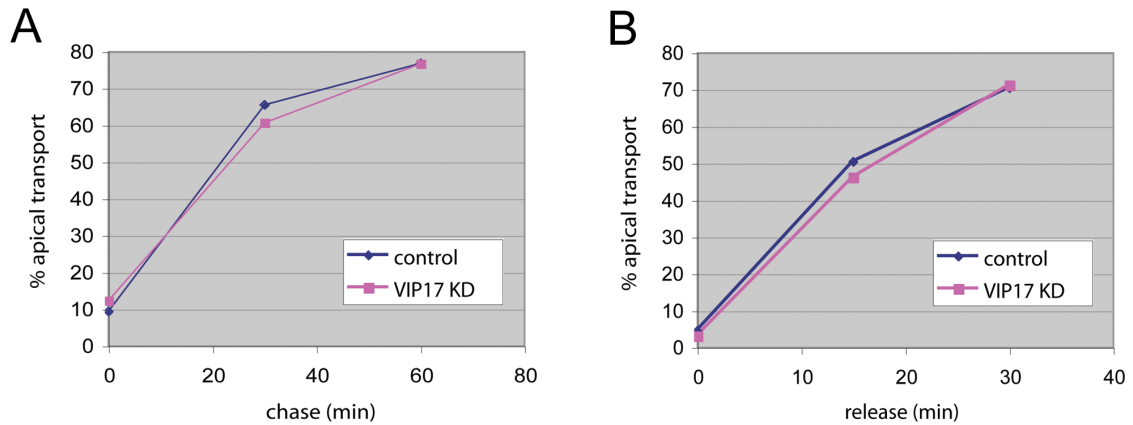


**Figure 5.2.** Influenza virus hemagglutinin transport assay in control and VIP17 knockdown cells. The band intensities of HA, HA<sub>1</sub> and HA<sub>2</sub> from the gels shown in Figure 5.1. were quantified. The apical transport index in % apical transport was calculated by dividing the band intensities of apically cleaved hemagglutinin (HA<sub>1</sub> + HA<sub>2</sub>) by the total hemagglutinin intensity (HA + HA<sub>1</sub> + HA<sub>2</sub>). The results were multiplied by 100 to obtain per cent values.

The depletion of VIP17 in knockdown cells was confirmed by immunoblotting (Figure 5.3.). Hence, reducing VIP17 to virtually undetectable levels inhibited neither ER-to-apical membrane nor TGN-to-apical membrane transport of HA.

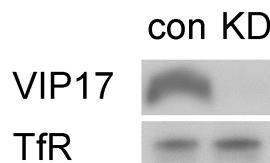


**Figure 5.3.** Confirmation of the VIP17 knockdown. Equal aliquots of the cell lysates obtained during the HA transport assay shown in Figure 5.1. from control and VIP17 knockdown cells (KD) were separated by SDS-PAGE. The VIP17 knockdown was assessed by immunoblotting, transferrin receptor was used as loading control.

Next, HA transport was measured in annexin 2, annexin 13, TI-VAMP, syntaxin-3 and KIFC3 knockdown cells. Transport efficiencies in control and knockdown cells were indistinguishable in all cases. As a positive control, the assay was performed in the presence of nocodazole, which is known to inhibit apical transport (Lafont et al., 1994). As expected, HA transport was strongly reduced (data not shown).

One reason for why RNAi did not affect HA transport could be the presence of residual target protein. This is plausible for syntaxin-3 and KIFC3, whose mRNAs were depleted by less than 80% (see Table 4.1.). However, this concern seems less relevant for annexin 2, annexin 13, TI-VAMP and VIP17, whose protein levels were reduced by at least 90% (see Figure 4.1. and 4.2.). Alternatively, the apical transport machinery may be redundant, or in some other way able to compensate the depletion of one of its components.

To address this possibility, HA transport was analysed in VIP17/annexin 13 and VIP17/MAL2 double knockdown cells. The VIP17/annexin 13 pair was chosen because the role of annexin 13 in surface transport in MDCK cells is reasonably well established (Lafont et al., 1998; Lecat et al., 2000). The rationale for the VIP17/MAL2 pair was that MAL2, which mediates transcytotic apical delivery in hepatocytes (de Marco et al., 2002), might functionally replace the closely related VIP17. However, neither double knockdown inhibited HA transport to the apical or basolateral membrane (Figure 5.4.).

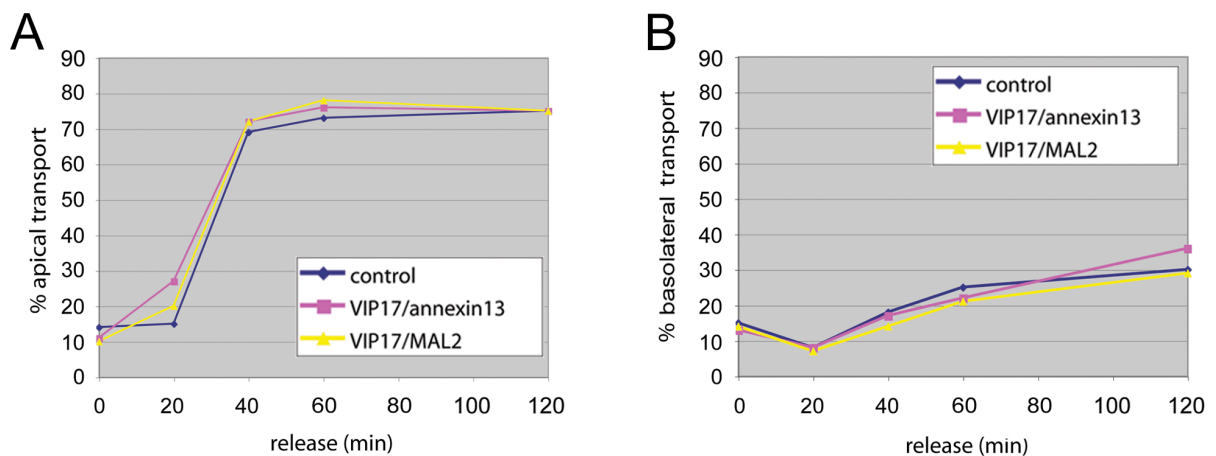


**Figure 5.4.** Influenza virus hemagglutinin transport assay in control cells, VIP17/anx13 and VIP17/MAL2 double knockdown cells. The hemagglutinin transport assay was carried out as in Figure 5.1 B. At the end of the chase, cells were subjected to apical or basolateral trypsinisation. Apical (**A**) and basolateral (**B**) transport efficiencies were determined as described in Figure 5.2.

These observations conflict with several previous studies (Puertollano et al., 1999; Lafont et al., 1998; Lafont et al., 1999), which reported delays of HA transport when the functions of VIP17, annexin 13 or TI-VAMP were impaired by different means. Most importantly, evidence for a role of VIP17 in HA transport has previously been obtained by an RNAi-like knockdown strategy using an experimental set-up similar to the one in Figure 5.1. A (Puertollano et al., 1999). However, a notable difference to the experiments described above was that HA transport was assayed two days after electroporating MDCK cells with VIP17 antisense RNA oligonucleotides, whereas here HA transport was analysed at least six days after retroviral infection. It therefore appears possible that prolonged depletion of VIP17 by retrovirus-mediated RNAi induced compensatory mechanisms that enabled knockdown cells to carry out HA transport with wild type efficiency.

To test whether such a scenario might apply, the kinetics of VIP17 depletion after retroviral infection were determined. MDCK cells were infected with empty RVH1-puro virus or retrovirus directed against VIP17, and selected with puromycin 32 h later. Samples from control and knockdown cells were taken 0, 32, 48, 60, 72, and 96 h post infection, and VIP17 mRNA and protein levels were analysed (Figure 5.5.).

32 h after infection, when the knockdown cell population still contained at least 30% non-transduced cells, VIP17 mRNA levels had already dropped to 50%. The maximal mRNA depletion of 90% was reached 60 h post infection (Figure 5.5. A). The decline of VIP17 protein levels was only slightly delayed and minimal levels were reached about 72 h post infection, indicating that the half-life of VIP17 is short. (Figure 5.5. B). Hence, when the HA transport assay is performed six days after retroviral infection, knockdown cells are exposed to severe VIP17 depletion for at least three days.



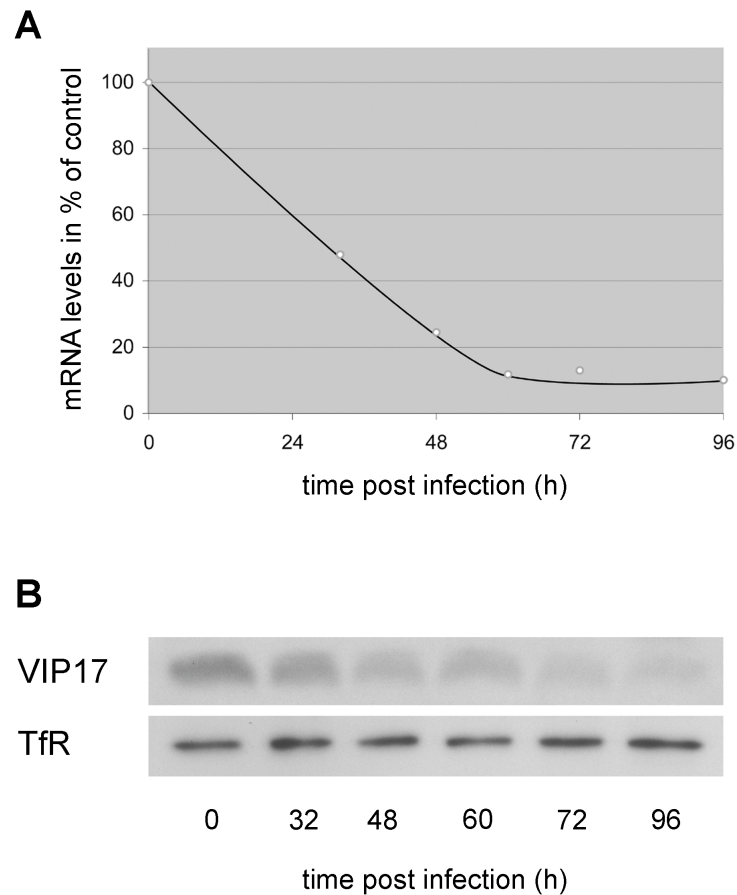


**Figure 5.5.** Kinetics of the VIP17 mRNA and protein depletion following retroviral transduction. MDCK cells were transduced with empty RVH1-puro or with RVH1-puro/VIP17. 32 h post infection, cells were split into puromycin to eliminate non-transduced cells. Aliquots of control and VIP17 knockdown cells were taken at the indicated time points, and analysed for the presence of VIP17 mRNA and protein by quantitative RT-PCR and immunoblotting, respectively. In **(A)** VIP17 mRNA levels are shown in % of control cells. In **(B)**, the VIP17 protein levels in knockdown cells are shown. The VIP17 protein levels in control cells were virtually identical at all time points.

In summary, the results obtained with the biochemical HA transport assay show that several proteins proposed to play a role in apical sorting can be strongly depleted without obvious defects in apical trafficking. This finding shows that a number of putative apical sorters, most notably VIP17, are not required for virally expressed HA to reach the apical membrane. A possible explanation is that cells may be able to adapt to the depletion of proteins like VIP17 within a few days, so that transport defects go undetected under the experimental regime used here.

## 5.2. A visual assay for surface transport

As a consequence of these results, a new RNAi-based assay for protein transport to the cell surface was designed which minimised the time between the retroviral infection and the analysis of surface transport. The two factors delaying the analysis in the previous set-up were the need to allow cells to express the antibiotic resistance gene for at least 24 h before they could be selected, and the time required for polarisation on filter supports. To remove these factors, a visual assay was established that eliminated the antibiotic selection step and allowed analysis of surface transport in cells grown on glass coverslips.

First, a new variant of the retroviral vector was generated, called RVH1-RFP, which encodes GPI-anchored monomeric red fluorescent protein (mRFP) instead of a protein conferring antibiotic resistance. This vector allows transduced cells to be identified by fluorescence microscopy, thus obviating the need for antibiotic selection. To test the efficiency of RNAi with this vector, MDCK cells were transduced with RVH1-RFP virus directed against caveolin-1, and analysed by immunofluorescence three days post infection. Figure 5.6. shows that an efficient knockdown can be achieved in this way, because expression of mRFP correlated well with a strong reduction of caveolin-1 levels.

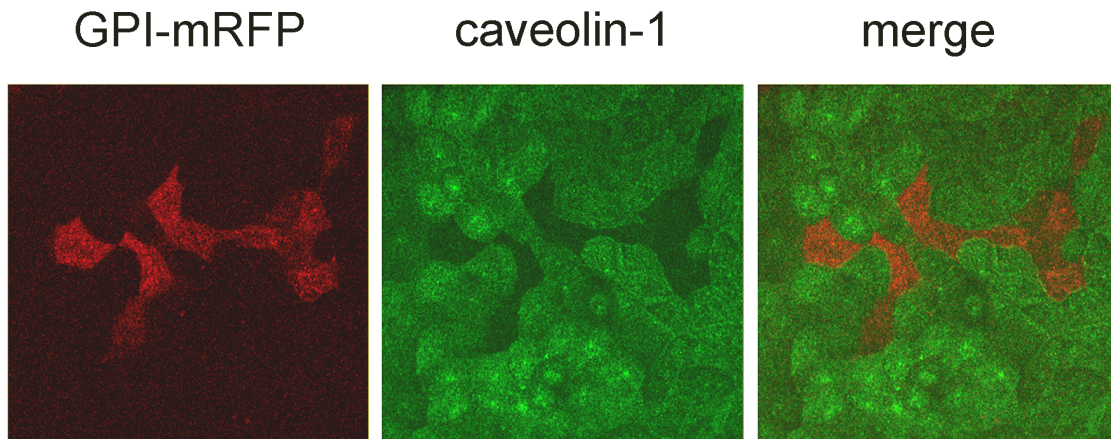


**Figure 5.6.** Correlation between knockdown efficiency and marker expression. MDCK cells transduced with RVH1-RFP/cav-1, which targets the caveolin-1 mRNA and encodes GPI-anchored monomeric RFP, were analysed by caveolin-1 immunofluorescence (middle panel). Transduced cells can be identified by RFP expression (left panel). Magnification was 100x.

Next, a number of fusion proteins tagged with green or yellow fluorescent protein (GFP or YFP) were tested as marker proteins for surface transport. These were a GFP-tagged variant of VSV-G that is efficiently transported to the basolateral membrane (referred to as bVSV-G, Keller et al., 2001), a GFP-tagged variant of VSV-G that is targeted to the apical membrane due to mutation of the tyrosine-based basolateral sorting determinant of the wild type protein (referred to as aVSV-G), a YFP-tagged version of HA that is efficiently transported to the apical membrane due to fusion with the cytoplasmic tail of the influenza virus M2 protein (referred to as M2-HA), a GPI-anchored GFP with added glycosylation sites for efficient apical transport (referred to as GPI-GFP, Keller et al., 2001), a YFP-tagged version of the apically sorted sucrase-isomaltase, and a GFP-tagged version of the apically sorted lactase-phlorizin hydrolase (Jacob and Naim, 2001).

Subconfluent MDCK cells on coverslips were infected with adenoviruses encoding these proteins. To capture the first wave of marker protein moving through the biosynthetic pathway, the proteins were expressed only for the minimum time necessary to obtain visible GFP or YFP fluorescence. bVSV-G and aVSV-G, which aggregate at elevated temperature due to the ts045 mutation, were accumulated in the ER by incubation at 39.5°C. The other marker proteins were accumulated in the TGN by incubation at 19.5°C in the presence of cycloheximide, an inhibitor of protein biosynthesis. Proteins were released from ER and TGN by shifting the temperature to 32°C or 37°C, respectively, cells were fixed after various chase times and immunostained for the Golgi protein giantin.

Sucrase-isomaltase and lactase-phlorizin hydrolase were largely retained in the ER even after prolonged incubation at 19.5°C in the presence of cycloheximide (data not shown) and therefore not used for further experiments. Figure 5.7. shows the transport of bVSV-G to the basolateral membrane. Immediately after the temperature shift to 32°C, bVSV-G localised to the ER, as judged its reticulated distribution throughout the cytosol (Figure 5.7. A and A'). After 20 min of chase, the protein was present in the perinuclear Golgi region and co-localised with giantin, but plasma membrane staining was absent (Figure 5.7. B and B'). After 40 min of chase, a significant fraction of bVSV-G localised to the lateral membrane (Figure 5.7. C and C'), and after 60 min of chase most of the protein was at the lateral membrane and the co-localisation with giantin had largely disappeared and (Figure 5.7. D and D').

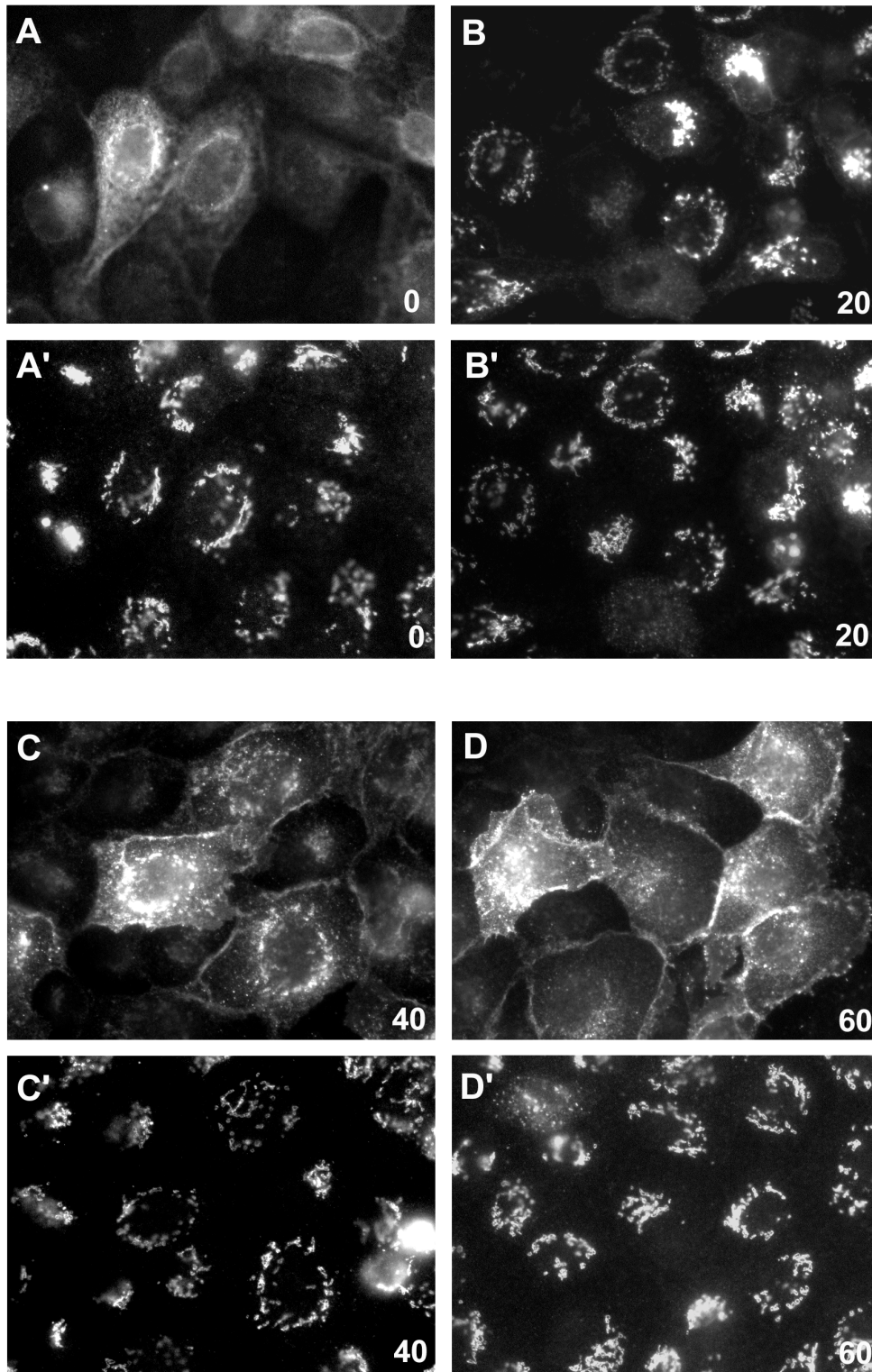


**Figure 5.7.** Surface transport of basolateral VSV-G. MDCK cells were infected with adenovirus encoding GFP-tagged basolateral VSV-G, and newly synthesised protein was accumulated in the ER at 39.5°C. Following a temperature shift to 32°C to allow ER exit, VSV-G was chased to the plasma membrane for 0, 20, 40 or 60 min in the presence of cycloheximide. The distribution of VSV-G is revealed by GFP fluorescence (**A - D**), the Golgi complex in the same cells was visualised by giantin immunofluorescence (**A' - D'**). Magnification was 100x.

aVSV-G was transported to the apical membrane, but much more slowly than its basolateral counterpart (Figure 5.8.). Even after 70 min of chase, only some apical plasma membrane staining had appeared and a significant fraction of aVSV-G still co-localised with giantin. By contrast, M2-HA was rapidly transported from the TGN to the apical membrane (Figure 5.9.). Already 10 min after the temperature shift from 19.5°C to 37°C, the TGN-accumulated M2-HA started to disperse, and after 20 min of chase a significant fraction had reached the apical membrane. After 30 min of chase, co-localisation with giantin was almost completely lost and the characteristic, granular apical staining predominated. These transport kinetics are similar to those observed with wild type HA in filter-grown cells (see Figure 5.2. B and 5.4. A). GPI-GFP was transported to the apical membrane much more efficiently than aVSV-G, but not as rapidly as M2-HA (Figure 5.10.). These time-courses show that bVSV-G, aVSV-G, M2-HA and GPI-GFP are useful marker proteins to follow surface transport in coverslip-grown MDCK cells.

Finally, transduction with RVH1-RFP retrovirus and adenoviral expression of the above GFP- and YFP-tagged marker proteins were combined. It was tested whether sequential infection with a retrovirus and an adenovirus yielded a sufficient proportion of double-infected cells for microscopic analysis. The retroviral infection rate was about 50%, whereas the proportion of adenovirus-infected cells that gave a strong enough fluorescent signal was in the range of 30-70% depending on the marker protein (data not shown). This seemed sufficient for further analysis, although it can not be excluded that the double-infected cells were in some way special and thus not representative of the whole cell population. It was then checked whether retroviral expression of the GPI-anchored mRFP alone affected surface transport. Cells were transduced with empty RVH1-RFP virus, infected with adenovirus encoding bVSV-G, the protein was accumulated in the ER and chased for 40 min in the presence of cycloheximide. During this time, bVSV-G partially reached the plasma membrane, regardless of whether or not cells also expressed GPI-anchored mRFP (Figure 5.11.). Similar results were obtained with aVSV-G as a marker (data not shown). Thus, retroviral transduction alone did not seem to interfere with transport to the cell surface.

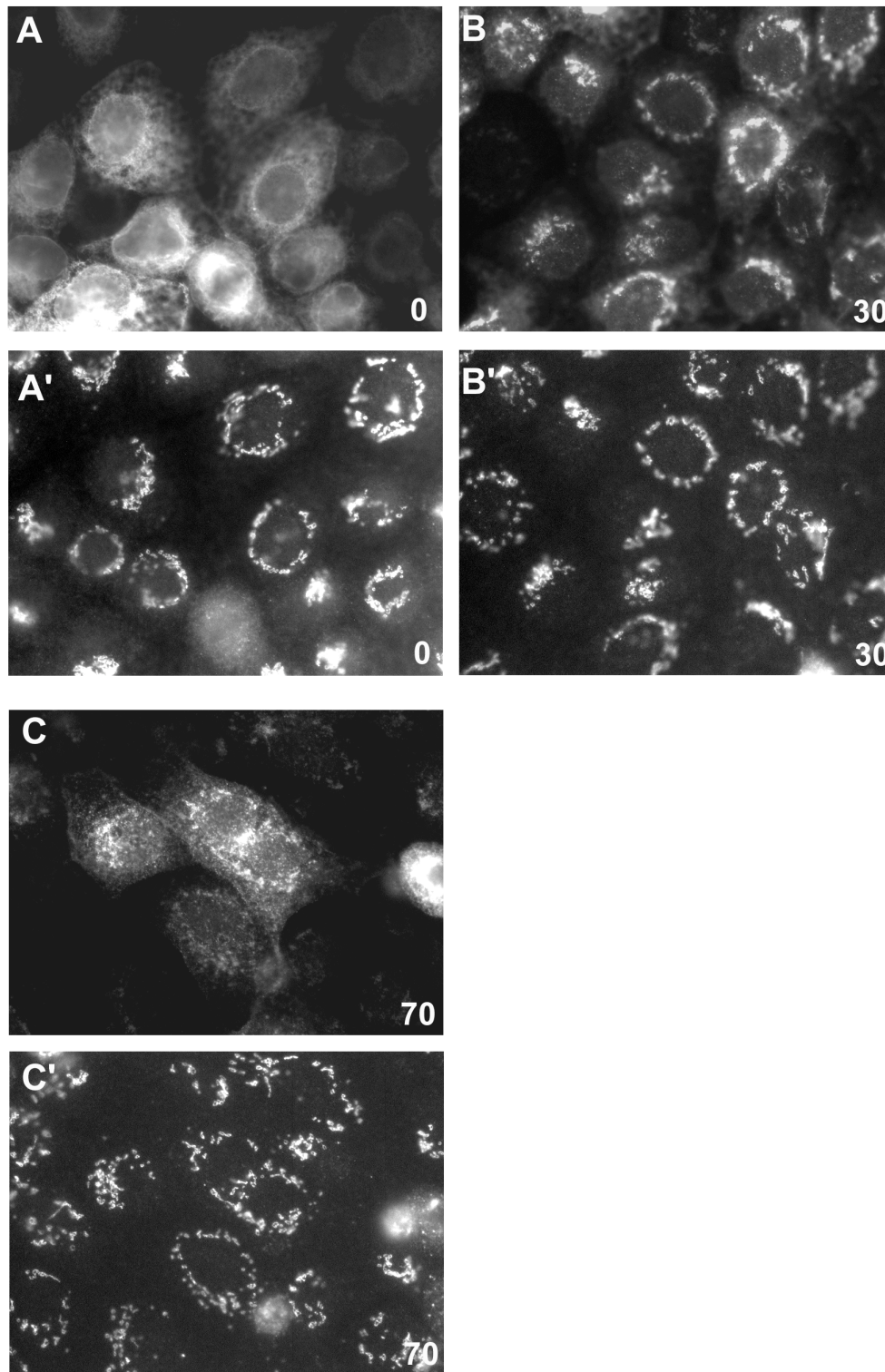


**Figure 5.8.** Surface transport of apical VSV-G. MDCK cells were infected with adenovirus encoding GFP-tagged apical VSV-G, and newly synthesised protein was accumulated in the ER at 39.5°C. Following a temperature shift to 32°C to allow ER exit, VSV-G was chased to the plasma membrane for 0, 30, or 60 min in the presence of cycloheximide. The distribution of VSV-G is revealed by GFP fluorescence (A - C), the Golgi complex in the same cells was visualised by giantin immunofluorescence (A' - C'). Magnification was 100x.

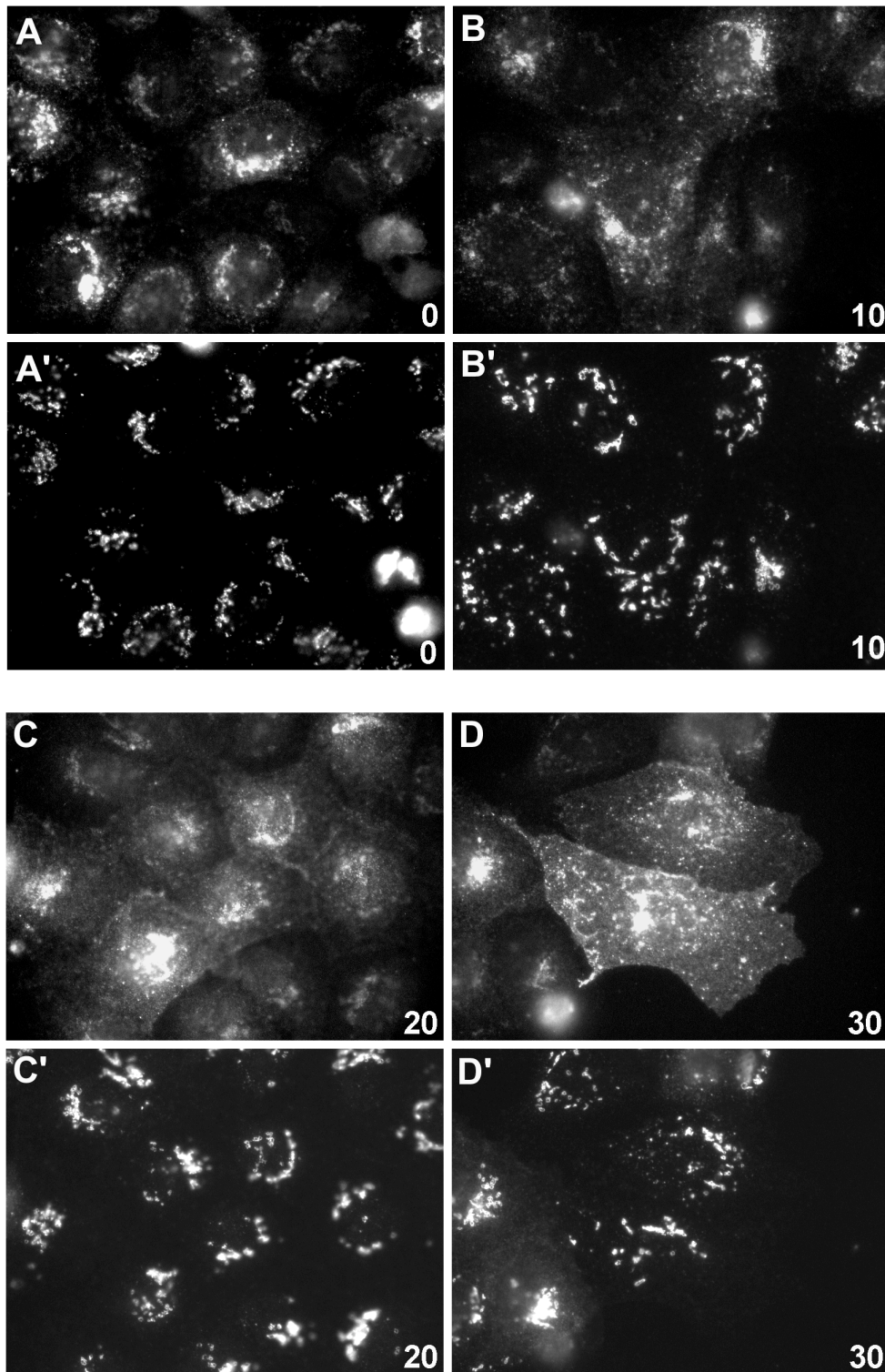


**Figure 5.9.** Surface transport of M2-HA. MDCK cells were infected with adenovirus encoding YFP-tagged M2-HA, and newly synthesised protein was accumulated in the TGN at 19.5°C. Following a temperature shift to 37°C to allow TGN exit, M2-HA was chased to the plasma membrane for 0, 10, 20 or 30 min in the presence of cycloheximide. The distribution of M2-HA is revealed by YFP fluorescence (A - D), the Golgi complex in the same cells was visualised by giantin immunofluorescence (A' - D'). Magnification was 100x.

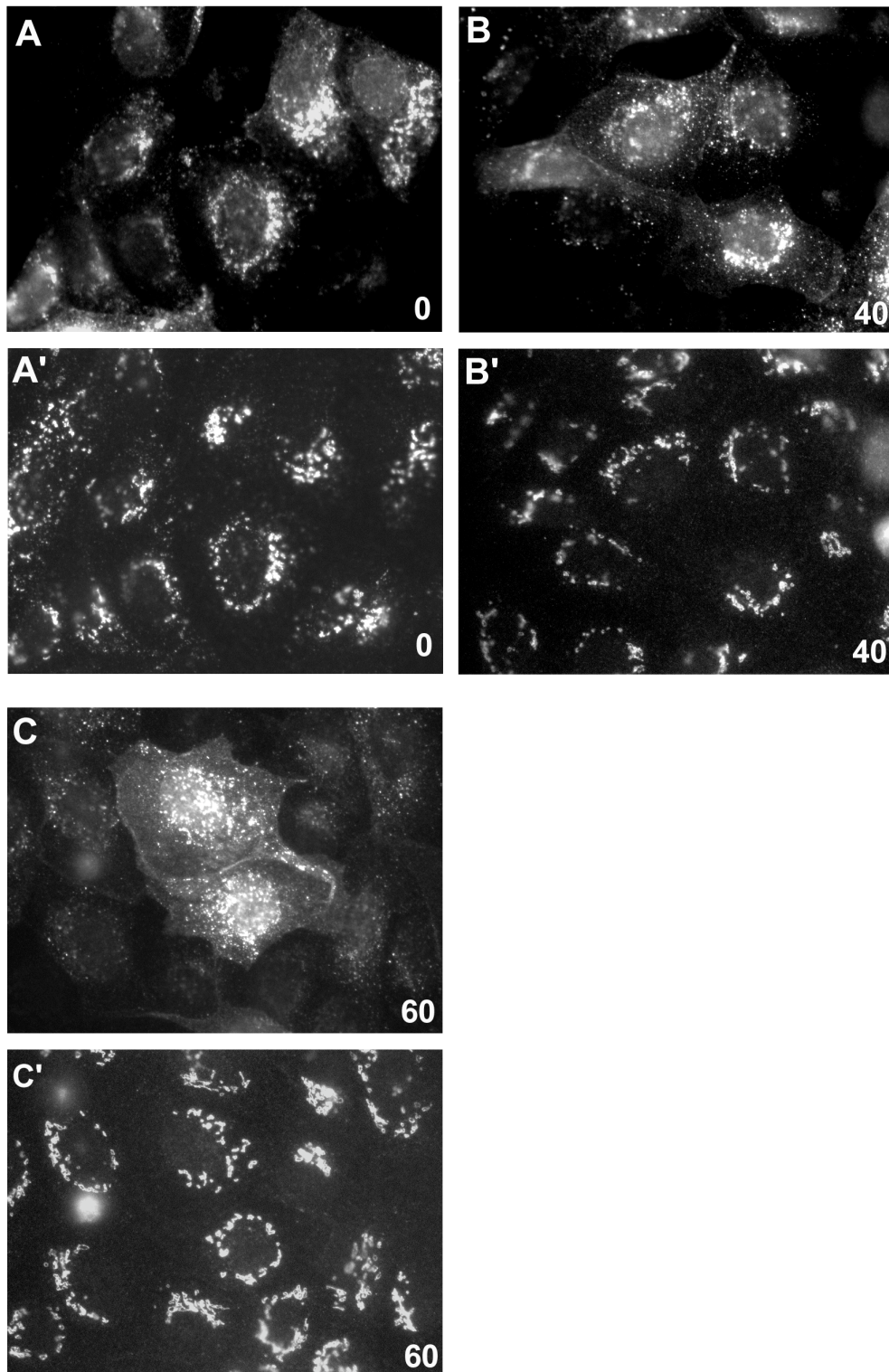


**Figure 5.10.** Surface transport of glycosylated GPI-GFP. MDCK cells were infected with adenovirus encoding GPI-anchored glycosylated GFP, and newly synthesised protein was accumulated in the TGN at 19.5°C. Following a temperature shift to 37°C to allow TGN exit, GPI-GFP was chased to the plasma membrane for 0, 40 or 60 min in the presence of cycloheximide. The distribution of GPI-GFP is revealed by GFP fluorescence (A - C), the Golgi complex in the same cells was visualised by giantin immunofluorescence (A' - C'). Magnification was 100x.



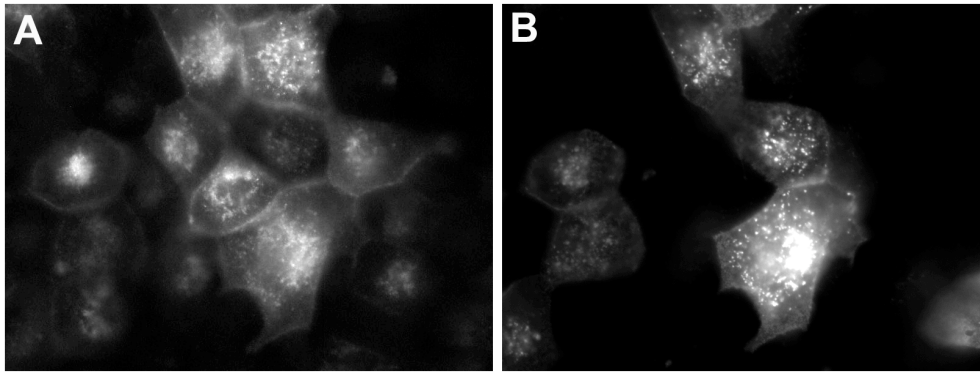


**Figure 5.11.** Surface transport of basolateral VSV-G in retrovirus-transduced cells. MDCK cells transduced with retrovirus encoding GPI-anchored mRFP were infected with adenovirus encoding GFP-tagged basolateral VSV-G. Following ER accumulation, VSV-G was chased to the plasma membrane for 40 min in the presence of cycloheximide. The distribution of VSV-G is revealed by GFP fluorescence (**A**), the distribution of GPI-anchored mRFP in the same cells is revealed by RFP fluorescence (**B**). Magnification was 100x.

### 5.3. Rab 10 as a putative regulator of membrane trafficking

Rab GTPases are involved in the regulation of almost all known membrane trafficking pathways (Zerial and McBride, 2001). In yeast, the rab GTPase SEC4 regulates post-Golgi transport to the cell surface, possibly by interacting with components of the exocyst complex (Guo et al., 1999). The closest mammalian homologues of SEC4 are rab8, rab13, and rab10 (Bock et al., 2001). Rab8 regulates basolateral transport in MDCK cells (Huber et al., 1993; Ang et al., 2003), whereas rab13 mediates tight junction assembly (Kohler et al., 2004). However, no function has yet been attributed to the ubiquitously expressed rab10. Given its close homology to rab8 and its localisation to the TGN (Chen et al., 1993), it appeared likely that rab10 plays a role in post-Golgi trafficking.

To test this possibility, constitutively active and inactive mutants of rab10 were generated, called rab10 Q67L and rab10 T23N. Adenoviruses were produced that encoded mRFP-tagged forms of wild type rab10, rab10 Q67L or rab10 T23N. These proteins were expressed in MDCK cells which were then used for the visual transport assay described in the preceding section. Figure 5.12. shows that the constitutively inactive rab10, which localised to the perinuclear region and to dot-like structures throughout the cytosol, had no effect on basolateral transport of bVSV-G (compare with Figure 5.7.).

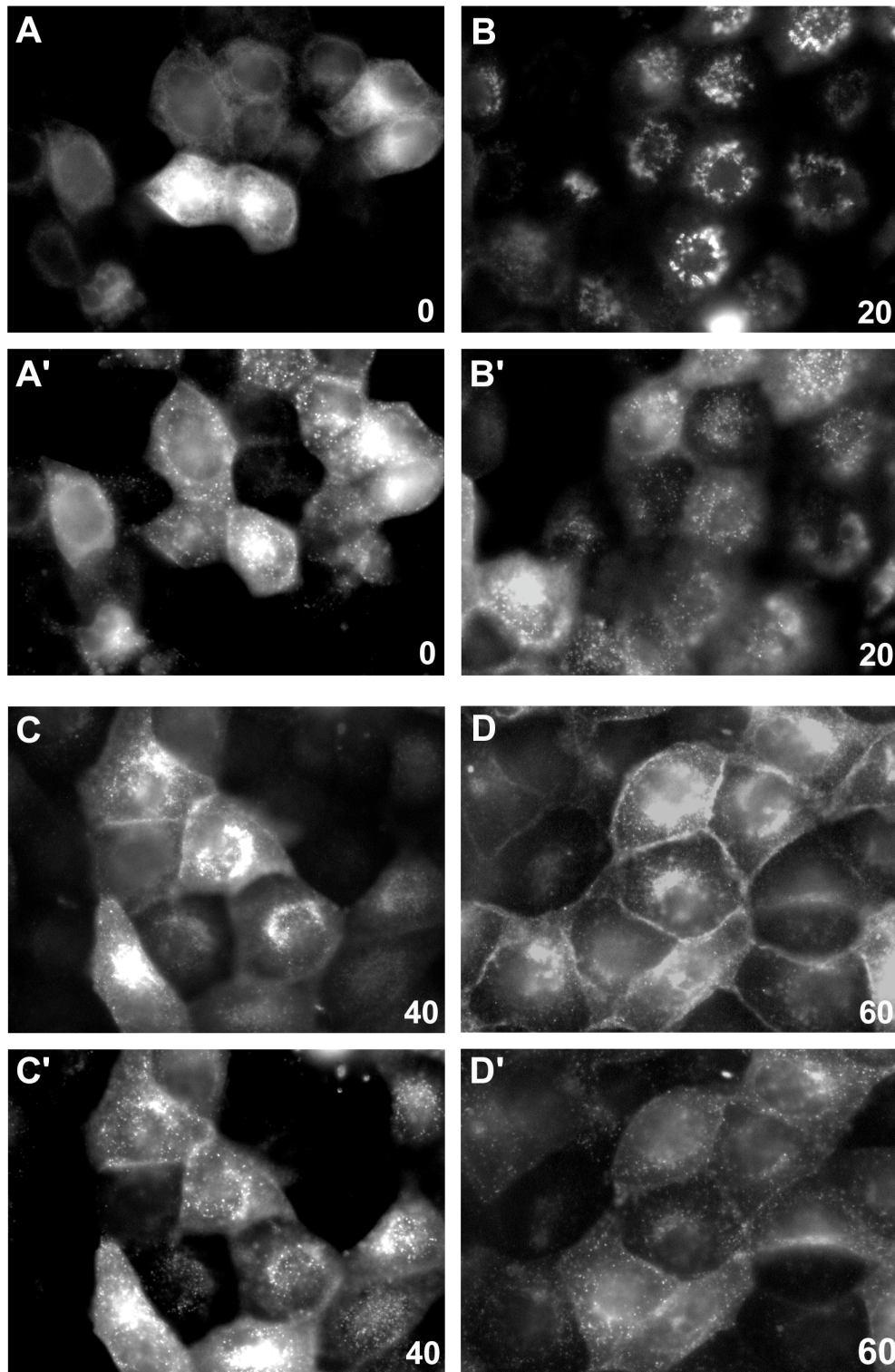


**Figure 5.12.** Surface transport of basolateral VSV-G in cells expressing constitutively inactive rab10 T23N. MDCK cells were infected with adenovirus encoding mRFP-tagged rab10 T23N. They were infected with adenovirus encoding GFP-tagged basolateral VSV-G 12 h later, newly synthesised VSV-G was accumulated in the ER at 39.5°C, and then chased to the plasma membrane for 0, 20, 40 or 60 min in the presence of cycloheximide at 32°C. The distribution of VSV-G is revealed by GFP fluorescence (A - D), the distribution of rab10 T23N in the same cells is revealed by RFP fluorescence (A' - D'). Magnification was 100x.

Overexpression of wild type rab10 also had no marked effect on bVSV-G trafficking (data not shown). However, expression of constitutively active rab10 Q67L lead to bVSV-G accumulation in the perinuclear region and completely blocked its surface delivery (Figure 5.13.). No dramatic effects on the apical transport of aVSV-G and GPI-GFP were observed in cells expressing constitutively active rab10 (data not shown).

These findings prompt the hypothesis that rab10 regulates transport to the basolateral membrane and provide a starting point for the functional analysis of this protein.

#### **5.4. Conclusions**

The results in this chapter show that apical transport of influenza virus HA in fully polarised MDCK cell is unaffected by the virtual absence of VIP17, annexin 13, annexin 2 or TI-VAMP, or the combined depletion of VIP17/annexin 13 or VIP17/MAL2. Therefore, these putative apical sorters are dispensable for HA trafficking.

Cells might adapt to RNAi-mediated depletion of proteins involved in sorting to the plasma membrane. The visual assay for surface transport in MDCK cells allows transport of adenovirally expressed marker proteins to be analysed as soon as target protein levels have been depleted by RNAi. With this assay, it should be possible to screen the knockdowns described in the previous chapter for transport phenotypes. Furthermore, the visual assay revealed that basolateral transport of VSV-G is blocked in the presence of a constitutively active mutant of rab10, thus demonstrating the usefulness of the assay and implicating rab10 in intracellular membrane trafficking.

However, the original goal of this chapter, i.e. to find conditions under which RNAi-induced transport phenotypes can be detected, has not yet been accomplished. The RNAi-based approach to define the apical sorting machinery in MDCK cells therefore remains to be validated.

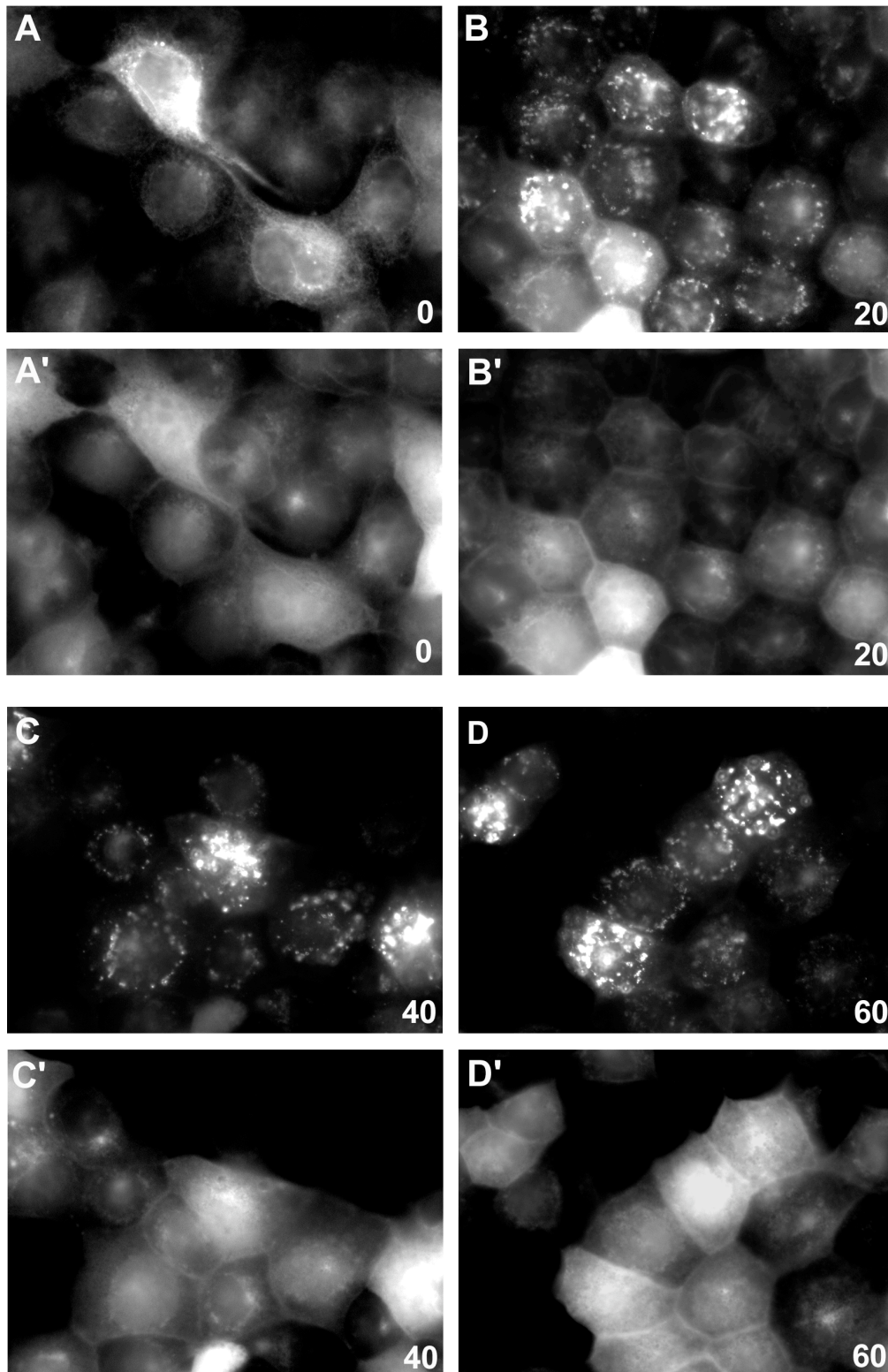


**Figure 5.13.** Surface transport of basolateral VSV-G in cells expressing constitutively active rab10 Q67L. The effect of rab10 Q67L on the transport of bVSV-G was assayed as in Figure 5.12. The distribution of VSV-G is revealed by GFP fluorescence (A - D), the distribution of rab10 Q67L in the same cells is revealed by RFP fluorescence (A' - D'). Magnification was 100x.

## 6. Discussion

In this study, a number of experimental tools that might help to learn more about the molecular organisation of polarised sorting in epithelial cells have been generated and characterised. The usefulness of several mild detergents for studying the architecture of cell membranes was evaluated, a retroviral RNAi system suitable for gene suppression in MDCK cells was established, and a new visual assay for the transport of various marker proteins to the plasma membrane of MDCK cells was set up. In addition, it was shown that several proteins believed to be involved in apical transport are not absolutely required for this process, and preliminary data suggesting a role for rab10 in trafficking to the plasma membrane were obtained. Below, the implications of this work are discussed and directions for future research are indicated.

### 6.1. Detergents as tools for the analysis of membrane organisation and trafficking

The solubilisation of cell membranes by an excess of detergent is essentially a three-step process. First, individual detergent molecules intercalate into the lipid bilayer. When the capacity of the bilayer is saturated, the strain introduced by the usually wedge-shaped detergent molecules causes membrane rupture and lamellar-micellar transition occurs. During this transition, the bilayered organisation of the membrane is lost and pieces of membrane become incorporated into mixed micelles. Finally, the membrane components redistribute among the available detergent micelles. The resulting micelles consist almost entirely of detergent molecules, and only a few membrane lipids and proteins are present in each micelle (Helenius and Simons, 1975; le Maire et al., 2000).

If parts of a cell membrane are particularly tightly packed, detergent intercalation will be restricted or even prevented in those areas. As a result, the number of detergent molecules that intercalate into an ordered membrane microdomain, for instance sphingolipid-cholesterol rafts, can be insufficient to effect lamellar-micellar transition. In the case of the apical membrane of epithelial cells, mild detergents might even fail to cause overall membrane disruption and only introduce holes or selectively solubilise membrane components not firmly integrated into the membrane "backbone". The components that

constitute such ordered membrane domains remain associated after detergent treatment and can be isolated as DRMs by flotation on density gradients.

DRM association may only imperfectly reflect the distribution of proteins between ordered domains and the surrounding membrane, for example because the interaction of some proteins with ordered domains may be too weak to survive detergent extraction (London and Brown, 2000). In addition, detergent intercalation can even promote the formation of DRMs, at least in model membranes (Heerklotz, 2002). Nevertheless, the results of DRM experiments have in many cases been confirmed by independent, detergent-free methods (Ahmed et al., 1997; Dietrich et al., 2001). Thus, insolubility in mild detergents appears to be a useful criterion to test association of lipids and proteins with ordered membrane domains such as sphingolipid-cholesterol rafts.

However, detergent treatment, at least in the case of Triton, leads to coalescence of detergent resistant micodomains, which come together to form aggregates or fuse into continuous membrane sheets (Kurzchalia et al., 1995; Mayor and Maxfield, 1995). As a result, DRMs cannot reveal the spatial organisation of detergent resistant membrane components before solubilisation. Studies of polarised cells that show readily discernible separation of different membrane domains illustrate this. In migrating T lymphocytes, several proteins and the glycolipids GM1 and GM3, all of which associate with DRMs, localise to different regions of the cells, the leading edge and the uropod (Gomez-Mouton et al., 2001). During yeast mating, a number of DRM-associated proteins re-localise to the mating projection of the cells. However, DRM-associated proteins are also found outside the mating projection (Bagnat and Simons, 2002). Hence, separate detergent-resistant domains exist in those cells, but they are indistinguishable by the DRM criterion.

Different types of detergent-resistant domains may be present in cell membranes (Madore et al., 1999; Röper et al., 2000). However, only if different detergents yielded DRMs with complementary sets of constituents, one could hope to distinguish compositionally distinct types of membrane domains by differential detergent insolubility alone. This is not the case, as shown by the results presented in chapter 3. DRMs prepared with very mild detergents such as Brij 58 and Lubrol contained the proteins and lipids also present in DRMs obtained with Triton or CHAPS. As the detergent selectivity increased, more and

more membrane components were removed from DRMs, resulting in an enrichment of a defined set of proteins, sphingolipids, cholesterol and saturated glycerophospholipids. Moreover, DRMs isolated with the least selective detergents did not reveal any significant enrichment or depletion as compared to total cell membranes. Thus, they were uninformative with regard to the possible presence of membrane microdomains.

This leads to the question of how the DRM criterion should best be applied to test association of a particular protein with specialised membrane domains. Given the relatively low DRM selectivities of some detergents, it appears best to first use a rather strong detergent. If the chosen detergent disrupts lipid association of the protein of interest, weaker detergent may be tried or the detergent concentration may be lowered. For instance, some gp114 and TfR were insoluble in 20 mM CHAPS, while they were fully solubilised by 65 mM CHAPS (data not shown). Regardless of the conditions for detergent treatment, a completely soluble membrane protein localised at the same membrane as the protein of interest should be included in the analysis. This is an essential negative control for incomplete solubilisation of bulk membrane. In addition, lipid analysis of DRMs should complement the analysis of DRM protein contents. There clearly are no universally applicable conditions for DRM isolation. Instead, optimisation will be required in each case.

If a protein is found to be DRM-associated, treatment with cyclodextrin, saponin and sphingomyelinase may be applied to test whether DRM association depends on cholesterol and sphingomyelin. In MDCK cells, cyclodextrin and saponin reduce DRM association of the plasma membrane proteins PLAP, Yes, caveolin-1 and VIP17/MAL, but only when cells were mechanically disrupted before cyclodextrin treatment. It is not clear why cyclodextrin was ineffective on live MDCK cells. Possibly, cholesterol is difficult to extract from the unusually stable apical plasma membrane.

There are more precedents of proteins whose DRM association is unaffected by cyclodextrin treatment. In BHK cells, DRM association of the bacterial toxin aerolysin is not significantly reduced by cyclodextrin, even though the integrity of the domains it interacts with was shown to depend on cholesterol by using saponin (Abrami and van der Goot, 1999). In microvillar vesicles derived from the small intestinal brush border

membrane, galectin-4 remains detergent-resistant despite cholesterol depletion by more than 70% (Hansen et al., 2001). In agreement with studies of liposomes (Schroeder et al., 1994), cholesterol might even be dispensable for the formation of detergent-resistant domains in membranes extremely rich in sphingolipids like the brush border membrane.

Sphingomyelinase treatment augments the effect of cyclodextrin, which, at first sight, is consistent with the idea that stability of detergent-resistant domains requires both cholesterol and sphingomyelin. However, the cleavage product of sphingomyelin, ceramide, strongly supports the formation of liquid-ordered domains in model membranes (Xu et al., 2001). In addition, it has recently been shown that ceramide is able to displace cholesterol from liquid-ordered domains in model membranes (London and London, 2004). Therefore, sphingomyelinase may be a useful tool to disrupt sphingolipid-rich membrane domains, but may in fact exert its effects through the displacement of cholesterol. It is interesting that sphingomyelinase, which degraded only 30% of the sphingomyelin in MDCK cells, is much more effective in fibroblasts, where more than 90% of the sphingomyelin is susceptible to sphingomyelinase (Slotte and Bierman, 1988). Thus, sphingomyelinase treatment may have stronger effects in these cells and render DRM-associated proteins Triton-soluble without additional cyclodextrin treatment.

These tools to manipulate DRM association of proteins, like DRM association itself, constitute 'inclusive' criteria. In case of a positive result, they can support a hypothesis, but a negative result does not necessarily provide contradicting evidence. For instance, reduction of DRM association of a protein by cholesterol depletion suggests interaction with a domain whose integrity depends on cholesterol. If no reduction is found, no conclusions can be drawn, since the remaining cholesterol may keep such domains intact. As discussed above, detergent insolubility of a protein indicates association with detergent-resistant domains, but detergent solubility does not exclude interaction with these domains as the interaction may not be strong enough to survive DRM preparation.

Overall, it appears that the isolation of DRMs will remain a valuable tool for probing the organisation of biological membranes. DRMs are a most useful starting point for defining the composition of membrane subdomains, including sphingolipid-cholesterol rafts, with Triton and CHAPS being the most reliable detergents for analysing possible raft-



association. Applying a variety of detergents may reveal subtle differences in lipid-protein interactions or changes in the lipid environment of proteins during processes like T cell activation (Janes et al., 1999). However, caution is needed when drawing conclusions from DRM experiments, and when comparing results obtained with different detergents and from different cell types.

With regard to the use of detergents in the study of membrane trafficking, detergent insolubility can reflect changes in the lipid environment of proteins during transport to the cell surface, as has been shown for influenza virus hemagglutinin and PLAP (Skibbens et al., 1989; Brown and Rose, 1992). Given that Brij 96 and Brij 98 are detergents that, in MDCK cells, produce DRMs selectively enriched in a subset of proteins and lipids, but are milder than Triton or CHAPS, they might be informative reagents with regard to apical transport. For instance, it could be interesting to follow the Brij 96 and Brij 98 insolubility of Triton-soluble proteins like gp114 and gp135 during their transport to the apical membrane in MDCK cells. This could address the question whether these proteins are really targeted to the apical membrane by a different mechanism than influenza virus hemagglutinin and PLAP, or use a similar pathway but with lower affinity for apically directed raft domains. Interestingly, Brij 96 has already been used to detect DRM association of Triton-soluble proteins in Golgi membranes derived from CHO cells (Gkantiragas et al., 2001), further indicating the potential utility of this detergent in membrane trafficking studies.

## **6.2. Retroviral RNAi as a tool for gene inhibition in epithelial cell**

The results described in chapter 4 show that gene expression in MDCK cells can be strongly and specifically inhibited using retroviral RNAi. Since expression could substantially be reduced for each of the 13 target genes, they support the notion that any mRNA can be targeted by RNAi.

What remains unknown is whether knockdowns of greater than 90% can be obtained for any given gene, and if so, how many target sequences will have to be tested to achieve this. Much will depend on refining the criteria for selecting target sequences. Several studies, including this one, have revealed certain characteristics of functional siRNAs.

They are marked by a low stability of the 5' antisense end compared to the 5' sense end, an overall relatively low stability, as well as a preference for adenosine at position 11 of the antisense strand (Khvorova et al., 2003; Aza-Blanc et al., 2003; Schwarz et al., 2003; Reynolds et al., 2004). These features have already been used to construct an algorithm for the rational design of siRNAs that significantly improves the chances of choosing functional siRNAs (Reynolds et al., 2004). Moreover, the characteristics of functional siRNAs that emerged during this study have been very helpful for creating further knockdowns in our laboratory. It is now usually sufficient to test only two target sequences in order to obtain at least one functional one. However, it is not clear how accurately the efficiency of an individual siRNA can be predicted. It is conceivable that factors unrelated to the properties of the siRNAs, like mRNA secondary structure, can interfere with target recognition by the RISC (Vickers et al., 2003). This may explain why there are relatively recalcitrant transcripts like the syntaxin-3 mRNA, for which none of the six target sequences that were tested gave a knockdown of more than 70%.

An additional point to consider when introducing siRNAs into cells by means of shRNA expression is that not all shRNAs may be transcribed equally well. The U6 promoter, which has been employed for expression of shRNAs (Paddison et al., 2002), has a strict requirement for guanosine in the +1 position, whereas the H1 promoter used in this study is more flexible (Dykxhoorn et al., 2003). Whether the H1 promoter has any preferences for certain bases downstream of the start site of transcription is not known.

Many genes are functionally redundant, as suggested by the large number of knockout mice without obvious phenotypes. Interfering with a particular function may therefore require removal of several gene activities. In mammalian cells, this can be achieved by RNAi using transient transfection of synthetic siRNAs or plasmids expressing shRNAs (Elbashir et al., 2002; Yu et al., 2003). In principle, there is no reason why shRNA expression vectors could not be used to derive stably transfected double knockdown MDCK cell lines, but the disadvantages of this approach, namely the time required to generate these lines and the drawbacks of clonal selection, remain. The retroviral system, on the other hand, avoids both problems. Double knockdowns can be produced within a week and the high transduction rates ensure that effects arising from the integration into a particular locus of the host genome will be averaged out in a cell population.

The capacity of the cellular RNAi machinery is not easily saturated, as shown by the facts that knockdowns can be improved by increasing the virus titer and that efficient double knockdowns can be generated. Triple or quadruple knockdowns might therefore be possible. Using a retroviral system, this could be achieved by introducing yet another selectable marker. Alternatively, retroviruses could be combined with adenoviruses, which have been successfully used for RNAi (Wilson and Richardson, 2003), and can also infect non-dividing cells including fully polarised MDCK cells. However, overloading the RNAi machinery may at some point compromise the regulatory functions of endogenously expressed micro RNAs (Bartel, 2004) and lead to unspecific side effects. In addition, exceedingly high levels of siRNAs might activate aspects of the interferon response (Bridge et al., 2003), even though this defense mechanism is not normally activated by double-stranded RNAs shorter than 30 nucleotides (Elbashir et al., 2001).

### **6.3. Defining components of the apical sorting machinery**

The ability to efficiently sort proteins to the apical and basolateral membrane is vital to maintain the organisation of epithelial cells. Disrupting the machinery for polarised sorting should therefore impair the barrier and exchange functions of various epithelial tissues. However, mice lacking putative elements of the apical sorting machinery such as VIP17, annexin 2, caveolin-1 and KIF3C are viable, and display only rather specific phenotypes (Schaeren-Wiemers et al., 2004; Ling et al., 2004; Drab et al., 2001; Yang et al., 2001; Xu et al., 2002). For example, VIP17 knockout mice show minor myelination defects in the central nervous system of adult animals, consistent with a role in VIP17 in the maintenance, but not the formation of myelin. Knockout animals showed disorganised axon-glia contacts in the paranodal regions of axons and reduced levels of various myelin proteins in purified myelin. A possible explanation is that proteins required for axon-glia interactions are less efficiently sorted to the paranodal regions in adult animals in the absence of VIP17, thus giving rise to the morphological aberrations observed (Schaeren-Wiemers et al., 2004). Annexin 2 knockout mice do not show any phenotype obviously related to membrane trafficking (Ling et al., 2004), and data revealing a block in surface transport of GPI-anchored proteins in cells derived from caveolin-1 knockout mice (Sotgia et al., 2002) could not be reproduced in our laboratory (Manninen, A., Füllekrug, J. and Simons, K., unpublished).

Similarly, only a few proteins involved in exocytic transport from the trans-Golgi are known in yeast, despite extensive genetic screens. The main reason for this may be that these screens searched for lethal mutations. Due to the existence of at least two pathways to the yeast plasma membrane, which can compensate each other (Harsay and Schekman, 2002), most genes involved in post-Golgi trafficking are probably non-essential. These genetic data from yeast and mammals suggest that the machinery for protein sorting and surface transport is redundant. It is likely that even when a particular transport route is blocked, cells can adapt so that proteins usually travelling along this pathway still reach their correct destination by taking alternative routes.

This raises the questions of why delays or even blocks in apical transport have been observed in tissue culture cells when the function of certain proteins was impaired. In part, this could be explained by pleiotropic effects of the methodology used. For example, a common method to interfere with the function of a protein is the intracellular application of specific antibodies, which mask the proteins they recognise and sterically hinder their activity. This approach has yielded evidence for the involvement of annexin 13b, TI-VAMP, syntaxin-3 and caveolin-1 in apical sorting (Fiedler et al., 1995; Lafont et al., 1999; Scheiffele et al., 1998). However, antibody shielding may simultaneously block the function of other proteins in close proximity to the antigen. It is therefore possible that the results obtained for annexin 13b, TI-VAMP, syntaxin-3 and caveolin-1 reflect their association with the apical pathway but overestimate their functional importance. Similar concerns apply to overexpression or intracellular application of proteins. Syntaxin-3 has been implicated in apical transport because its overproduction leads to accumulation of apical transport carriers beneath the apical membrane, whereas overexpression of wild type or dominant negative KIFC3 accelerated or inhibited apical transport, respectively (Low et al., 1998; Noda et al., 2001). Intracellular application of recombinant wild type or mutant annexin 13b in permeabilised MDCK cells stimulated or inhibited apical transport, respectively (Lafont et al., 1998). However, increasing the levels or introducing dominant negative mutants of these proteins may have disturbed apical transport much more than their simple removal would have done.

The most convincing evidence for the role of a protein in apical transport in tissue culture cells has come from experiments using RNAi or related techniques. Knocking down

annexin 2 strongly inhibited Golgi export of sucrase-isomaltase in MDCK cells (Jacob et al., 2004), and depletion of VIP17 or MAL2 by antisense RNA oligonucleotides impaired apical transport of a variety of proteins in MDCK cells and hepatocytes, including influenza virus HA and GPI-anchored proteins (Cheong et al., 1999; Puertollano et al., 1999; Martin-Belmonte et al., 2000; de Marco et al., 2002). Removal of these proteins by RNAi could have strong effects compared to the mild phenotypes in knockout mice because RNAi-induced protein depletion occurs very rapidly. As a result, the depletion of a protein may, for a limited amount of time, evade adaptive mechanisms which can compensate the loss of functionally important proteins. Moreover, such compensatory mechanisms may act more stringently in living organisms than in tissue culture cells.

These considerations may explain why removing a protein by RNAi can fail to confirm results obtained with other, less specific methods. In addition, they indicate that cell adaptation may limit the time window for detecting RNAi effects. Knockdown phenotypes clearly can be obtained with the retroviral system. This is illustrated by the reduced transferrin uptake in rab11a/b double knockdown cells, as described in chapter 4. Other examples are the podocalyxin knockdown, which leads to a delay in cell growth as well as epithelial polarisation (Meder, D., Simons, K. and Füllekrug, J., unpublished), and the galectin-9 knockdown, which impairs the organisation of the apical membrane (Manninen, A. and Simons, K., unpublished). Hence, it appears possible that effects on HA transport were not observed in the experiments in chapter 5 because the time window for detecting HA trafficking phenotypes was missed. However, it can also not be excluded that cells adapt so rapidly that there is no such time window.

Cell adaptation notwithstanding, the results demonstrate that VIP17, annexin 2, annexin 13, TI-VAMP and MAL2 are unlikely to be essential elements of the apical transport machinery. A caveat for this interpretation is that the sorting of HA in cells infected with influenza virus may to a large extent be independent of the endogenous transport machinery. It is interesting to note that wild type HA is only inefficiently transported to the apical membrane in cells that do not express also the other influenza virus proteins (Keller, P. and Simons, K., unpublished). Efficient apical transport only occurs when HA is fused to the cytoplasmic tail of the influenza virus M2 protein, which is involved in controlling the shape of the viral particle (Roberts et al., 1998). These observations

indicate that the proteins responsible for sorting of influenza virus transmembrane proteins such as HA are partially provided by the virus itself. As a result, HA transport may only require very fundamental protein components of the cellular transport machinery such as microtubules and microtubule motors, and it is not entirely clear whether transport of HA in cells infected with influenza virus accurately recapitulates normal apical trafficking.

The newly-established visual transport assay may avoid the problem of cell adaptation as it allows knockdown cells to be analysed much earlier than was possible with the HA transport assay on filter-grown cells. This assay could therefore be more suitable to detect RNAi-induced transport defects. As it is based on visually inspecting the distribution of fluorescent marker proteins, this assay is probably most sensitive with regard to alterations that affect the most conspicuous cellular structures. For instance, the perinuclear Golgi region has a very characteristic morphology and the disappearance of fluorescent signal from this structure is easily recognised. Therefore, delays in export from this region should be readily detectable. The assay also provides a simple means of testing new candidate proteins for a functional role in polarised sorting, as illustrated by the experiments implicating rab10 in post-Golgi trafficking.

#### **6.4. Future directions**

It remains to be established whether defects in biosynthetic transport to the plasma membrane can be produced by depleting proteins with the help of retroviral RNAi. The logical next step to address this is to screen the existing knockdowns by means of the visual transport assay.

Regarding the function of rab10, the finding that basolateral VSV-G is trapped at an intracellular site by expression of constitutively active rab10 needs to be extended. First, the site of VSV-G accumulation needs to be characterised. Second, possible effects of wild type and the active and inactive mutant forms of rab10 on apical cargo proteins need to be tested in more detail to find out whether the function of rab10 is restricted to the basolateral pathway. In addition, testing the effects of a rab10 knockdown would be of interest. Finally, it could be attempted to identify rab10 interacting proteins by an affinity

chromatography approach, as has been successfully done for other rab GTPases (Christoforidis et al., 2000).

The protein machinery involved in polarised membrane trafficking to the plasma membrane remains to be defined. Interactions between machinery proteins should help to elucidate how polarised sorting works at the molecular level. The interactions of this machinery with lipid microdomains should provide further clues about the role of rafts in polarised sorting. In addition, the localisation of the machinery should help to clarify at which cellular sites segregation of different cargo molecules occurs. This will lead to a better understanding of how different mechanisms and trafficking routes are employed by epithelial cells solve the tremendously complicated molecular sorting problem they face with such impressive accuracy.

## 7. Materials and Methods

### 7.1. Cell culture techniques

#### 7.1.1. Cell culture

Madin-Darby canine kidney (MDCK) strain II cells (ATCC No. CCL-34) and MDCK strain II cells expressing human placental alkaline phosphatase (MDCK-PLAP cells; Brown et al., 1989) were maintained on tissue culture plates in MEM (Invitrogen) with 5% FCS (PAA Laboratories), 2 mM glutamine (Invitrogen) and 100 U/ml penicillin/streptomycin (Invitrogen). For subculturing, confluent cells were detached by two rounds of treatment with trypsin/EDTA (Invitrogen), first at room temperature for 15 min, then at 37°C for another 15 min. Trypsin was inhibited by addition of normal culture medium, and cells were re-plated. For growth on permeable filter supports,  $3 \times 10^5$  cells in normal medium containing 10% FCS were plated per 12 mm polycarbonate filter (Corning). Cells were allowed to polarise for at least three days, during which time the medium was exchanged daily.

Jurkat T lymphocytes (ATCC No. TIB-152) were kept in suspension in RPMI 1640 medium (Sigma) supplemented with 10% FCS, 2 mM glutamine and 100 U/ml penicillin/streptomycin. Phoenix gag-pol cells (obtained from the ATCC with authorisation from Garry Nolan, School of Medicine, Stanford University, Stanford, CA) and QBI-293A cells (Qbiogene) were maintained on tissue culture plates in high-glucose DMEM (4.5 g/l, PAA Laboratories) containing 10% FCS, 2 mM glutamine and 100 U/ml penicillin/streptomycin.

#### 7.1.2. Metabolic labelling of MDCK and Jurkat cells

For metabolic labelling, confluent MDCK on a 10 cm tissue culture plate or  $10^7$  Jurkat cells were incubated in normal medium supplemented with 10  $\mu$ Ci  $^{14}$ C-acetate or 50  $\mu$ Ci  $^{32}$ P-orthophosphate (Amersham Pharmacia) for 16 h.



### 7.1.3. Cyclodextrin, saponin and sphingomyelinase treatment

For cyclodextrin treatment of live cells, MDCK-PLAP cells on a 10 cm tissue culture plate were washed twice with PBS and treated with 10 mM methyl-beta-cyclodextrin (Sigma) in MEM at 37°C for 30 or 60 min. For cyclodextrin treatment of cell homogenates, MDCK-PLAP cells on a 6 cm tissue culture plate were washed PBS, collected by scraping and centrifugation at 2000 rpm for 5 min and resuspended in 180 µl TNE (150 mM NaCl, 2 mM EDTA in 50 mM Tris-HCl, pH 7.4) with CLAP (chymostatin, leupeptin, antipain, pepstatin, 25 µg/ml each, all from Sigma). Cells were homogenised by passing through a 25 G needle 20 times. 160 µl cell homogenate were mixed with 20 µl 100 mM methyl-beta-cyclodextrin and incubated at 37°C for 30 min. For saponin treatment, MDCK-PLAP cells were treated with 0.2% (w/v) saponin from Quillaja Bark (Sigma) in PBS at 4°C for 1 h. For sphingomyelinase (SMase) treatment, cells were incubated with 0.5 U/ml SMase from *Staphylococcus aureus* (Sigma) in MEM at 37°C for 1 h. Homogenate from saponin or SMase treated cells was prepared, and either used directly for subsequent detergent extraction (see 7.2.2.), or first treated with cyclodextrin as described above.

## 7.2. Biochemical methods

### 7.2.1. Cell lysis

For the preparation of cell lysates for SDS-PAGE, cells were washed once with PBS and lysed by addition of a small volume of lysis buffer consisting of 2% (w/v) NP-40 (Fluka) and 0.2% (w/v) SDS (Serva) in PBS. The lysate was collected by scraping, vortexed at 4°C for 1 min and centrifuged at 17,000 xg for 15 min to remove insoluble material. The supernatant was collected and the protein concentration was determined using the BCA assay kit (Perbio).

### 7.2.2. Detergent extraction and equilibrium density centrifugation

For equilibrium density centrifugation (also referred to as flotation) on sucrose step gradients, confluent MDCK cells from a 10 cm tissue culture plate or 10<sup>7</sup> Jurkat cells (approximately 1 mg protein) were washed with homogenisation buffer (HB, 250 mM

sucrose, 10 mM HEPES, pH 7.4) and collected by scraping and centrifugation at 200 xg for 5 min. Cells were resuspended in 500  $\mu$ l HB with CLAP and homogenised by passing through a 25 G needle 20 times. 500  $\mu$ l HB/CLAP were added containing either no detergent, 2% (w/v) Tween 20 (Sigma), 2% (w/v) Brij 58 (Sigma), 1% (w/v) Lubrol WX (Serva), 2% (w/v) Brij 98 (Sigma), 1% (w/v) Brij 96 (Fluka), 2% (w/v) Triton X-100 (Perbio) or 8% (w/v) CHAPS (Anatrace). Extraction was done on ice for 30 min, except for Brij 98, which was applied at 37°C for 10 min. Samples were adjusted to 42% (w/w) sucrose with 2 ml 56% (w/w) sucrose in 10 mM HEPES, transferred into SW40 centrifuge tubes (Beckman), overlaid with 8.5 ml 38% (w/w) and 0.5 ml 5% (w/w) sucrose/HEPES, and centrifuged at 39,000 rpm (271,000 xg) for 18 h. 2.5 ml were collected from the top as the floating fraction.

For flotation on linear sucrose gradients, detergent extracts from MDCK-PLAP cells were prepared as above, except that HB was replaced by TNE. Samples were adjusted to 40% (w/w) sucrose with 2 ml 56% (w/w) sucrose in TNE, transferred into SW40 tubes, overlaid with 9 ml linear 5 - 35% sucrose gradients in TNE and centrifuged as above. 12 fractions of 1 ml were collected from the top unless stated otherwise.

For flotation on Optiprep step gradients, homogenates from MDCK-PLAP cells from 6 cm dishes were prepared as above, except that cells were resuspended in 180  $\mu$ l TNE before disruption. Homogenates were extracted with 20  $\mu$ l 10% Triton X-100 on ice for 30 min, adjusted to 40% (w/v) iodixanol with 400  $\mu$ l Optiprep (Nycomed Pharma), transferred into TLS55 centrifuge tubes (Beckman), overlaid with 1.2 ml 30% (w/v) iodixanol in TNE and 0.2 ml TNE, and centrifuged at 55,000 rpm (259,000 xg) for 2 h. Two fractions of 1 ml were collected from the top.

### *7.2.3. SDS polyacrylamid gel electrophoresis (SDS-PAGE)*

Mini gels (5.5 cm x 8 cm x 1.5 mm) were cast and run using the SE 250 gel system (Hoefer). Separating gels of the appropriate acrylamide concentration were prepared using 4x separating buffer (1.5 M Tris-HCl pH 8.8, 0.4% (w/v) SDS), 30% acrylamide stock solution (30% w/v acrylamide, 0.8% w/v bisacrylamide), TEMED (Sigma) and 10% (w/v) APS stock solution. Stacking gels were prepared with 4x stacking buffer (0.5 M Tris-HCl

pH 6.8, 0.4% (w/v) SDS), acrylamide, TEMED and APS, and had a final acrylamide concentration of 4.5% (w/v).

Large gradient gels (11 cm x 16 cm x 1.5 mm) were cast and run using the SE 600 gel system (Hoefer). For the separating gels, two 13 ml gel solutions without APS were prepared, containing a low and a high concentration of acrylamide, respectively. Solutions were cooled on ice, APS was added, and gels were cast at 4°C using a gradient maker and a peristaltic pump. Gels were allowed to polymerise at room temperature for 2 h before casting the stacking gels as described above.

Cell lysates (prepared as described under 7.2.1.) or fractions from equilibrium density gradients were mixed with 0.2 volumes of 5x sample buffer (250 mM Tris pH 6.8, 12.5 mM EDTA, 10% SDS, 25% glycerol, containing 10% beta-mercaptoethanol or not, depending on whether the samples were run under reducing or non-reducing conditions), boiled for 5 min, cooled on ice, centrifuged briefly, and loaded. Minigels were run at a constant voltage of 100 V. Large gels were run at a constant voltage of 250 V, or at 60 V over night.

#### *7.2.4. Immunoblotting*

SDS-PAGE gels were removed from the gel chamber and soaked blotting buffer (25 mM Tris, 192 mM glycine, 20% methanol) for 2 min. Proteins were blotted onto PVDF membranes (Immobilon P, Millipore) that had been activated with methanol and soaked in blotting buffer for 5 min. Blotting was performed with a semidry blotting apparatus (Semiphor, Hoefer) at a constant current of 100 mA per membrane for 1 h. Membranes were washed once with TBS/Tween (20 mM Tris, 0.15 mM NaCl, 0.1% (w/v) Tween 20, pH 7.4) and incubated in blocking solution (5% (w/v) dry milk powder in TBS/Tween) at room temperature for 1 h. Incubation with the primary antibody diluted in blocking solution was done at room temperature for 1 h or at 4°C over night. Membranes were washed 3 x 5 min with TBS/Tween, and incubated with HRP-coupled secondary antibody (goat anti-rabbit HRP or goat anti-mouse HRP antibody from Biorad) diluted 1:5000 in blocking solution at room temperature for 1 h. After washing with TBS/Tween for 4 x 15 min, bands were revealed with the ECL kit (Amersham) and detected using Biomax Light

films (Kodak). Table 7.1. lists the primary antibodies used, the sources they were obtained from, and their working dilutions.

<b>Antigen</b>	<b>Antibody</b>	<b>Source</b>	<b>Dilution</b>
annexin 2	HH7 mouse anti-human annexin 2	Volker Gerke (Thiel et al., 1992)	1:5000
annexin 13/2	rabbit anti-dog annexin 13/2	Simons lab (Lecat et al., 2000)	1:1000
annexin 13b	172 rabbit anti-dog annexin 13b	Simons lab (Fiedler et al., 1995)	1:1000
calnexin	mouse anti-human calnexin	BD Transduction laboratories	1:500
caveolin-1	N20 rabbit anti-human caveolin-1	Santa Cruz	1:5000
gp114	4.6.5. mouse anti-canine gp114	Simons lab (Balcarova-Ständer et al., 1984)	1:1000
gp135	mouse anti-dog gp135	George Ojakian (Ojakian and Schwimmer, 1988)	1:1000
PLAP	4679 rabbit anti-human PLAP	Simons lab (Verkade et al., 2000)	1:5000
rab-5	46-4 rabbit anti-human rab-5	Marino Zerial	1:1000
rab-8	66320 mouse anti-human rab-8	BD Transduction laboratories	1:1000
rab-11	mouse anti-human rab-11	BD Transduction laboratories	1:2000
stomatin	GARP50 mouse anti-human stomatin	Rainer Prohaska (Snyers et al., 1999)	1:500
syntaxin 3	rabbit anti-human syntaxin-3	Vesa Olkkonen (Riento et al., 1998)	1:1000
TI-VAMP	CI 158.2 mouse anti-rat TI-VAMP	Thierry Galli (Muzerelle et al., 2003)	1:1000
transferrin receptor	H68.4 mouse anti-human transferrin receptor	Zymed	1:2000
transferrin receptor	MRC OX-26 mouse anti-rat transferrin receptor	Serotec	1:500
VIP17/MAL	26iR rabbit anti-canine VIP17	Simons lab	1:5000
VIP36	1534 rabbit anti-dog VIP36	Simons lab (Fiedler and Simons, 1996)	1:2000
Yes	mouse anti-human Yes	BD Transduction laboratories	1:500

#### 7.2.5. Cell surface biotinylation

Confluent MDCK cells on 10 cm tissue culture plates were washed twice with PBS and biotinylated with 1 mg/ml Sulfo-NHS-LC-Biotin (Pierce) in PBS containing 0.5 mM magnesium and 1 mM calcium (PBS+) at 4°C for 30 min. Cells were washed once with

quenching buffer (PBS+ with 0.3% (w/v) BSA and 0.1 M glycine) and unreacted biotinylation reagent was quenched by three additional 5 min incubations with quenching buffer at 4°C. For the quantification of biotinylated protein, dilution series of each sample were dotted onto a nitrocellulose membrane, probed with peroxidase-extravidin (Sigma), and ECL images were quantified using the Image Gauge V3.3 software (Fuji). Background signal arising from endogenously biotinylated proteins was negligible.

#### *7.2.6. Lipid extraction*

Lipids were extracted according to Folch (Folch et al., 1957), using chloroform-washed 16 x 100 mm screw cap pyrex tubes (Corning). 2 ml methanol were added to 300 µl sample (e.g. a fraction from a sucrose gradient), and mixed by shaking for 5 min. 4 ml chloroform were added, followed by shaking for 5 min. Insoluble material such as sucrose was removed by centrifugation at 3000 xg for 5 min. Supernatants were transferred into fresh glass tubes and 1.2 ml water were added to induce phase separation. After 5 min shaking, samples were centrifuged at 500 xg for 5 min. The lower, organic phase was collected with chloroform-washed glass Pasteur pipettes, transferred into fresh tubes and dried in a speedvac (Heto RC 10.22., Jouan). Lipids were resuspend in 400 µl methanol/chloroform (1:1 v/v), transferred into 0.5 ml microfuge tubes and dried again. Lipids were resuspended in 20 µl methanol/chloroform (1:1 v/v) and used for thin-layer chromatography or mass spectrometric analysis.

#### *7.2.7. Mild alkaline hydrolysis of ester lipids*

Mild alkaline hydrolysis of ester lipids was performed according to Schnaar (Schnaar, 1994). Dried lipids were dissolved in 1 ml freshly prepared 0.1M NaOH in methanol. Samples were incubated at 37°C for 2 h, and 100 µl 1 M sodium phosphate pH 7.0 and 100 µl 1 M hydrochloric acid were added to neutralise the sodium hydroxide. Samples were dried, and lipids were extracted twice as described above to remove the sodium chloride.

### 7.2.8. Cholesterol determination

Cholesterol was determined using the cholesterol oxidase-based Amplex red kit (Molecular Probes). Cells were washed twice with PBS, collected by scraping and centrifugation at 2000 rpm for 5 min, and resuspended in water. Lipids were prepared as described above. Dried lipids were resuspended in the reaction buffer supplied with the Amplex red kit, and cholesterol was measured according to the manufacturer's instructions.

### 7.2.9. Thin layer chromatography (TLC)

Lipids were resolved on 20 x 10 cm silica high-performance TLC plates (Merck) using chloroform/methanol/water 60:35:8 (v/v/v) or chloroform/methanol/acetic acid/water 60:50:1:4 (v/v/v).  $^{14}\text{C}$ - and  $^{32}\text{P}$ -labelled lipids were revealed by phosphorimaging on a BAS 1800 II bioimager (Fuji), and quantified using the Image Gauge V3.3 software (Fuji). When non-radioactive samples were analysed, lipids were visualised by sulfuric acid spraying. Lipids were identified by co-migration with synthetic standards (Avanti) and by susceptibility to mild alkaline hydrolysis (see 7.2.7.).

### 7.2.10. Mass spectrometric analysis of phosphatidylcholine

Mass spectrometric analysis was performed using multiple precursor ion scanning (MPIS) (Ekroos et al., 2002). To enable quantitative analysis of different samples, each sample was spiked with an equal amount of  $^{13}\text{C}$ -labelled lipid extract from *P. pastoris* as internal standard. For detection of phosphatidylcholine (PC), MPIS was performed in positive ion mode with the selected characteristic fragment ion of the choline head group. To determine percent fractions, the peak area of individual PC species was divided by the sum peak area of all PC species. To determine relative concentrations, the peak area of individual PC species was divided by the sum peak area of a selected set of five  $^{13}\text{C}$ -labelled PC species as internal standard.

### 7.3. Molecular biology methods

#### 7.3.1. Cloning of retroviral RVH1 vectors

To create pRVH1-puro, the puromycin resistance gene of pSVpaX1 (Buchholz et al., 1996; provided by Frank Buchholz, Max-Planck-Institute of Molecular Cell Biology and Genetics, Dresden, Germany) was amplified by PCR, introducing XbaI and NotI restriction sites in the process. The PCR product was cloned into the XbaI/NotI site of pRVH1 (Barton and Medzhitov, 2002; provided by Ruslan Medzhitov, Howard Hughes Medical Institute, Yale University, New Haven), replacing the CD4 gene of the original vector. By the same procedure, pRVH1-hygro was created by inserting the hygromycin resistance gene of pRAD54B-hyg (Miyagawa et al., 2002; provided by Kiyoshi Miyagawa, Department of Molecular Pathology, University of Hiroshima, Hiroshima, Japan) into pRVH1, and pRVH1-RFP was created by inserting the mRFP sequence of pRFP-GL-GPI (provided by Aki Manninen, Max-Planck-Institute of Molecular Cell Biology and Genetics, Dresden, Germany) into pRVH1. To generate pRVH1-GFP vectors, the GFP gene of pEGFP-N2 (Clontech) was excised with NheI/NotI and inserted into the XbaI/NotI side of pRVH1 vectors already containing shRNA oligonucleotides.

#### 7.3.2. Cloning of adenoviral pAdeasy-RFP-rab10 vectors

The coding sequence of canine rab10 was excised from pGEM-rab10 (provided by Marino Zerial, Max-Planck-Institute of Molecular Cell Biology and Genetics, Dresden, Germany) using SacI/PstI and inserted into the SacI/PstI site of pEGFP-C1 (Clontech), thus generating pGFP-rab10 which encodes N-terminally GFP-tagged rab10. Point mutations generating pGFP-rab10 Q67L and pGFP-rab10 T23N, which encode constitutively active and constitutively inactive mutants of rab10, respectively, were introduced using the QuikChange site-directed mutagenesis kit (Stratagene) according to the manufacturer's instructions. The GFP tag of wild type and mutant rab10 was replaced by mRFP by insertion of the AgeI/BsrGI fragment of pRFP-GL-GPI into the AgeI/BsrGI sites of pGFP-rab10, pGFP-rab10 Q67L and pGFP-rab10 T23N, generating pRFP-rab10, pRFP-rab10 Q67L and pRFP-rab10 T23N. Subsequent cloning of pAdeasy vectors was done as suggested by the AdEasy manual (Qbiogene). The coding sequences of wild type and mutant rab10 was excised from pRFP-rab10, pRFP-rab10 Q67L and pRFP-rab10 T23N

using NheI/XbaI and cloned into the XbaI site of pShuttle-CMV (Qbiogene), generating pShuttle-RFP-rab10, pShuttle-RFP-rab10 Q67L and pShuttle-RFP-rab10 T23N. The plasmids were linearised with PmeI and used for transformation of BJ5183-AD-1 electrocompetent cells (Stratagene). Correct recombination to yield pAdeasy-RFP-rab10, pAdeasy-RFP-rab10 Q67L, and pAdeasy-RFP-rab10 T23N was confirmed by PacI digest. Plasmids were linearised with PacI and transfected into QBI-293A cells (see 7.4.3.).

### 7.3.3. Design of shRNAs and cloning into retroviral RVH1 vectors

As a complete and assembled dog genome sequence is not yet available, the coding sequence of several target genes had to be re-constructed from partial sequences, which were obtained from the NCBI canis familiaris trace archive using the discontinuous Mega BLAST search tool (<http://www.ncbi.nlm.nih.gov/BLAST/tracemb.shtml>). Unique sequences conforming to either AAN<sub>19</sub> as suggested by Elbashir and co-workers (Elbashir et al., 2002) or to GN<sub>20</sub> were selected. Target sequences containing EcoRI or XhoI sites (which would interfere with the subsequent cloning), TTT at their 3' end (which would create a cluster of transcription-terminating thymidines), or stretches of more than three identical bases (which have been proposed to reduce RNAi efficiency) were avoided. Oligonucleotides encoding shRNAs directed against the different target genes were designed according to Brummelkamp et al., 2002 (see Figure 7.1.).

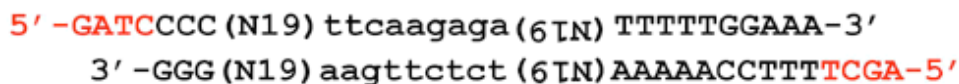


**Figure 7.1.** Design of shRNA oligonucleotides. The sense oligonucleotide (top strand) is shown in 5'-3' direction, the antisense oligonucleotide (bottom strand) in 3'-5' direction. The red sequences at 5' ends indicate the BglII and HindIII sites, which were used to clone the annealed shRNA oligonucleotides into pSUPER. Each oligonucleotide contains the target sequence in sense orientation (N19), followed by a short loop sequence, and the target sequence in antisense orientation. For target sequences conforming to AAN<sub>19</sub>, only the N19 sequence had to be incorporated into the shRNA oligonucleotides as the TT 3' overhang present in the siRNA that result from the processing of the expressed shRNAs provided the remaining two nucleotides (see Figure 4.4. for a schematic representation of the processing of expressed shRNA into siRNAs). For target sequences conforming to GN<sub>20</sub>, the full 21 nucleotide sequence was incorporated into the shRNA oligonucleotides. The shRNA oligonucleotides were thus 64 or 68 nucleotides long. From Brummelkamp et al., 2002.



To clone these oligonucleotides into RVH1 vectors, sense and antisense oligonucleotides were annealed, phosphorylated and cloned into the BglIII/HindIII site of dephosphorylated pSUPER (provided by Reuven Agami, The Netherlands Cancer Institute, Amsterdam). Positive colonies were identified by colony PCR using T3 and T7 primers, which yielded a 440 bp PCR product in case of correct insertion of the shRNA oligonucleotide, as opposed to a 380 bp PCR product in case of vector re-ligation. Integrity of the shRNA oligonucleotides was confirmed by sequencing with the T7 primer. The H1 expression cassette containing the shRNA oligonucleotide was then excised with EcoRI/XhoI and cloned into the EcoRI/XhoI site of pRVH1-puro, pRVH1-hygro, or pRVH1-RFP. Correct insertion was confirmed by DNA sequencing with the RVH1 sequencing primer (TACATCGTGACCTGGGAAGC).

#### *7.3.4. RNA isolation and cDNA synthesis*

RNA isolation was done with the RNeasy kit (Qiagen) according to the manufacturer's instructions. RNA was eluted in 30  $\mu$ l RNase-free water (Qiagen). To remove potential contaminations with genomic DNA, the RNA solution was treated with 10 U RNase-free DNase I (Boehringer) in DNase buffer (40 mM Tris, 10 mM NaCl, 6 mM MgCl<sub>2</sub> in RNase-free water, pH 7.5) at 37°C for 30 min, followed by a 20 min incubation at 65°C to denature the DNase. For photometric RNA determination, RNA was diluted 1:50 in water.

For cDNA synthesis, 1  $\mu$ l 0.5 mg/ml oligo-(dT) was added to 1  $\mu$ g RNA, and the volume was adjusted to 12  $\mu$ l with RNase-free water. For destruction of secondary structures, the sample was heated to 70°C for 10 min, cooled on ice and spun down. cDNA synthesis was carried out with 200 U M-MLV reverse transcriptase (Promega) at 42°C for 50 min in a 20  $\mu$ l reaction mix containing the RNA, the oligo-(dT) primer, 50 mM Tris, 75 mM KCl, 3 mM MgCl<sub>2</sub>, pH 8.3, 10 mM DTT and 1 mM of each dNTP. The reverse transcriptase was inactivated by a 15 min incubation at 70°C, and samples were diluted 1:10 with water.

#### *7.3.5. Quantitative real time-PCR (QRT-PCR)*

QRT-PCR, as it was used here, relies on the intercalation of the fluorescent dye SYBR Green into double-stranded DNA, which results in a shift in its fluorescence. The amounts

of PCR product after each amplification cycle can thus be determined by measuring the fluorescence that stems from SYBR Green bound to double-stranded DNA. Provided the amount of PCR product doubles with each amplification cycle, the resulting amplification curves allow the calculation of the levels of an mRNA of interest relative to an internal standard, usually an abundant mRNA of a house keeping gene.

For each reaction, 2  $\mu$ l of cDNA were mixed with 1.2  $\mu$ l forward and reverse primers (2.5  $\mu$ M stock solutions, resulting in final concentrations of 300 nM), 0.6  $\mu$ l water and 5  $\mu$ l 2x SYBR Green master mix (Applied Biosystems). For each cDNA and primer pair, duplicate reactions were performed. The PCR was performed using Mx3000 96-well PCR plates (Stratagene) on an Mx3000 QRT-PCR system (Stratagene) with an annealing temperature of 60°C. Table 7.2. lists the primers used.

<b>Gene</b>	<b>Forward primer</b>	<b>Reverse primer</b>
annexin 2	GCATCAGCATTGAAGTCAGCC	CAGGTGTTTTCAATAGGCCCA
annexin 13a/b	ACTGCTGGTGGCCCTCTTG	TTGACAAAGGTGGCTTCTCCA
annexin 13b	AGAAGGCAGTCAACAGTTGCC	GATGGGTGGCTGAGAGGCT
caveolin-1	CACCAAGGAAATCGACCTGG	CAATCTTGACCACGTCGTCGT
KIFC3	TCCGCAACTCCAAGCTCAC	ACCACCATGAGGGTCTTGCT
MAL2	TGTTTCGTGCCGTGACAGCT	GAGTCACCATGCCAGAGAGGA
rab 8a	CACAGCTGGTCAAGAACGGTT	CAGCATGATGCCATTGC
rab 11a	GGCACAGATATGGGACACAGC	GGCACCTACAGCTCCACGAT
rab 11b	ATTGTGTCACAGAAGCAGATTGC	CTGATGTCCACCACGTTGTTG
syntaxin 3	TGGATGAGTTCTTCGCCGAG	CACGTGCTCCGAGATCTTGTC
TI-VAMP	GAGCACAGACAGCACTCCCAT	ATGCTTCAACTGTGCAGCCA
ubiquitin	TCCAAGACAAGGAGGGCATC	TTCTAGCTGTTTGCCCGCA
VIP17	CCTGGATGCAGCCTACCACT	GCCAAAGCTTCCAGCACAG
VIP36	GGAACCTTGGCCTTATTACCCT	AATTGCTCCTCCAGCCACAC

Relative mRNA levels in samples from control and knockdown cells were determined as follows. First, cycle threshold (ct) values, which indicate the cycle at which the amount of PCR product rises significantly over background levels, were determined for each reaction using the Mx3000 software (Stratagene). Average cycle threshold values were calculated for each duplicate. Next, the average cycle threshold values for a given primer pair were normalised to the amount of cDNA used for the PCR reaction. This was done by subtracting the average cycle threshold value for ubiquitin, the internal standard mRNA,

from the average cycle threshold value for the mRNA of interest, yielding  $\Delta\text{Ct}$  values. To compare the levels of a given mRNA between two cDNAs, for example between cDNAs derived from control and knockdown cells,  $\Delta\Delta\text{Ct}$  values were determined by subtracting the  $\Delta\text{Ct}$  value of the control cDNA from the  $\Delta\text{Ct}$  value of the knockdown cDNA. Positive  $\Delta\Delta\text{Ct}$  values indicated that in the knockdown sample the amount of PCR product resulting from the mRNA of interest reached the threshold at a later cycle than in the control sample, i.e. that the starting amounts of cDNA of the gene of interest were lower in the knockdown than in the control sample. Finally, the  $\Delta\Delta\text{Ct}$  values, which are on a logarithmic scale due to the exponential increase of product during the PCR, were converted to relative mRNA levels, which are on a linear scale. This was done using the relation  $\text{mRNA levels} = 2^{-\Delta\Delta\text{Ct}}$ .

Whenever a new primer pair was established for a given gene, the following tests were carried out to ensure that the primers led to a duplication of the amount of PCR product with each cycle. PCR reactions were carried out using a dilution series of cDNA from untreated MDCK cells, ranging from 2  $\mu\text{l}$  to 0.125  $\mu\text{l}$ . In addition, a no template control was included to detect the possible formation of primer dimers. Provided a single PCR product of the right size was detected on 2.5% agarose gels in all samples except for the no template control, the relative mRNA concentrations in each sample were calculated from the cycle threshold values (relative mRNA levels =  $2^{-\text{Ct}}$ ) and plotted against the amount of cDNA used. Ideally, a straight line with unity slope should result. Primers were regarded as acceptable if the slope was between 0.95 and 1, and the linear fit better than  $R^2 = 0.98$ .

### 7.3.6. Internal energy calculation

Internal energy profiles of siRNA duplexes, as well as the duplex stabilities at the 5' ends of sense and antisense strands were calculated with the RNAstructure 3.71 software using the OligoWalk program (Zuker, 2003; <http://www.bioinfo.rpi.edu/applications/mfold>). Starting from the 5' end of the antisense strand, pentamer hybridisation energies along the length of the siRNA duplexes were determined. Depending on the target sequence format (AAN<sub>19</sub> or GN<sub>20</sub>, see 7.3.3.), the duplexed regions were 19 or 21 nucleotides long, giving 15 or 17 pentamer hybridisation energies. These were then used to construct internal

energy profiles. This procedure is similar to the one used by Khvorova et al., 2003, except that the sequences were not extended at the 3' end. The duplex stabilities at the 5' ends of sense and antisense strands were likewise calculated on the basis of pentamer hybridisation energies.

#### **7.4. Virus techniques**

##### *7.4.1. Production of retroviruses*

Nearly confluent Phoenix gag-pol cells in 6-wells were transfected with 4 µg pRVH1-puro, pRVH1-hygro, pRVH1-GFP or pRVH1-RFP and 0.4 µg pMD.G (which expresses the vesicular stomatitis virus glycoprotein under control of the human CMV immediate-early promoter, provided by Richard Mulligan, Harvard Medical School, Boston) using Lipofectamine 2000 (Invitrogen) according to the manufacturer's protocol. 24 h post transfection, the medium was changed to low glucose DMEM (1 g/L, PAA Laboratories) containing 10% FCS, 2 mM glutamine and 100 U/ml penicillin/streptomycin (1 ml per 6-well), and placed at 32°C. 48 h post transfection the medium was collected, centrifuged at 200 xg for 5 min to remove cell debris and used for infection of MDCK cells.

For producing virus stocks, Phoenix gag-pol cells on 10 cm dishes were transfected with 24 µg retroviral vector and 2.4 µg pMD.G, the medium was changed to low glucose DMEM (5 ml per dish) 24 hours post transfection, and cells were placed at 32°C. Batches of virus-containing supernatant were collected every 24 hours for up to seven days. The supernatant was passed through a 0.45 µm syringe filter and frozen in liquid nitrogen.

Where indicated, the virus was concentrated immediately before infection. For this, virus-containing supernatant was transferred into SW40 tubes, the total volume was brought to at least 10 ml with MEM, and 1 M HEPES pH 7.4 was added to a final concentration of 10 mM. The virus was pelleted by centrifugation at 16,800 rpm (50,000 xg) for 1.5 h. The supernatant was removed, and an appropriate volume of MEM containing 5% FCS and 10 mM HEPES was added to the pellet. The centrifugation tube was incubated at 4°C for at least 1 h to loosen the pellet, and the virus was resuspended by gentle pipetting.

#### 7.4.2. Retroviral transduction of MDCK cells

For infection,  $1.5 \times 10^5$  MDCK cells were mixed with 450  $\mu$ l virus containing supernatant in the presence of 4  $\mu$ g/ml polybrene (Sigma), seeded into 12-wells, and incubated at 32°C. 12 post infection, the medium was changed to normal culture medium, and cells were returned to 37°C. 36 to 48 h post infection, cells were trypsinised and seeded into 6-wells in the presence of 4  $\mu$ g/ml puromycin or 800  $\mu$ g/ml hygromycin (both from BD Biosciences). Selection was done for 48 or 60 h, respectively. For double knockdowns, cells were sequentially infected with RVH1-puro virus, selected with puromycin, infected with RVH1-hygro virus, and selected with hygromycin as above.

#### 7.4.3. Generation and amplification of adenoviruses

For the generation of adenoviruses, confluent QBI-293A cells in 6-wells were transfected with 5  $\mu$ g PacI-linearised pAdeasy vector using Lipofectamine 2000 according to the manufacturer's protocol. After seven days, cells were collected, pelleted by centrifugation at 500  $\times$ g at 4 °C for 5 min and resuspended in 2 ml OptiMEM (Invitrogen). Cells were disrupted and recombinant adenovirus released by four freeze-thaw cycles. Cell debris was removed by centrifugation at 2500  $\times$ g at 4°C for 10 min. For the first round of amplification, the supernatant was used for infection of QBI-293A cells on 10 cm dishes. When at least half of the cells had detached, cells were collected and subjected to lysis by freeze-thawing. One and eight 175 cm<sup>2</sup> flasks QBI-293A cells were used for the second and third amplification round, respectively.

For the final preparation, infected QBI-293A cells from eight 175 cm<sup>2</sup> flasks were collected when at least half of the cells had detached, pelleted by centrifugation, and resuspended in 8 ml OptiMEM. After freeze-thawing and removal of cells debris, 4 ml supernatant each were placed on top of two 8 ml Optiprep gradients in SW40 centrifugation tubes consisting of steps of 15, 25, 40 and 54% (w/v) iodixanol. Gradients were centrifuged at 31,500 rpm (177,000  $\times$ g) at 4°C over night. The virus bands were collected, mixed with 1 volume 90% (v/v) glycerol and 1 volume 3x adenovirus storage buffer (15 mM Tris pH 8.0, 150 mM NaCl, 0.15% (w/v) BSA, 50% (v/v) glycerol), and stored at -20°C.

## 7.5. Cell biology methods

### 7.5.1. Immunofluorescence

MDCK cells grown on 11 mm glass cover slips were washed once with PBS and fixed with 4% (w/v) paraformaldehyde at room temperature for 20 min. Unreacted paraformaldehyde was quenched with 50 mM NH<sub>4</sub>Cl in PBS for 10 min. Cells were washed three times with PBS and permeabilised with saponin or Triton X-100. If saponin was used, cells were permeabilised and blocked in one step by a 10 min incubation with PBS-SG (0.1% (w/v) saponin from Quillaja Bark (Sigma), 0.2% (w/v) Teleostan gelatin (Sigma) in PBS). In the case of Triton X-100, cells were treated with 0.1% (w/v) Triton X-100 (Serva) in PBS for 5 min, washed three times with PBS, and blocked with PBS-G (PBS with 0.5% (w/v) BSA and 0.2% (w/v) gelatin) for 20 min. The coverslips were dried and placed upside down on 20 µl droplets of PBS containing the primary antibody (PBS-SG was used instead of PBS for this and all subsequent steps when the permeabilisation had been done with saponin). Table 7.3. lists the primary antibodies used, the sources they were obtained from, and their working dilutions.

Antigen	Antibody	Source	Dilution
caveolin-1	N20 rabbit anti-human caveolin-1	Santa Cruz	1:200
E-cadherin	rr1 mouse anti-dog E-cadherin	Simons lab (Gumbiner and Simons, 1986)	1:40
giantin	mouse anti-human giantin	Hans-Peter Hauri (Linstedt and Hauri, 1993)	1:1000
gp114	4.6.5. mouse anti-dog gp114	Simons lab (Balcarova-Ständer et al., 1984)	1:50
gp135	mouse anti-dog gp135	George Ojakian (Ojakian and Schwimmer, 1988)	1:200
p58	6.23.3 mouse anti-dog p58	Simons lab (Balcarova-Ständer et al., 1984)	1:50
PLAP	4679 rabbit anti-human PLAP	Simons lab (Verkade et al., 2000)	1:200

The coverslips were incubated for 60 min in a moist chamber, transferred into 24-well plates and washed three times with PBS. The PBS was removed and 250 µl PBS were added containing secondary antibodies conjugated to Cy3 or FITC (Jackson Immuno Research), diluted 1:1000 and 1:250, respectively. After a 1 h incubation, coverslips were

washed three times with PBS, once with water, and mounted on a droplet of Mowiol containing 100 mg/ml DABCO. The Mowiol was allowed to dry at room temperature over night, the coverslips were sealed with nail polish and stored at -20°C.

Images were acquired with an Olympus BX-61 fluorescence microscope (Olympus) or an Leica TCS SP2 laser scanning confocal microscope (Leica Microsystems).

#### *7.5.2. Transferrin uptake assay*

MDCK cells were seeded onto coverslips and grown over night so that they reached approximately 50% confluence. They were washed twice with PBS and starved in MEM for 3 h. Coverslips were dried and placed upside down on 25 µl droplets of internalisation medium (DMEM with 10 mM HEPES pH 7.25, 2 mg/ml BSA) containing 60 µg/ml iron-loaded dog transferrin (Sigma) coupled to Alexa-488 (Molecular Probes). Cells were allowed to take up transferrin at 37°C for 10 min, washed twice with ice cold PBS by dipping, and fixed with 4% (w/v) paraformaldehyde.

To quantify internalised Alexa-transferrin, fluorescence images were acquired with an Olympus BX-61 fluorescence microscope (Olympus) using a magnification of 40x and identical settings for all images. Cells at the edges of cell islands took up transferrin more efficiently than those at the centres. Therefore, images were taken only from the centres of cell islands in such a way that the entire field was filled with cells. The total fluorescence intensity of each image was quantified using the IpLab software (Scanalytics). The fluorescence intensities from 20 images per coverslip were averaged. The experiment was performed in triplicate, and the average fluorescence per condition was calculated from the average values for each of the three coverslips.

#### *7.5.3. Hemagglutinin transport assay*

The hemagglutinin (HA) transport assay (Matlin and Simons, 1984) uses the fact that infection with influenza virus leads to a shut-off of host protein synthesis. Subsequent radioactive pulse-labelling therefore labels only viral proteins. Labelled viral membrane proteins can be accumulated in the TGN by incubation at 19.5°C and then chased to the

cell surface at 37°C as a synchronous wave. Using a virus that encodes the N variant of HA allows cell surface HA to be distinguished from intracellular HA by trypsin treatment at the end of the chase. This HA variant is inefficiently cleaved by the TGN-localised protease furin so that intracellular HA is unprocessed, whereas surface HA can be cleaved by trypsin into two fragments, HA<sub>1</sub> and HA<sub>2</sub>. Figure 7.2. gives an overview of the assay.

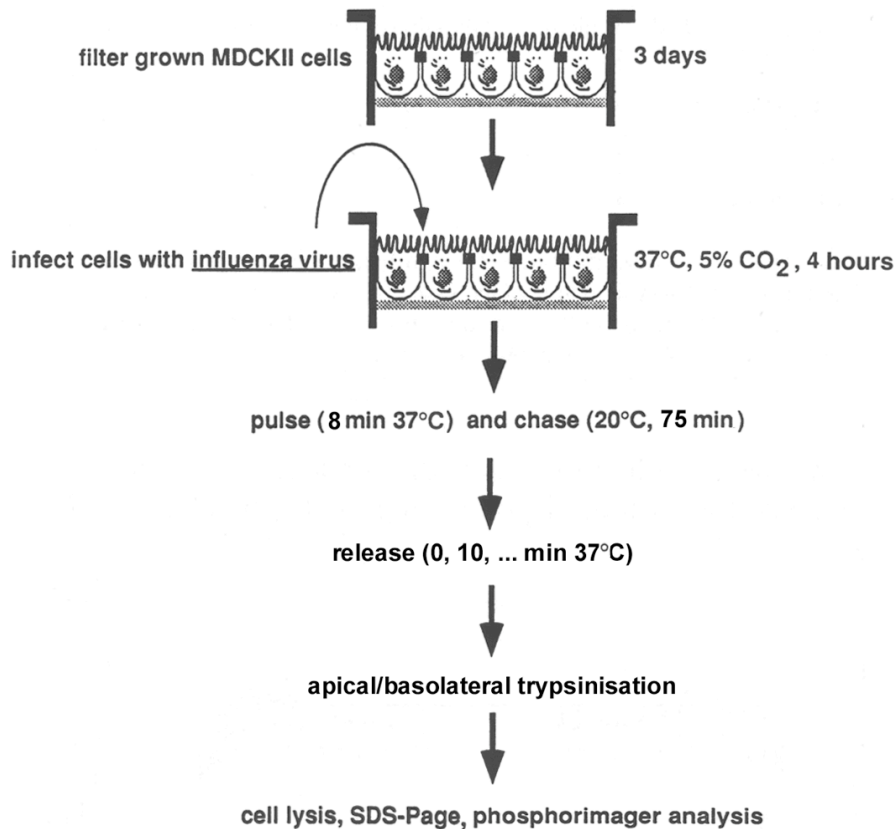


**Figure 7.2.** Influenza virus hemagglutinin transport assay. Filter grown MDCK are infected with influenza virus, followed by a 4 h incubation to allow the virus to shut off host protein synthesis. Newly synthesised proteins are pulse-labelled for 8 min with <sup>35</sup>S-methionine. Labelled proteins are accumulated in the TGN by incubation at 20°C for 75 min. They are then released and chased to the cell surface at 37°C. Transport is stopped by incubation on ice, and surface hemagglutinin is cleaved by trypsinisation from the apical or basolateral side. Cells are lysed, the cell lysate is separated by SDS-PAGE, and radioactively labelled proteins are revealed by autoradiography.

MDCK cells were grown on 12 mm filters for 3 days to allow full polarisation. For infection with influenza virus, cells were washed twice with PBS containing 0.5 mM magnesium and 1 mM calcium (PBS+) by dipping, and once with pre-warmed infection



medium (MEM with 50 mM HEPES pH 7.3, 100 U/ml penicillin, 100 µg/ml streptomycin, 2 mM glutamine). Per filter, 10 to 20 plague-forming units fowl-plague virus N20 were diluted in 100 µl infection medium and used for infection from the apical side. After a 1 h incubation at 37°C, 750 µl and 1.5 ml infection medium were added to the apical and basolateral side, respectively. Cells were incubated for 4 h to allow host protein shut-off. Filters were washed twice with pre-warmed PBS+ by dipping, 500 µl pre-warmed labelling medium (methionine-free MEM containing 0.35 g/l sodium bicarbonate, 50 mM HEPES pH 7.3 and 2 mM glutamine) were added to the apical side, and filters were placed onto 20 µl droplets of labelling medium containing 10 µCi <sup>35</sup>S-methionine. After 8 min incubation at 37°C, filters were washed twice with room temperature PBS+, chase medium (labelling medium supplemented with 150 µg/ml methionine and 20 µg/ml cycloheximide) was added to both the apical and basolateral side. Labelled protein was either directly chased to the cell surface at 37°C, or first accumulated in the TGN by incubating the cells at 19.5°C for 75 min. Medium was removed, replaced by fresh chase medium pre-warmed to 37°C, and labelled proteins were chased to the cell surface by incubation at 37°C. At the end of the chase, cells were washed twice with ice-cold PBS+ and treated with 0.1 mg/ml TPCK-treated trypsin (Worthington Biochemical Corporation) from the apical or basolateral side at 4°C for 30 min. Trypsin was inactivated by addition of soy bean trypsin inhibitor (Sigma) to a final concentration of 0.1 mg/ml. Cells were washed three times for 5 min with PBS+ containing 0.1 mg/ml trypsin inhibitor. Filters were excised from the plastic holders and cells were lysed as described under 7.2.1. using 200 µl lysis buffer. 40 µl aliquots of the lysates were separated on 10% SDS-PAGE gels. Gels were dried, and radioactive proteins were detected and quantified by phosphorimager analysis as described under 7.2.9.

The transport efficiency of HA can be calculated by dividing the radioactivity of the HA cleavage products by the radioactivity of the uncleaved HA. The cleavage products HA<sub>1</sub> and HA<sub>2</sub> remain associated through a disulfide bond, so that no label is lost to the medium. Hence, % surface transport is given by  $100 \times (HA_1 + HA_2) / (HA + HA_1 + HA_2)$ . As both HA<sub>1</sub> and HA<sub>2</sub> contain seven methionine residues, % surface transport can alternatively be obtained by  $100 \times (2 \times HA_1) / (HA + 2 \times HA_1)$ .

#### 7.5.4. Surface transport of adenovirally expressed marker proteins

$5 \times 10^4$  MDCK cells each were seeded onto 11 mm glass coverslips placed into wells of a 24-well plate (1.9 cm<sup>2</sup> surface area) and grown for 2.5 days. Cells were infected with adenoviruses encoding basolaterally targeted VSV-G-GFP (referred to as bVSV-G, Keller et al., 2001), apically targeted VSV-G-GFP, in which the tyrosine-based basolateral sorting determinant is mutated (referred to as aVSV-G, provided by Aki Manninen, Max-Planck-Institute of Molecular Cell Biology and Genetics, Dresden, Germany), apically targeted M2-HA-YFP, in which the cytoplasmic tail of the influenza virus M2 protein is fused to HA (referred to as M2-HA, provided by Patrick Keller, Max-Planck-Institute of Molecular Cell Biology and Genetics, Dresden, Germany) or apically targeted, glycosylated GPI-GL-GFP (referred to as GPI-GFP, Keller et al., 2001) in 250  $\mu$ l OptiMEM at 37°C for 1 h (M2-HA and GPI-GFP) or 2 h (bVSV-G and aVSV-G). Cells infected with virus encoding bVSV-G or aVSV-G were then incubated at 39.5°C for 6 h to accumulate the VSV-G variants in the ER, the medium was changed to normal culture medium containing 20  $\mu$ g/ml cycloheximide (Sigma), and VSV-G was chased to the cell surface at 32°C for 0, 20, 40 and 60 min (bVSV-G) or 0, 30, 50 and 70 min (aVSV-G). Cells infected with virus encoding M2-HA were incubated at 37°C for 8 h, the medium was changed to CO<sub>2</sub>-independent medium containing 20  $\mu$ g/ml cycloheximide, cells were transferred to 19.5°C for 2 h to accumulate M2-HA in the TGN, and the protein was chased to the cell surface at 37°C for 0, 15, 30 and 60 min. Cells infected with virus encoding GPI-GFP were incubated at 37°C for 5 h, the medium was changed to CO<sub>2</sub>-independent medium containing 20  $\mu$ g/ml cycloheximide, cells were transferred to 19.5°C for 1 h to accumulate GPI-GFP in the TGN, and the protein was chased to the cell surface at 37°C for 0, 20, 40 and 60 min. Following the chase, cells were fixed in ice-cold 4% (w/v) paraformaldehyde and processed for immunofluorescence as described under 7.5.1.

## 8. References

- Abrami, L., and F.G. van Der Goot. 1999. Plasma membrane microdomains act as concentration platforms to facilitate intoxication by aerolysin. *J Cell Biol.* 147:175-84.
- Ahmed, S.N., D.A. Brown, and E. London. 1997. On the origin of sphingolipid/cholesterol-rich detergent-insoluble cell membranes: physiological concentrations of cholesterol and sphingolipid induce formation of a detergent-insoluble, liquid-ordered lipid phase in model membranes. *Biochemistry.* 36:10944-53.
- Al-Awqati, Q. 2003. Terminal differentiation of intercalated cells: the role of hensin. *Annu Rev Physiol.* 65:567-83.
- Altschuler, Y., C. Hodson, and S.L. Milgram. 2003. The apical compartment: trafficking pathways, regulators and scaffolding proteins. *Curr Opin Cell Biol.* 15:423-9.
- Ang, A.L., H. Folsch, U.M. Koivisto, M. Pypaert, and I. Mellman. 2003. The Rab8 GTPase selectively regulates AP-1B-dependent basolateral transport in polarized Madin-Darby canine kidney cells. *J Cell Biol.* 163:339-50.
- Ang, L.A., T. Taguchi, S. Francis, H. Folsch, L. Murrells, M. Pypaert, G. Warren, and I. Mellman. in press. Recycling endosomes can serve as intermediates during transport from the Golgi to the plasma membrane of MDCK cells. *J Cell Biol.*
- Aza-Blanc, P., C.L. Cooper, K. Wagner, S. Batalov, Q.L. Deveraux, and M.P. Cooke. 2003. Identification of modulators of TRAIL-induced apoptosis via RNAi-based phenotypic screening. *Mol Cell.* 12:627-37.
- Bagnat, M., A. Chang, and K. Simons. 2001. Plasma membrane proton ATPase Pma1p requires raft association for surface delivery in yeast. *Mol Biol Cell.* 12:4129-38.
- Bagnat, M., and K. Simons. 2002. Cell surface polarization during yeast mating. *Proc Natl Acad Sci U S A.* 99:14183-8.
- Balcarova-Stander, J., S.E. Pfeiffer, S.D. Fuller, and K. Simons. 1984. Development of cell surface polarity in the epithelial Madin-Darby canine kidney (MDCK) cell line. *Embo J.* 3:2687-94.
- Barman, S., and D.P. Nayak. 2000. Analysis of the transmembrane domain of influenza virus neuraminidase, a type II transmembrane glycoprotein, for apical sorting and raft association. *J Virol.* 74:6538-45.
- Bartel, D.P. 2004. MicroRNAs: genomics, biogenesis, mechanism, and function. *Cell.* 116:281-97.
- Barton, G.M., and R. Medzhitov. 2002. Retroviral delivery of small interfering RNA into primary cells. *Proc Natl Acad Sci U S A.* 99:14943-5.
- Bastaki, M., L.T. Braiterman, D.C. Johns, Y.H. Chen, and A.L. Hubbard. 2002. Absence of direct delivery for single transmembrane apical proteins or their "Secretory" forms in polarized hepatic cells. *Mol Biol Cell.* 13:225-37.
- Baumgart, T., S.T. Hess, and W.W. Webb. 2003. Imaging coexisting fluid domains in biomembrane models coupling curvature and line tension. *Nature.* 425:821-4.
- Beitel, G.J., and M.A. Krasnow. 2000. Genetic control of epithelial tube size in the *Drosophila* tracheal system. *Development.* 127:3271-82.
- Benharouga, M., M. Sharma, J. So, M. Haardt, L. Drzymala, M. Popov, B. Schwapach, S. Grinstein, K. Du, and G.L. Lukacs. 2003. The role of the C terminus and Na<sup>+</sup>/H<sup>+</sup> exchanger regulatory factor in the functional expression of cystic fibrosis

- transmembrane conductance regulator in nonpolarized cells and epithelia. *J Biol Chem.* 278:22079-89.
- Benting, J.H., A.G. Rietveld, I. Ansorge, and K. Simons. 1999a. Acyl and alkyl chain length of GPI-anchors is critical for raft association in vitro. *FEBS Lett.* 462:47-50.
- Benting, J.H., A.G. Rietveld, and K. Simons. 1999b. N-Glycans mediate the apical sorting of a GPI-anchored, raft-associated protein in Madin-Darby canine kidney cells. *J Cell Biol.* 146:313-20.
- Bock, J.B., H.T. Matern, A.A. Peden, and R.H. Scheller. 2001. A genomic perspective on membrane compartment organization. *Nature.* 409:839-41.
- Bohuslav, J., T. Cinek, and V. Horejsi. 1993. Large, detergent-resistant complexes containing murine antigens Thy-1 and Ly-6 and protein tyrosine kinase p56lck. *Eur J Immunol.* 23:825-31.
- Bomsel, M., K. Prydz, R.G. Parton, J. Gruenberg, and K. Simons. 1989. Endocytosis in filter-grown Madin-Darby canine kidney cells. *J Cell Biol.* 109:3243-58.
- Braccia, A., M. Villani, L. Immerdal, L.L. Niels-Christiansen, B.T. Nystrom, G.H. Hansen, and E.M. Danielsen. 2003. Microvillar membrane microdomains exist at physiological temperature. Role of galectin-4 as lipid raft stabilizer revealed by "superrafts". *J Biol Chem.* 278:15679-84.
- Bretscher, M.S., and S. Munro. 1993. Cholesterol and the Golgi apparatus. *Science.* 261:1280-1.
- Brewer, C.F., M.C. Miceli, and L.G. Baum. 2002. Clusters, bundles, arrays and lattices: novel mechanisms for lectin-saccharide-mediated cellular interactions. *Curr Opin Struct Biol.* 12:616-23.
- Bridge, A.J., S. Pebernard, A. Ducraux, A.L. Nicoulaz, and R. Iggo. 2003. Induction of an interferon response by RNAi vectors in mammalian cells. *Nat Genet.* 34:263-4.
- Brown, D.A., B. Crise, and J.K. Rose. 1989. Mechanism of membrane anchoring affects polarized expression of two proteins in MDCK cells. *Science.* 245:1499-501.
- Brown, D.A., and E. London. 1998. Functions of lipid rafts in biological membranes. *Annu Rev Cell Dev Biol.* 14:111-36.
- Brown, D.A., and J.K. Rose. 1992. Sorting of GPI-anchored proteins to glycolipid-enriched membrane subdomains during transport to the apical cell surface. *Cell.* 68:533-44.
- Brown, P.S., E. Wang, B. Aroeti, S.J. Chapin, K.E. Mostov, and K.W. Dunn. 2000. Definition of distinct compartments in polarized Madin-Darby canine kidney (MDCK) cells for membrane-volume sorting, polarized sorting and apical recycling. *Traffic.* 1:124-40.
- Brummelkamp, T.R., R. Bernards, and R. Agami. 2002. A system for stable expression of short interfering RNAs in mammalian cells. *Science.* 296:550-3.
- Buchholz, F., P.O. Angrand, and A.F. Stewart. 1996. A simple assay to determine the functionality of Cre or FLP recombination targets in genomic manipulation constructs. *Nucleic Acids Res.* 24:3118-9.
- Bunnell, S.C., D.I. Hong, J.R. Kardon, T. Yamazaki, C.J. McGlade, V.A. Barr, and L.E. Samelson. 2002. T cell receptor ligation induces the formation of dynamically regulated signaling assemblies. *J Cell Biol.* 158:1263-75.
- Cambi, A., F. De Lange, N.M. Van Maarseveen, M. Nijhuis, B. Joosten, E.M. Van Dijk, B.I. De Bakker, J.A. Fransen, P.H. Bovee-Geurts, F.N. Van Leeuwen, N.F. Van Hulst, and C.G. Figdor. 2004. Microdomains of the C-type lectin DC-SIGN are portals for virus entry into dendritic cells. *J Cell Biol.* 164:145-55.

- Chen, W., Y. Feng, D. Chen, and A. Wandinger-Ness. 1998. Rab11 is required for trans-golgi network-to-plasma membrane transport and a preferential target for GDP dissociation inhibitor. *Mol Biol Cell*. 9:3241-57.
- Chen, Y.T., C. Holcomb, and H.P. Moore. 1993. Expression and localization of two low molecular weight GTP-binding proteins, Rab8 and Rab10, by epitope tag. *Proc Natl Acad Sci U S A*. 90:6508-12.
- Cheong, K.H., D. Zacchetti, E.E. Schneeberger, and K. Simons. 1999. VIP17/MAL, a lipid raft-associated protein, is involved in apical transport in MDCK cells. *Proc Natl Acad Sci U S A*. 96:6241-8.
- Cherukuri, A., R.H. Carter, S. Brooks, W. Bornmann, R. Finn, C.S. Dowd, and S.K. Pierce. 2004. B cell signaling is regulated by induced palmitoylation of CD81. *J Biol Chem*.
- Christoforidis, S., and M. Zerial. 2000. Purification and identification of novel Rab effectors using affinity chromatography. *Methods*. 20:403-10.
- Crane, J.M., and L.K. Tamm. 2004. Role of cholesterol in the formation and nature of lipid rafts in planar and spherical model membranes. *Biophys J*. 86:2965-79.
- de Marco, M.C., F. Martin-Belmonte, L. Kremer, J.P. Albar, I. Correas, J.P. Vaerman, M. Marazuela, J.A. Byrne, and M.A. Alonso. 2002. MAL2, a novel raft protein of the MAL family, is an essential component of the machinery for transcytosis in hepatoma HepG2 cells. *J Cell Biol*. 159:37-44.
- Dietrich, C., L.A. Bagatolli, Z.N. Volovyk, N.L. Thompson, M. Levi, K. Jacobson, and E. Gratton. 2001. Lipid rafts reconstituted in model membranes. *Biophys J*. 80:1417-28.
- Drab, M., P. Verkade, M. Elger, M. Kasper, M. Lohn, B. Lauterbach, J. Menne, C. Lindschau, F. Mende, F.C. Luft, A. Schedl, H. Haller, and T.V. Kurzchalia. 2001. Loss of caveolae, vascular dysfunction, and pulmonary defects in caveolin-1 gene-disrupted mice. *Science*. 293:2449-52.
- Drevot, P., C. Langlet, X.J. Guo, A.M. Bernard, O. Colard, J.P. Chauvin, R. Lasserre, and H.T. He. 2002. TCR signal initiation machinery is pre-assembled and activated in a subset of membrane rafts. *Embo J*. 21:1899-908.
- Dykxhoorn, D.M., C.D. Novina, and P.A. Sharp. 2003. Killing the messenger: short RNAs that silence gene expression. *Nat Rev Mol Cell Biol*. 4:457-67.
- Ekroos, K., I.V. Chernushevich, K. Simons, and A. Shevchenko. 2002. Quantitative profiling of phospholipids by multiple precursor ion scanning on a hybrid quadrupole time-of-flight mass spectrometer. *Anal Chem*. 74:941-9.
- Elbashir, S.M., J. Harborth, W. Lendeckel, A. Yalcin, K. Weber, and T. Tuschl. 2001a. Duplexes of 21-nucleotide RNAs mediate RNA interference in cultured mammalian cells. *Nature*. 411:494-8.
- Elbashir, S.M., J. Harborth, K. Weber, and T. Tuschl. 2002. Analysis of gene function in somatic mammalian cells using small interfering RNAs. *Methods*. 26:199-213.
- Elbashir, S.M., J. Martinez, A. Patkaniowska, W. Lendeckel, and T. Tuschl. 2001b. Functional anatomy of siRNAs for mediating efficient RNAi in *Drosophila melanogaster* embryo lysate. *Embo J*. 20:6877-88.
- Fiedler, K., F. Lafont, R.G. Parton, and K. Simons. 1995. Annexin XIIIb: a novel epithelial specific annexin is implicated in vesicular traffic to the apical plasma membrane. *J Cell Biol*. 128:1043-53.
- Fiedler, K., and K. Simons. 1996. Characterization of VIP36, an animal lectin homologous to leguminous lectins. *J Cell Sci*. 109 ( Pt 1):271-6.
- Folch, J., M. Lees, and G.H. Sloane Stanley. 1957. A simple method for the isolation and purification of total lipides from animal tissues. *J Biol Chem*. 226:497-509.

- Folsch, H., H. Ohno, J.S. Bonifacino, and I. Mellman. 1999. A novel clathrin adaptor complex mediates basolateral targeting in polarized epithelial cells. *Cell*. 99:189-98.
- Folsch, H., M. Pypaert, S. Maday, L. Pelletier, and I. Mellman. 2003. The AP-1A and AP-1B clathrin adaptor complexes define biochemically and functionally distinct membrane domains. *J Cell Biol*. 163:351-62.
- Foster, L.J., C.L. De Hoog, and M. Mann. 2003. Unbiased quantitative proteomics of lipid rafts reveals high specificity for signaling factors. *Proc Natl Acad Sci U S A*. 100:5813-8.
- Füllekrug, J., P. Scheiffele, and K. Simons. 1999. VIP36 localisation to the early secretory pathway. *J Cell Sci*. 112 ( Pt 17):2813-21.
- Futter, C.E., C.N. Connolly, D.F. Cutler, and C.R. Hopkins. 1995. Newly synthesized transferrin receptors can be detected in the endosome before they appear on the cell surface. *J Biol Chem*. 270:10999-1003.
- Galli, T., A. Zahraoui, V.V. Vaidyanathan, G. Raposo, J.M. Tian, M. Karin, H. Niemann, and D. Louvard. 1998. A novel tetanus neurotoxin-insensitive vesicle-associated membrane protein in SNARE complexes of the apical plasma membrane of epithelial cells. *Mol Biol Cell*. 9:1437-48.
- Gkantiragas, I., B. Brugger, E. Stuken, D. Kaloyanova, X.Y. Li, K. Lohr, F. Lottspeich, F.T. Wieland, and J.B. Helms. 2001. Sphingomyelin-enriched microdomains at the Golgi complex. *Mol Biol Cell*. 12:1819-33.
- Gomez-Mouton, C., J.L. Abad, E. Mira, R.A. Lacalle, E. Gallardo, S. Jimenez-Baranda, I. Illa, A. Bernad, S. Manes, and A.C. Martinez. 2001. Segregation of leading-edge and uropod components into specific lipid rafts during T cell polarization. *Proc Natl Acad Sci U S A*. 98:9642-7.
- Gu, C., Y.N. Jan, and L.Y. Jan. 2003. A conserved domain in axonal targeting of Kv1 (Shaker) voltage-gated potassium channels. *Science*. 301:646-9.
- Gumbiner, B., and K. Simons. 1986. A functional assay for proteins involved in establishing an epithelial occluding barrier: identification of a uvomorulin-like polypeptide. *J Cell Biol*. 102:457-68.
- Guo, W., D. Roth, C. Walch-Solimena, and P. Novick. 1999. The exocyst is an effector for Sec4p, targeting secretory vesicles to sites of exocytosis. *Embo J*. 18:1071-80.
- Gut, A., F. Kappeler, N. Hyka, M.S. Balda, H.P. Hauri, and K. Matter. 1998. Carbohydrate-mediated Golgi to cell surface transport and apical targeting of membrane proteins. *Embo J*. 17:1919-29.
- Hansen, G.H., L. Immerdal, E. Thorsen, L.L. Niels-Christiansen, B.T. Nystrom, E.J. Demant, and E.M. Danielsen. 2001. Lipid rafts exist as stable cholesterol-independent microdomains in the brush border membrane of enterocytes. *J Biol Chem*. 276:32338-44.
- Hansen, G.H., L.L. Niels-Christiansen, E. Thorsen, L. Immerdal, and E.M. Danielsen. 2000. Cholesterol depletion of enterocytes. Effect on the Golgi complex and apical membrane trafficking. *J Biol Chem*. 275:5136-42.
- Hara-Kuge, S., T. Ohkura, H. Ideo, O. Shimada, S. Atsumi, and K. Yamashita. 2002. Involvement of VIP36 in intracellular transport and secretion of glycoproteins in polarized Madin-Darby canine kidney (MDCK) cells. *J Biol Chem*. 277:16332-9.
- Harder, T., and K.R. Engelhardt. 2004. Membrane domains in lymphocytes - from lipid rafts to protein scaffolds. *Traffic*. 5:265-75.
- Harder, T., and M. Kuhn. 2000. Selective accumulation of raft-associated membrane protein LAT in T cell receptor signaling assemblies. *J Cell Biol*. 151:199-208.

- Harder, T., P. Scheiffele, P. Verkade, and K. Simons. 1998. Lipid domain structure of the plasma membrane revealed by patching of membrane components. *J Cell Biol.* 141:929-42.
- Harsay, E., and R. Schekman. 2002. A subset of yeast vacuolar protein sorting mutants is blocked in one branch of the exocytic pathway. *J Cell Biol.* 156:271-85.
- Heerklotz, H. 2002. Triton promotes domain formation in lipid raft mixtures. *Biophys J.* 83:2693-701.
- Helenius, A., and K. Simons. 1975. Solubilization of membranes by detergents. *Biochim Biophys Acta.* 415:29-79.
- Hirschberg, K., C.M. Miller, J. Ellenberg, J.F. Presley, E.D. Siggia, R.D. Phair, and J. Lippincott-Schwartz. 1998. Kinetic analysis of secretory protein traffic and characterization of golgi to plasma membrane transport intermediates in living cells. *J Cell Biol.* 143:1485-503.
- Hoekstra, D., D. Tyteca, and I.S.C. van. 2004. The subapical compartment: a traffic center in membrane polarity development. *J Cell Sci.* 117:2183-92.
- Horton, A.C., and M.D. Ehlers. 2003. Neuronal polarity and trafficking. *Neuron.* 40:277-95.
- Huber, L.A., S. Pimplikar, R.G. Parton, H. Virta, M. Zerial, and K. Simons. 1993. Rab8, a small GTPase involved in vesicular traffic between the TGN and the basolateral plasma membrane. *J Cell Biol.* 123:35-45.
- Huttner, W.B., and J. Zimmerberg. 2001. Implications of lipid microdomains for membrane curvature, budding and fission. *Curr Opin Cell Biol.* 13:478-84.
- Ihrke, G., J.R. Bruns, J.P. Luzio, and O.A. Weisz. 2001. Competing sorting signals guide endolyn along a novel route to lysosomes in MDCK cells. *Embo J.* 20:6256-64.
- Jacob, R., M. Heine, J. Eikemeyer, N. Frerker, K.P. Zimmer, U. Rescher, V. Gerke, and H.Y. Naim. 2004. Annexin II is required for apical transport in polarized epithelial cells. *J Biol Chem.* 279:3680-4.
- Jacob, R., and H.Y. Naim. 2001. Apical membrane proteins are transported in distinct vesicular carriers. *Curr Biol.* 11:1444-50.
- Jacob, R., U. Preuss, P. Panzer, M. Alfalah, S. Quack, M.G. Roth, H. Naim, and H.Y. Naim. 1999. Hierarchy of sorting signals in chimeras of intestinal lactase-phlorizin hydrolase and the influenza virus hemagglutinin. *J Biol Chem.* 274:8061-7.
- Janes, P.W., S.C. Ley, and A.I. Magee. 1999. Aggregation of lipid rafts accompanies signaling via the T cell antigen receptor. *J Cell Biol.* 147:447-61.
- Jing, S.Q., and I.S. Trowbridge. 1987. Identification of the intermolecular disulfide bonds of the human transferrin receptor and its lipid-attachment site. *Embo J.* 6:327-31.
- Keller, P., and K. Simons. 1998. Cholesterol is required for surface transport of influenza virus hemagglutinin. *J Cell Biol.* 140:1357-67.
- Keller, P., D. Toomre, E. Diaz, J. White, and K. Simons. 2001. Multicolour imaging of post-Golgi sorting and trafficking in live cells. *Nat Cell Biol.* 3:140-9.
- Khvorova, A., A. Reynolds, and S.D. Jayasena. 2003. Functional siRNAs and miRNAs exhibit strand bias. *Cell.* 115:209-16.
- Kipp, H., and I.M. Arias. 2000. Newly synthesized canalicular ABC transporters are directly targeted from the Golgi to the hepatocyte apical domain in rat liver. *J Biol Chem.* 275:15917-25.
- Klopfenstein, D.R., and R.D. Vale. 2004. The Lipid Binding Pleckstrin Homology Domain in UNC-104 Kinesin is Necessary for Synaptic Vesicle Transport in *Caenorhabditis elegans*. *Mol Biol Cell.* 15:3729-39.
- Kohler, K., D. Louvard, and A. Zahraoui. 2004. Rab13 regulates PKA signaling during tight junction assembly. *J Cell Biol.* 165:175-80.

- Korlach, J., P. Schwille, W.W. Webb, and G.W. Feigenson. 1999. Characterization of lipid bilayer phases by confocal microscopy and fluorescence correlation spectroscopy. *Proc Natl Acad Sci U S A.* 96:8461-6.
- Kreitzer, G., A. Marmorstein, P. Okamoto, R. Vallee, and E. Rodriguez-Boulan. 2000. Kinesin and dynamin are required for post-Golgi transport of a plasma-membrane protein. *Nat Cell Biol.* 2:125-7.
- Kundu, A., R.T. Avalos, C.M. Sanderson, and D.P. Nayak. 1996. Transmembrane domain of influenza virus neuraminidase, a type II protein, possesses an apical sorting signal in polarized MDCK cells. *J Virol.* 70:6508-15.
- Kurzchalia, T.V., P. Dupree, R.G. Parton, R. Kellner, H. Virta, M. Lehnert, and K. Simons. 1992. VIP21, a 21-kD membrane protein is an integral component of trans-Golgi-network-derived transport vesicles. *J Cell Biol.* 118:1003-14.
- Kurzchalia, T.V., E. Hartmann, and P. Dupree. 1995. Guilty by insolubility--does a protein's detergent insolubility reflect a caveolar location? *Trends Cell Biol.* 5:187-9.
- Kusumi, A., I. Koyama-Honda, and K. Suzuki. 2004. Molecular dynamics and interactions for creation of stimulation-induced stabilized rafts from small unstable steady-state rafts. *Traffic.* 5:213-30.
- Lafont, F., J.K. Burkhardt, and K. Simons. 1994. Involvement of microtubule motors in basolateral and apical transport in kidney cells. *Nature.* 372:801-3.
- Lafont, F., S. Lecat, P. Verkade, and K. Simons. 1998. Annexin XIIIb associates with lipid microdomains to function in apical delivery. *J Cell Biol.* 142:1413-27.
- Lafont, F., P. Verkade, T. Galli, C. Wimmer, D. Louvard, and K. Simons. 1999. Raft association of SNAP receptors acting in apical trafficking in Madin-Darby canine kidney cells. *Proc Natl Acad Sci U S A.* 96:3734-8.
- le Maire, M., P. Champeil, and J.V. Moller. 2000. Interaction of membrane proteins and lipids with solubilizing detergents. *Biochim Biophys Acta.* 1508:86-111.
- Lecat, S., P. Verkade, C. Thiele, K. Fiedler, K. Simons, and F. Lafont. 2000. Different properties of two isoforms of annexin XIII in MDCK cells. *J Cell Sci.* 113 ( Pt 14):2607-18.
- Lecuit, T., and F. Pilot. 2003. Developmental control of cell morphogenesis: a focus on membrane growth. *Nat Cell Biol.* 5:103-8.
- Leitinger, B., A. Hille-Rehfeld, and M. Spiess. 1995. Biosynthetic transport of the asialoglycoprotein receptor H1 to the cell surface occurs via endosomes. *Proc Natl Acad Sci U S A.* 92:10109-13.
- Lin, S., H.Y. Naim, A.C. Rodriguez, and M.G. Roth. 1998. Mutations in the middle of the transmembrane domain reverse the polarity of transport of the influenza virus hemagglutinin in MDCK epithelial cells. *J Cell Biol.* 142:51-7.
- Ling, Q., A.T. Jacovina, A. Deora, M. Febbraio, R. Simantov, R.L. Silverstein, B. Hempstead, W.H. Mark, and K.A. Hajjar. 2004. Annexin II regulates fibrin homeostasis and neoangiogenesis in vivo. *J Clin Invest.* 113:38-48.
- Linstedt, A.D., and H.P. Hauri. 1993. Giantin, a novel conserved Golgi membrane protein containing a cytoplasmic domain of at least 350 kDa. *Mol Biol Cell.* 4:679-93.
- Lipardi, C., L. Nitsch, and C. Zurzolo. 2000. Detergent-insoluble GPI-anchored proteins are apically sorted in fischer rat thyroid cells, but interference with cholesterol or sphingolipids differentially affects detergent insolubility and apical sorting. *Mol Biol Cell.* 11:531-42.
- Lipowsky, R. 1993. Domain-induced budding of fluid membranes. *Biophys J.* 64:1133-38.
- Lipowsky, R. 2002. Domains and rafts in membranes - hidden dimensions of self-organization. *J Biol Phys.* 28:195-210.



- Lisanti, M.P., I.W. Caras, M.A. Davitz, and E. Rodriguez-Boulan. 1989. A glycosphospholipid membrane anchor acts as an apical targeting signal in polarized epithelial cells. *J Cell Biol.* 109:2145-56.
- London, E., and D.A. Brown. 2000. Insolubility of lipids in triton X-100: physical origin and relationship to sphingolipid/cholesterol membrane domains (rafts). *Biochim Biophys Acta.* 1508:182-95.
- London, M., and E. London. 2004. Ceramide selectively displaces cholesterol from ordered lipid domains (rafts): implications for lipid raft structure and function. *J Biol Chem.* 279:9997-10004.
- Low, S.H., S.J. Chapin, C. Wimmer, S.W. Whiteheart, L.G. Komuves, K.E. Mostov, and T. Weimbs. 1998. The SNARE machinery is involved in apical plasma membrane trafficking in MDCK cells. *J Cell Biol.* 141:1503-13.
- Low, S.H., M. Miura, P.A. Roche, A.C. Valdez, K.E. Mostov, and T. Weimbs. 2000. Intracellular redirection of plasma membrane trafficking after loss of epithelial cell polarity. *Mol Biol Cell.* 11:3045-60.
- Lubarsky, B., and M.A. Krasnow. 2003. Tube morphogenesis: making and shaping biological tubes. *Cell.* 112:19-28.
- Lundbaek, J.A., O.S. Andersen, T. Werge, and C. Nielsen. 2003. Cholesterol-induced protein sorting: an analysis of energetic feasibility. *Biophys J.* 84:2080-9.
- Madore, N., K.L. Smith, C.H. Graham, A. Jen, K. Brady, S. Hall, and R. Morris. 1999. Functionally different GPI proteins are organized in different domains on the neuronal surface. *Embo J.* 18:6917-26.
- Martin-Belmonte, F., R. Puertollano, J. Millan, and M.A. Alonso. 2000. The MAL proteolipid is necessary for the overall apical delivery of membrane proteins in the polarized epithelial Madin-Darby canine kidney and fischer rat thyroid cell lines. *Mol Biol Cell.* 11:2033-45.
- Matlin, K.S., and K. Simons. 1984. Sorting of an apical plasma membrane glycoprotein occurs before it reaches the cell surface in cultured epithelial cells. *J Cell Biol.* 99:2131-9.
- Matter, K. 2000. Epithelial polarity: sorting out the sorters. *Curr Biol.* 10:R39-42.
- Matter, K., and I. Mellman. 1994. Mechanisms of cell polarity: sorting and transport in epithelial cells. *Curr Opin Cell Biol.* 6:545-54.
- Mayor, S., and F.R. Maxfield. 1995. Insolubility and redistribution of GPI-anchored proteins at the cell surface after detergent treatment. *Mol Biol Cell.* 6:929-44.
- Mayor, S., and H. Riezman. 2004. Sorting GPI-anchored proteins. *Nat Rev Mol Cell Biol.* 5:110-20.
- Mayran, N., R.G. Parton, and J. Gruenberg. 2003. Annexin II regulates multivesicular endosome biogenesis in the degradation pathway of animal cells. *Embo J.* 22:3242-53.
- Mays, R.W., K.A. Siemers, B.A. Fritz, A.W. Lowe, G. van Meer, and W.J. Nelson. 1995. Hierarchy of mechanisms involved in generating Na/K-ATPase polarity in MDCK epithelial cells. *J Cell Biol.* 130:1105-15.
- Mellman, I. 1996. Endocytosis and molecular sorting. *Annu Rev Cell Dev Biol.* 12:575-625.
- Misek, D.E., E. Bard, and E. Rodriguez-Boulan. 1984. Biogenesis of epithelial cell polarity: intracellular sorting and vectorial exocytosis of an apical plasma membrane glycoprotein. *Cell.* 39:537-46.
- Miyagawa, K., T. Tsuruga, A. Kinomura, K. Usui, M. Katsura, S. Tashiro, H. Mishima, and K. Tanaka. 2002. A role for RAD54B in homologous recombination in human cells. *Embo J.* 21:175-80.

- Monier, S., R.G. Parton, F. Vogel, J. Behlke, A. Henske, and T.V. Kurzchalia. 1995. VIP21-caveolin, a membrane protein constituent of the caveolar coat, oligomerizes in vivo and in vitro. *Mol Biol Cell*. 6:911-27.
- Monlauzeur, L., A. Rajasekaran, M. Chao, E. Rodriguez-Boulan, and A. Le Bivic. 1995. A cytoplasmic tyrosine is essential for the basolateral localization of mutants of the human nerve growth factor receptor in Madin-Darby canine kidney cells. *J Biol Chem*. 270:12219-25.
- Montixi, C., C. Langlet, A.M. Bernard, J. Thimonier, C. Dubois, M.A. Wurbel, J.P. Chauvin, M. Pierres, and H.T. He. 1998. Engagement of T cell receptor triggers its recruitment to low-density detergent-insoluble membrane domains. *Embo J*. 17:5334-48.
- Mostov, K.E., M. Verges, and Y. Altschuler. 2000. Membrane traffic in polarized epithelial cells. *Curr Opin Cell Biol*. 12:483-90.
- Munro, S. 2003. Lipid rafts: elusive or illusive? *Cell*. 115:377-88.
- Musch, A. 2004. Microtubule organization and function in epithelial cells. *Traffic*. 5:1-9.
- Muth, T.R., and M.J. Caplan. 2003. Transport protein trafficking in polarized cells. *Annu Rev Cell Dev Biol*. 19:333-66.
- Muzerelle, A., P. Alberts, S. Martinez-Arca, O. Jeannequin, P. Lafaye, J.C. Mazie, T. Galli, and P. Gaspar. 2003. Tetanus neurotoxin-insensitive vesicle-associated membrane protein localizes to a presynaptic membrane compartment in selected terminal subsets of the rat brain. *Neuroscience*. 122:59-75.
- Naim, H.Y., D.T. Dodds, C.B. Brewer, and M.G. Roth. 1995. Apical and basolateral coated pits of MDCK cells differ in their rates of maturation into coated vesicles, but not in the ability to distinguish between mutant hemagglutinin proteins with different internalization signals. *J Cell Biol*. 129:1241-50.
- Nakagawa, T., M. Setou, D. Seog, K. Ogasawara, N. Dohmae, K. Takio, and N. Hirokawa. 2000. A novel motor, KIF13A, transports mannose-6-phosphate receptor to plasma membrane through direct interaction with AP-1 complex. *Cell*. 103:569-81.
- Nebl, T., K.N. Pestonjamas, J.D. Leszyk, J.L. Crowley, S.W. Oh, and E.J. Luna. 2002. Proteomic analysis of a detergent-resistant membrane skeleton from neutrophil plasma membranes. *J Biol Chem*. 277:43399-409.
- Neumann-Giesen, C., B. Falkenbach, P. Beicht, S. Claasen, G. Luers, C.A. Stuermer, V. Herzog, and R. Tikkanen. 2004. Membrane and raft association of reggie-1/flotillin-2: role of myristoylation, palmitoylation and oligomerization and induction of filopodia by overexpression. *Biochem J*. 378:509-18.
- Nishimura, N., H. Plutner, K. Hahn, and W.E. Balch. 2002. The delta subunit of AP-3 is required for efficient transport of VSV-G from the trans-Golgi network to the cell surface. *Proc Natl Acad Sci U S A*. 99:6755-60.
- Noda, Y., Y. Okada, N. Saito, M. Setou, Y. Xu, Z. Zhang, and N. Hirokawa. 2001. KIFC3, a microtubule minus end-directed motor for the apical transport of annexin XIIIb-associated Triton-insoluble membranes. *J Cell Biol*. 155:77-88.
- Ojakian, G.K., and R. Schwimmer. 1988. The polarized distribution of an apical cell surface glycoprotein is maintained by interactions with the cytoskeleton of Madin-Darby canine kidney cells. *J Cell Biol*. 107:2377-87.
- Oling, F., W. Bergsma-Schutter, and A. Brisson. 2001. Trimers, dimers of trimers, and trimers of trimers are common building blocks of annexin a5 two-dimensional crystals. *J Struct Biol*. 133:55-63.

- Orzech, E., S. Cohen, A. Weiss, and B. Aroeti. 2000. Interactions between the exocytic and endocytic pathways in polarized Madin-Darby canine kidney cells. *J Biol Chem.* 275:15207-19.
- Ostedgaard, L.S., C. Randak, T. Rokhlina, P. Karp, D. Vermeer, K.J. Ashbourne Excoffon, and M.J. Welsh. 2003. Effects of C-terminal deletions on cystic fibrosis transmembrane conductance regulator function in cystic fibrosis airway epithelia. *Proc Natl Acad Sci U S A.* 100:1937-42.
- Paddison, P.J., A.A. Caudy, E. Bernstein, G.J. Hannon, and D.S. Conklin. 2002. Short hairpin RNAs (shRNAs) induce sequence-specific silencing in mammalian cells. *Genes Dev.* 16:948-58.
- Paladino, S., D. Sarnataro, R. Pillich, S. Tivodar, L. Nitsch, and C. Zurzolo. in press. Protein oligomerization modulates raft partitioning and apical sorting of GPI-anchored proteins. *J Cell Biol.*
- Perego, C., C. Vanoni, A. Villa, R. Longhi, S.M. Kaech, E. Frohli, A. Hajnal, S.K. Kim, and G. Pietrini. 1999. PDZ-mediated interactions retain the epithelial GABA transporter on the basolateral surface of polarized epithelial cells. *Embo J.* 18:2384-93.
- Pfeiffer, S., S.D. Fuller, and K. Simons. 1985. Intracellular sorting and basolateral appearance of the G protein of vesicular stomatitis virus in Madin-Darby canine kidney cells. *J Cell Biol.* 101:470-6.
- Polishchuk, R., A. Di Pentima, and J. Lippincott-Schwartz. 2004. Delivery of raft-associated, GPI-anchored proteins to the apical surface of polarized MDCK cells by a transcytotic pathway. *Nat Cell Biol.* 6:297-307.
- Pralle, A., P. Keller, E.L. Florin, K. Simons, and J.K. Horber. 2000. Sphingolipid-cholesterol rafts diffuse as small entities in the plasma membrane of mammalian cells. *J Cell Biol.* 148:997-1008.
- Prior, I.A., C. Muncke, R.G. Parton, and J.F. Hancock. 2003. Direct visualization of Ras proteins in spatially distinct cell surface microdomains. *J Cell Biol.* 160:165-70.
- Puertollano, R., F. Martin-Belmonte, J. Millan, M.C. de Marco, J.P. Albar, L. Kremer, and M.A. Alonso. 1999. The MAL proteolipid is necessary for normal apical transport and accurate sorting of the influenza virus hemagglutinin in Madin-Darby canine kidney cells. *J Cell Biol.* 145:141-51.
- Ren, M., G. Xu, J. Zeng, C. De Lemos-Chiarandini, M. Adesnik, and D.D. Sabatini. 1998. Hydrolysis of GTP on rab11 is required for the direct delivery of transferrin from the pericentriolar recycling compartment to the cell surface but not from sorting endosomes. *Proc Natl Acad Sci U S A.* 95:6187-92.
- Rescher, U., and V. Gerke. 2004. Annexins--unique membrane binding proteins with diverse functions. *J Cell Sci.* 117:2631-9.
- Reynolds, A., D. Leake, Q. Boese, S. Scaringe, W.S. Marshall, and A. Khvorova. 2004. Rational siRNA design for RNA interference. *Nat Biotechnol.* 22:326-30.
- Riento, K., T. Galli, S. Jansson, C. Ehnholm, E. Lehtonen, and V.M. Olkkonen. 1998. Interaction of Munc-18-2 with syntaxin 3 controls the association of apical SNAREs in epithelial cells. *J Cell Sci.* 111 ( Pt 17):2681-8.
- Roberts, P.C., R.A. Lamb, and R.W. Compans. 1998. The M1 and M2 proteins of influenza A virus are important determinants in filamentous particle formation. *Virology.* 240:127-37.
- Robinson, M.S. 2004. Adaptable adaptors for coated vesicles. *Trends Cell Biol.* 14:167-74.

- Roper, K., D. Corbeil, and W.B. Huttner. 2000. Retention of prominin in microvilli reveals distinct cholesterol-based lipid micro-domains in the apical plasma membrane. *Nat Cell Biol.* 2:582-92.
- Schaeren-Wiemers, N., A. Bonnet, M. Erb, B. Erne, U. Bartsch, F. Kern, N. Mantei, D. Sherman, and U. Suter. 2004. The raft-associated protein MAL is required for maintenance of proper axon--glia interactions in the central nervous system. *J Cell Biol.* 166:731-42.
- Scheiffele, P., J. Peranen, and K. Simons. 1995. N-glycans as apical sorting signals in epithelial cells. *Nature.* 378:96-8.
- Scheiffele, P., M.G. Roth, and K. Simons. 1997. Interaction of influenza virus haemagglutinin with sphingolipid-cholesterol membrane domains via its transmembrane domain. *Embo J.* 16:5501-8.
- Scheiffele, P., P. Verkade, A.M. Fra, H. Virta, K. Simons, and E. Ikonen. 1998. Caveolin-1 and -2 in the exocytic pathway of MDCK cells. *J Cell Biol.* 140:795-806.
- Schmidt, K., M. Schrader, H.F. Kern, and R. Kleene. 2001. Regulated apical secretion of zymogens in rat pancreas. Involvement of the glycosylphosphatidylinositol-anchored glycoprotein GP-2, the lectin ZG16p, and cholesterol-glycosphingolipid-enriched microdomains. *J Biol Chem.* 276:14315-23.
- Schnaar, R.L. 1994. Isolation of glycosphingolipids. *Methods Enzymol.* 230:348-70.
- Schroeder, R., E. London, and D. Brown. 1994. Interactions between saturated acyl chains confer detergent resistance on lipids and glycosylphosphatidylinositol (GPI)-anchored proteins: GPI-anchored proteins in liposomes and cells show similar behavior. *Proc Natl Acad Sci U S A.* 91:12130-4.
- Schwarz, D.S., G. Hutvagner, T. Du, Z. Xu, N. Aronin, and P.D. Zamore. 2003. Asymmetry in the assembly of the RNAi enzyme complex. *Cell.* 115:199-208.
- Setou, M., T. Nakagawa, D.H. Seog, and N. Hirokawa. 2000. Kinesin superfamily motor protein KIF17 and mLin-10 in NMDA receptor-containing vesicle transport. *Science.* 288:1796-802.
- Sheff, D.R., E.A. Daro, M. Hull, and I. Mellman. 1999. The receptor recycling pathway contains two distinct populations of early endosomes with different sorting functions. *J Cell Biol.* 145:123-39.
- Shelly, M., Y. Mosesson, A. Citri, S. Lavi, Y. Zwang, N. Melamed-Book, B. Aroeti, and Y. Yarden. 2003. Polar expression of ErbB-2/HER2 in epithelia. Bimodal regulation by Lin-7. *Dev Cell.* 5:475-86.
- Shenolikar, S., and E.J. Weinman. 2001. NHERF: targeting and trafficking membrane proteins. *Am J Physiol Renal Physiol.* 280:F389-95.
- Short, D.B., K.W. Trotter, D. Reczek, S.M. Kreda, A. Bretscher, R.C. Boucher, M.J. Stutts, and S.L. Milgram. 1998. An apical PDZ protein anchors the cystic fibrosis transmembrane conductance regulator to the cytoskeleton. *J Biol Chem.* 273:19797-801.
- Shvartsman, D.E., M. Kotler, R.D. Tall, M.G. Roth, and Y.I. Henis. 2003. Differently anchored influenza hemagglutinin mutants display distinct interaction dynamics with mutual rafts. *J Cell Biol.* 163:879-88.
- Simmen, T., S. Honing, A. Icking, R. Tikkanen, and W. Hunziker. 2002. AP-4 binds basolateral signals and participates in basolateral sorting in epithelial MDCK cells. *Nat Cell Biol.* 4:154-9.
- Simons, K., and E. Ikonen. 1997. Functional rafts in cell membranes. *Nature.* 387:569-72.
- Simons, K., and D. Toomre. 2000. Lipid rafts and signal transduction. *Nat Rev Mol Cell Biol.* 1:31-9.

- Simons, K., and G. van Meer. 1988. Lipid sorting in epithelial cells. *Biochemistry*. 27:6197-202.
- Simons, K., and W.L. Vaz. 2004. Model systems, lipid rafts, and cell membranes. *Annu Rev Biophys Biomol Struct.* 33:269-95.
- Skibbens, J.E., M.G. Roth, and K.S. Matlin. 1989. Differential extractability of influenza virus hemagglutinin during intracellular transport in polarized epithelial cells and nonpolar fibroblasts. *J Cell Biol.* 108:821-32.
- Slotte, J.P., and E.L. Bierman. 1988. Depletion of plasma-membrane sphingomyelin rapidly alters the distribution of cholesterol between plasma membranes and intracellular cholesterol pools in cultured fibroblasts. *Biochem J.* 250:653-8.
- Snyers, L., E. Umlauf, and R. Prohaska. 1999. Association of stomatin with lipid-protein complexes in the plasma membrane and the endocytic compartment. *Eur J Cell Biol.* 78:802-12.
- Sotgia, F., B. Razani, G. Bonuccelli, W. Schubert, M. Battista, H. Lee, F. Capozza, A.L. Schubert, C. Minetti, J.T. Buckley, and M.P. Lisanti. 2002. Intracellular retention of glycosylphosphatidyl inositol-linked proteins in caveolin-deficient cells. *Mol Cell Biol.* 22:3905-26.
- Spodsberg, N., M. Alfalah, and H.Y. Naim. 2001. Characteristics and structural requirements of apical sorting of the rat growth hormone through the O-glycosylated stalk region of intestinal sucrase-isomaltase. *J Biol Chem.* 276:46597-604.
- Sugimoto, H., M. Sugahara, H. Folsch, Y. Koide, F. Nakatsu, N. Tanaka, T. Nishimura, M. Furukawa, C. Mullins, N. Nakamura, I. Mellman, and H. Ohno. 2002. Differential recognition of tyrosine-based basolateral signals by AP-1B subunit mu1B in polarized epithelial cells. *Mol Biol Cell.* 13:2374-82.
- Swiatecka-Urban, A., M. Duhaime, B. Coutermarsh, K.H. Karlson, J. Collawn, M. Milewski, G.R. Cutting, W.B. Guggino, G. Langford, and B.A. Stanton. 2002. PDZ domain interaction controls the endocytic recycling of the cystic fibrosis transmembrane conductance regulator. *J Biol Chem.* 277:40099-105.
- Tai, A.W., J.Z. Chuang, and C.H. Sung. 2001. Cytoplasmic dynein regulation by subunit heterogeneity and its role in apical transport. *J Cell Biol.* 153:1499-509.
- Thiel, C., M. Osborn, and V. Gerke. 1992. The tight association of the tyrosine kinase substrate annexin II with the submembranous cytoskeleton depends on intact p11- and Ca(2+)-binding sites. *J Cell Sci.* 103 ( Pt 3):733-42.
- Thiele, C., and W.B. Huttner. 1998. Protein and lipid sorting from the trans-Golgi network to secretory granules-recent developments. *Semin Cell Dev Biol.* 9:511-6.
- Toomre, D., P. Keller, J. White, J.C. Olivo, and K. Simons. 1999. Dual-color visualization of trans-Golgi network to plasma membrane traffic along microtubules in living cells. *J Cell Sci.* 112 ( Pt 1):21-33.
- Traub, L.M., and G. Apodaca. 2003. AP-1B: polarized sorting at the endosome. *Nat Cell Biol.* 5:1045-7.
- Tsukita, S., M. Furuse, and M. Itoh. 2001. Multifunctional strands in tight junctions. *Nat Rev Mol Cell Biol.* 2:285-93.
- Ullrich, O., S. Reinsch, S. Urbe, M. Zerial, and R.G. Parton. 1996. Rab11 regulates recycling through the pericentriolar recycling endosome. *J Cell Biol.* 135:913-24.
- van Deurs, B., K. Roepstorff, A.M. Hommelgaard, and K. Sandvig. 2003. Caveolae: anchored, multifunctional platforms in the lipid ocean. *Trends Cell Biol.* 13:92-100.
- Vega-Salas, D.E., P.J. Salas, and E. Rodriguez-Boulan. 1987. Modulation of the expression of an apical plasma membrane protein of Madin-Darby canine kidney

- epithelial cells: cell-cell interactions control the appearance of a novel intracellular storage compartment. *J Cell Biol.* 104:1249-59.
- Vega-Salas, D.E., P.J. Salas, and E. Rodriguez-Boulan. 1988. Exocytosis of vacuolar apical compartment (VAC): a cell-cell contact controlled mechanism for the establishment of the apical plasma membrane domain in epithelial cells. *J Cell Biol.* 107:1717-28.
- Verkade, P., T. Harder, F. Lafont, and K. Simons. 2000. Induction of caveolae in the apical plasma membrane of Madin-Darby canine kidney cells. *J Cell Biol.* 148:727-39.
- Vickers, T.A., S. Koo, C.F. Bennett, S.T. Crooke, N.M. Dean, and B.F. Baker. 2003. Efficient reduction of target RNAs by small interfering RNA and RNase H-dependent antisense agents. A comparative analysis. *J Biol Chem.* 278:7108-18.
- von Haller, P.D., S. Donohoe, D.R. Goodlett, R. Aebersold, and J.D. Watts. 2001. Mass spectrometric characterization of proteins extracted from Jurkat T cell detergent-resistant membrane domains. *Proteomics.* 1:1010-21.
- Wilson, B.S., S.L. Steinberg, K. Liederman, J.R. Pfeiffer, Z. Surviladze, J. Zhang, L.E. Samelson, L.H. Yang, P.G. Kotula, and J.M. Oliver. 2004. Markers for detergent-resistant lipid rafts occupy distinct and dynamic domains in native membranes. *Mol Biol Cell.* 15:2580-92.
- Wilson, J.A., and C.D. Richardson. 2003. Induction of RNA interference using short interfering RNA expression vectors in cell culture and animal systems. *Curr Opin Mol Ther.* 5:389-96.
- Xu, X., R. Bittman, G. Duportail, D. Heissler, C. Vilcheze, and E. London. 2001. Effect of the structure of natural sterols and sphingolipids on the formation of ordered sphingolipid/sterol domains (rafts). Comparison of cholesterol to plant, fungal, and disease-associated sterols and comparison of sphingomyelin, cerebrosides, and ceramide. *J Biol Chem.* 276:33540-6.
- Xu, Y., S. Takeda, T. Nakata, Y. Noda, Y. Tanaka, and N. Hirokawa. 2002. Role of KIFC3 motor protein in Golgi positioning and integration. *J Cell Biol.* 158:293-303.
- Yang, Z., C. Xia, E.A. Roberts, K. Bush, S.K. Nigam, and L.S. Goldstein. 2001. Molecular cloning and functional analysis of mouse C-terminal kinesin motor KifC3. *Mol Cell Biol.* 21:765-70.
- Yeaman, C., K.K. Grindstaff, and W.J. Nelson. 1999. New perspectives on mechanisms involved in generating epithelial cell polarity. *Physiol Rev.* 79:73-98.
- Yeaman, C., A.H. Le Gall, A.N. Baldwin, L. Monlauzeur, A. Le Bivic, and E. Rodriguez-Boulan. 1997. The O-glycosylated stalk domain is required for apical sorting of neurotrophin receptors in polarized MDCK cells. *J Cell Biol.* 139:929-40.
- Yu, J.Y., J. Taylor, S.L. DeRuiter, A.B. Vojtek, and D.L. Turner. 2003. Simultaneous inhibition of GSK3alpha and GSK3beta using hairpin siRNA expression vectors. *Mol Ther.* 7:228-36.
- Zerial, M., and H. McBride. 2001. Rab proteins as membrane organizers. *Nat Rev Mol Cell Biol.* 2:107-17.
- Zuker, M. 2003. Mfold web server for nucleic acid folding and hybridization prediction. *Nucleic Acids Res.* 31:3406-15.

## 9. Abbreviations

A	adenosine
A	Ampere
AP	adaptor protein
APS	ammonium peroxodisulfate
ATCC	American Type Culture Collection
ATP	adenosine triphosphate
BCA	bicinchoninic acid
BLAST	basic local alignment search tool
bp	base pair(s)
BSA	bovine serum albumin
C	centigrade
C	cytosine
cDNA	complementary DNA
CFTR	cystic fibrosis transmembrane conductance regulator
CHAPS	3-[(3-Cholamidopropyl)-dimethylammonio]-1-propansulfonate
CHO	Chinese hamster ovary
Ci	Curie
CLAP	chymostatin, leupeptin, antipain, pepstatin
cm	centimetre
CMV	cytomegalovirus
DABCO	1,4-Diazabicyclo(2.2.2)octane hydrochloride
DMEM	Dulbecco's modified Eagle's medium
DNA	deoxyribonucleic acid
dNTPs	deoxynucleosidetriphosphates
DRMs	detergent-resistant membranes
dT	deoxythymidine
EDTA	ethylene-diamine-tetra-acetic acid
ER	endoplasmic reticulum
FCS	fetal calf serum
FITC	fluorescein
g	acceleration of gravity
g	gram
G	gauge
G	guanine
GFP	green fluorescent protein

---

gp	glycoprotein
GPI	glycosylphosphatidylinositol
h	hour(s)
HA	hemagglutinin
HB	homogenisation buffer
HEPES	4-(2-hydroxyethyl)-1-piperazineethanesulfonic acid
HRP	horseradish peroxidase
KD	knockdown
kDa	kilo Dalton
KIF	kinesin family
l	litre
μ	micro (10 <sup>-6</sup> )
m	metre
m	milli (10 <sup>-3</sup> )
M	molar = mol per liter
M-MLV	mouse Moloney murine leukemia virus
MAL	myelin and lymphocyte protein
MDCK	Madin-Darby canine kidney
MEM	minimal essential medium
min	minute(s)
MPIS	multiple precursor ion scanning
mRNA	messenger RNA
n	nano (10 <sup>-9</sup> )
N	nucleoside
NCBI	National Center for Biotechnology Information
NHERF	Na <sup>+</sup> /H <sup>+</sup> -exchanger regulatory factor
PAGE	polyacrylamide gel electrophoresis
PBS	phosphate buffered saline
PC	phosphatidylcholine
PCR	polymerase chain reaction
PDZ	PSD-95/Dlg/ZO-1 domain
pIgR	polymeric immunoglobulin receptor
PLAP	placental alkaline phosphatase
PM	plasma membrane
PVDF	polyvinylidene fluoride
QRT-PCR	quantitative RT-PCR
RISC	RNA-induced silencing complex
RFP	red fluorescent protein
RNA	ribonucleic acid



---

RNAi	RNA interference
rpm	revolutions per minute
RT-PCR	real time-PCR or reverse transcription-PCR
s	second(s)
SDS	sodium dodecyl sulfate
shRNA	small hairpin RNA
siRNA	small interfering RNAs
SMase	sphingomyelinase
SNAP	soluble NSF-sensitive attachment protein
SNARE	SNAP receptor
T	thymidine
TBS	Tris-buffered saline
TCMs	total cell membranes
TEMED	N,N,N',N'-tetramethyl ethylene diamine
TfR	transferrin receptor
TGN	<i>trans</i> -Golgi network
TI-VAMP	tetanus insensitive vesicle-associated membrane protein
TLC	thin-layer chromatography
TMD	transmembrane domain
TNE	Tris, NaCl, EDTA
TPCK	L-(tosylamido-2-phenyl) ethyl chloromethyl ketone
Tris	tris(hydroxymethyl)aminomethane
U	unit
v	volume
V	volt
VAC	vacuolar apical compartment
VIP	vesicular membrane protein
VSV	vesicular stomatitis virus
VSV-G	VSV glycoprotein
w	weight
YFP	yellow fluorescent protein

## Appendix 1

A.

Molecular species <sup>a</sup>	Mass, m/z	Detergents							
		TCM	Tween 20	Brij 58	Lubrol WX	Brij 98	Brij 96	Triton	CHAPS
30:0	706.5	62.73 ± 1.21	65.68 ± 11.05	56.81 ± 8.93	56.39 ± 4.95	41.56 ± 10.22	71.87 ± 12.89	15.69 ± 2.16	6.5 ± 0.96
31:1	718.5	66.69 ± 8.94	65.86 ± 4.31	37.77 ± 0.57	45.58 ± 0.64	21.7 ± 6.95	30.7 ± 4.58	4.35 ± 0.61	2.29 ± 0.39
31:0	720.5	33.29 ± 3.06	35.26 ± 4.18	21.01 ± 2.26	27.58 ± 2.67	20.39 ± 7.22	26.89 ± 2.29	9.46 ± 2.39	3.55 ± 0.80
32:2	730.5	44.76 ± 2.95	53.4 ± 4.15	21.11 ± 3.43	27.21 ± 4.29	12.75 ± 2.58	not detectable	not detectable	1.13 ± 0.20
32:1	732.5	267.91 ± 13.80	317.56 ± 25.18	132.98 ± 2.08	174.22 ± 16.03	73.66 ± 13.46	117.07 ± 9.6	14.91 ± 1.22	8.74 ± 0.43
32:0	734.5	94.96 ± 2.80	97.96 ± 5.42	60.79 ± 6.28	66.28 ± 3.63	45.81 ± 11.97	66.29 ± 6.78	21.98 ± 1.77	11.14 ± 0.28
33:2	744.5	82.64 ± 3.41	103.97 ± 9.12	43.31 ± 5.07	56.2 ± 2.17	22.34 ± 3.58	23.09 ± 2.77	3.04 ± 0.50	2.06 ± 0.09
33:1	746.5	463.44 ± 15.83	520.59 ± 47.10	252.58 ± 18.15	320.81 ± 7.03	136.18 ± 22.31	203.84 ± 17.48	26.32 ± 0.94	17.11 ± 2.44
34:2	758.5	242.72 ± 14.72	294.23 ± 12.49	128.68 ± 4.85	161.39 ± 12.6	69.49 ± 18.89	70.89 ± 3.73	8.57 ± 1.52	6.78 ± 0.55
34:1	760.5	1344.63 ± 22.19	1505.57 ± 19.67	767.37 ± 21.71	916.41 ± 7.07	403.96 ± 82.36	719.12 ± 27.53	83.44 ± 5.36	58.87 ± 2.02
34:0	762.5	139.54 ± 4.54	152.75 ± 6.54	76.52 ± 6.24	82.06 ± 11.92	41.74 ± 9.18	76.58 ± 2.59	14.97 ± 1.10	9.72 ± 2.05
35:2	772.5	187.54 ± 0.13	198.17 ± 8.14	92.74 ± 4.99	125.5 ± 9.11	50.45 ± 7.85	50.65 ± 3.28	6.6 ± 1.94	4.52 ± 0.79
35:1	774.5	99.34 ± 7.09	112.55 ± 5.87	53.19 ± 2.72	62.71 ± 10.79	34.67 ± 8.58	46.63 ± 4.21	6.19 ± 0.83	3.94 ± 0.23
36:3	784.5	73.98 ± 6.00	98.43 ± 5.64	38.71 ± 3.08	53.82 ± 6.47	22.24 ± 5.35	25.71 ± 0.88	2.06 ± 0.47	2.23 ± 0.19
36:2	786.5	725.37 ± 11.86	813.46 ± 16.27	389.5 ± 5.76	492.61 ± 5.67	211.69 ± 35.41	214.78 ± 19.73	24.34 ± 2.39	19.09 ± 2.03
36:1	788.5	435.47 ± 4.88	484.4 ± 6.91	247.36 ± 6.92	300.44 ± 8.84	143.26 ± 46.23	225.73 ± 20.83	34.26 ± 2.68	21.6 ± 2.18
38:3	812.5	62.46 ± 2.47	69.61 ± 1.68	25.76 ± 2.36	39.48 ± 4.56	17.43 ± 3.73	not detectable	2.08 ± 0.72	1.73 ± 0.2
Total amount:		4427.47 ± 125.88	4989.45 ± 193.72	2446.19 ± 126.4	3008.69 ± 118.44	1369.32 ± 295.87	1969.84 ± 139.17	278.26 ± 26.6	181.00 ± 15.83

B.

Molecular species <sup>a</sup>	Mass, m/z	Detergents							
		TCM	Tween 20	Brij 58	Lubrol WX	Brij 98	Brij 96	Triton	CHAPS
30:0	706.5	83.69 ± 20.28	123.51 ± 5.05	116.50 ± 11.17	92.99 ± 18.71	102.51 ± 39.97	79.96 ± 3.68	47.53 ± 4.31	8.12 ± 1.52
31:1	718.5	61.71 ± 7.54	06.21 ± 14.86	80.42 ± 7.25	66.28 ± 6.66	72.1 ± 23.97	52.59 ± 8.19	23.41 ± 1.66	5.25 ± 0.57
31:0	720.5	98.58 ± 3.96	97.18 ± 81.74	128.20 ± 5.82	81.56 ± 43.68	123.3 ± 38.58	100.67 ± 4.33	56.7 ± 6.76	12.18 ± 0.81
32:2	730.5	30.61 ± 1.77	35.85 ± 1.80	16.93 ± 2.26	18.98 ± 6.03	12.58 ± 4.44	12.55 ± 2.76	3.43 ± 1.44	1.12 ± 0.36
32:1	732.5	242.14 ± 8.93	302.83 ± 16.87	192.37 ± 4.66	180.70 ± 44.05	94.37 ± 17.4	120.53 ± 5.04	32.53 ± 0.73	9.65 ± 0.53
32:0	734.5	291.70 ± 42.62	478.13 ± 41.51	426.65 ± 19.19	395.36 ± 23.02	293.17 ± 2.52	301.45 ± 26.85	182.92 ± 14.70	42.01 ± 5.16
33:2	744.5	30.32 ± 2.27	42.12 ± 1.67	21.68 ± 4.55	21.57 ± 4.74	17.70 ± 4.34	19.45 ± 1.06	3.80 ± 0.33	1.40 ± 0.43
33:1	746.5	125.85 ± 20.64	186.02 ± 10.98	129.78 ± 8.78	125.61 ± 21.66	78.16 ± 15.04	84.41 ± 4.83	18.78 ± 4.66	6.10 ± 0.73
34:2	758.5	116.88 ± 22.64	132.14 ± 4.15	67.10 ± 9.63	73.78 ± 11.10	39.59 ± 8.02	48.19 ± 1.44	10.77 ± 0.54	4.58 ± 0.34
34:1	760.5	726.34 ± 21.70	952.69 ± 21.75	646.13 ± 22.13	599.27 ± 42.57	357.49 ± 29.55	457.57 ± 11.48	117.44 ± 15.77	34.93 ± 6.21
34:0	762.5	107.46 ± 12.77	167.26 ± 10.98	153.43 ± 14.31	150.84 ± 24.74	94.08 ± 23.68	104.01 ± 4.46	53.27 ± 8.23	12.73 ± 1.40
35:2	772.5	35.01 ± 3.59	42.04 ± 4.47	20.63 ± 4.24	28.03 ± 2.29	16.45 ± 10.21	16.57 ± 3.29	2.54 ± 0.19	1.61 ± 0.18
35:1	774.5	30.53 ± 7.09	48.47 ± 1.75	34.50 ± 8.35	39.83 ± 11.78	19.72 ± 2.10	21.77 ± 1.18	6.59 ± 0.30	1.86 ± 0.21
36:3	784.5	32.07 ± 6.86	39.65 ± 1.73	14.64 ± 3.00	23.91 ± 2.85	7.98 ± 3.62	13.08 ± 0.62	3.37 ± 0.96	1.39 ± 0.22
36:2	786.5	163.18 ± 24.91	203.40 ± 4.29	93.31 ± 9.97	121.32 ± 6.09	39.34 ± 20.79	77.57 ± 4.21	16.46 ± 0.85	6.05 ± 0.79
36:1	788.5	164.30 ± 25.01	226.53 ± 3.62	159.58 ± 9.91	161.60 ± 10.38	68.2 ± 15.54	109.25 ± 5.46	32.58 ± 1.08	8.22 ± 0.60
38:3	812.5	24.31 ± 2.45	28.65 ± 0.19	16.57 ± 5.47	18.61 ± 2.43	4.55 ± 2.95	9.46 ± 0.52	2.83 ± 0.79	0.90 ± 0.13
Total amount:		2364.68 ± 235.03	3212.68 ± 227.41	2318.42 ± 150.69	2200.24 ± 282.78	1441.29 ± 262.72	1629.08 ± 89.4	614.95 ± 63.3	158.1 ± 20.19

<sup>a</sup> Defined as total fatty acid carbon number:total number of double bonds.

**Appendix 1.** Relative concentrations of Phosphatidylcholine (PC) species in DRMs from MDCK (A) and Jurkat cells (B). TCMs and DRMs were obtained as before, lipids were extracted and analysed by mass spectrometry. Relative concentrations of all detectable species were calculated using  $^{13}\text{C}$ -labelled lipids from *P. pastoris* as internal standards. Odd-numbered fatty acids presumably are of plant origin; they derive from the fetal calf serum used for cell culture and subsequently are incorporated into cellular phospholipids. The total amount of PC in the floating fraction of the TCMs represents an underestimate of total membrane PC as a sizeable fraction of membranes is lost during preparation, probably due to incomplete homogenisation and adherence to non-floating material such as nuclei, mitochondria and the cytoskeleton. As some weak detergents like Tween 20 prevent these losses without extensively solubilizing cell membranes, some DRMs can contain nearly as much or even more PC than the TCMs.

## Appendix 2

Target gene	Reference	Target sequence	Construct	RT-PCR	Immunoblotting	Comments
<b>Annexin 2</b>	AW784365	<b>(AA)GACCAAAAGGTGGATGAG</b>	anx2	<b>82 ± 4% (77+86+83+82)</b>	Strong reduction (90%)	
<b>Annexin 13</b>	X80208/9	<b>(AA)GAGTGACCTGAGTGGGAAC</b>	anx13	<b>91 ± 2% (92+92+89)</b>	Strong reduction	
<b>Annexin 13b</b>	X80209	<b>GCTTACTCCCTCTCGAAGG</b>	anx13b/21	<b>74 ± 4% (77+76+70)</b>	Strong reduction (90%)	
Annexin 13b	X80209	(AA)GGCAGTCAACAGTTGCCCA	anx13b/38	56% (61+50)	n.t.	
Annexin 13b	X80209	GCAGTCAACAGTTGCCCAAG	anx13b/42	64%	n.t.	
Annexin 13b	X80209	(AA)CCCTCAGCAGCGGTGCAGC	anx13b/94	34%	n.t.	
<b>Caveolin-1</b>	Z12161	<b>(AA)GATGTGATTGCAGAACCCAG</b>	cav1	<b>90 ± 3% (94+89+87+88+90)</b>	Strong reduction (80%)	
KIFC3	Partial	GCACATCAACAAAGTCCTGTC	KIF/63	74%	n.t.	No antibody available
KIFC3	Partial	(AA)GACCCCTCATGGTGTGCAG	KIF/192	59%	n.t.	No antibody available
<b>KIFC3</b>	Partial	<b>(AA)GAACACCCAGTGAGACTCTG</b>	KIF/228	<b>73 ± 4% (70+77+69+74)</b>	n.t.	No antibody available
<b>MAL2</b>	Partial	<b>(AA)GGATGGTTCATGTTCCGTGT</b>	MAL/217	<b>88 ± 3% (91+86+88+85)</b>	n.t.	No antibody available
MAL2	Partial	(AA)GCAGCAGCCACATCCCTGC	MAL2/172	59%	n.t.	No antibody available
rab8a	X56385	(AA)TTAGGACCATTAGAGCTCGA	rab8a/140	24% (24+23)	n.t.	
<b>rab8a</b>	X56385	<b>(AA)GACAAAGTTCCAAAGGAACG</b>	rab8a/384	<b>93 ± 4% (95+95+88)</b>	Clear reduction*	* Antibody recognizes rab8a and b
rab8a	X56385	(AA)GGCCAAACATCAATGTGGAG	rab8a/437	94%	n.t.	
<b>rab11a</b>	X56388	<b>(AA)GGCACAGATATGGGACACA</b>	rab11a	<b>77 ± 6% (69+84+78+76)</b>	Mild reduction*	* Antibody recognizes rab11a and b
rab11b	Partial	(AA)GCACCTGACCTATGAGAAC	rab11b/283	83% (83+82)	n.t.	
<b>rab11b</b>	Partial	<b>(AA)GAACATCTCACAGAGATC</b>	rab11b/496	<b>96 ± 1% (97+95+95)</b>	Slight reduction*	* Antibody recognizes rab11a and b
Syntaxin 3	Partial	GCTGAACATCGACAGATCTC	six3/113	42%	n.t.	
Syntaxin 3	Partial	(AA)GATCTCGGAGCAGCTGGAC	six3/126	55% (46+63)	n.t.	
Syntaxin 3	Partial	GAGATCAAGAAAGAGCCCAAC	six3/232	68%	n.t.	
Syntaxin 3	Partial	GCCAAACGTCGGAAACAAG	six3/244	70%	n.t.	
<b>Syntaxin 3</b>	Partial	<b>(AA)GAGTATGGAGGGACATC</b>	six3/270	<b>71 ± 2% (73+70+68+73)</b>	Clear reduction (70-80%)	
Syntaxin 3	Partial	GATCATCGACTCCAGATCTC	six3/624	22%	n.t.	
<b>Ti-VAMP</b>	Partial	<b>(AA)GAAGAGGTTCCAGACTACA</b>	Ti-VAMP/230	<b>90 ± 4% (85+95+94+87+91)</b>	Strong reduction (>90%)	
Ti-VAMP	Partial	(AA)GGAATCATGGTCAGAAACA	Ti-VAMP/393	60%	n.t.	
Ti-VAMP	Partial	(AA)TAGAAATCTTGCACGAGC	Ti-VAMP/505	77%	Strong reduction	
VIP17	X92505	GCTTTCATCTTCGAGTTTAT	VIP17/98	77%	n.t.	
<b>VIP17</b>	X92505	<b>GCTTTCCTGTACATAATTGG</b>	VIP17/230	<b>91 ± 1% (90+92+90)</b>	Strong reduction	
VIP17	X92505	(AA)TTCTGGGTACCCCTGGAT	VIP17/267	37% (38+36)	n.t.	
VIP17	X92505	(AA)CAGTACCACGAAACATCT	VIP17/382	53 ± 16% (69+51+38)	Mild reduction	
VIP17	X92505	GTACGTGGTCCATGCAGTGT	VIP17/437	87%	n.t.	
VIP36	X76392	(AA)CTGACGGTAACAGTGAACA	VIP36/139	48%	n.t.	
VIP36	X76392	(AA)GGCAGCACTACTACTCACA	VIP36/234	65% (72+57)	n.t.	
VIP36	X76392	(AA)GACAACCTCCATGGCTTAG	VIP36/453	72% (70+73)	n.t.	
<b>VIP36</b>	X76392	<b>GTGATCATGATACCCTCCTAG</b>	VIP36/626	<b>81 ± 5% (81+86+76)</b>	Strong reduction	
VIP36	X76392	(AA)GAAITTCATTCGACATCAGC	VIP36/711	63%	n.t.	

**Appendix 2.** RNAi database. The table lists the 13 target genes, references for the target mRNA sequences, the 37 target sequences, the names of the respective constructs, and their effectiveness as judged by RT-PCR and immunoblotting. The best target sequence for each gene is in bold. GeneBank accession numbers for the target genes are given where available; "partial" indicates that these mRNA sequences were re-constructed from partial genomic sequences. All target sequences are 21 nucleotides long, but only 19 nucleotides were cloned into pSUPER in the case of target sequences starting with AA. Due to the design of the shRNAs, antisense strands of the resulting siRNAs have 3' overhangs consisting of UU, which can pair with AA at the 5' of the target sequences (see Figure 4.5.). This is indicated by "(AA)" where applicable. To distinguish between different target sequences in the same mRNA, the construct names have the format x/y, where x is the target gene and y denotes the position of the first nucleotide of a target sequence. Average mRNA reductions  $\pm$  standard deviation are given in percent relative to control cells transduced with empty RVH1-puro. In brackets are the results from the individual experiments. The protein reductions are given only in qualitative terms unless determined by immunoblotting using serial dilutions. n.t. = not tested.

## Acknowledgements

I am indebted to Kai Simons, my supervisor, for his enthusiastic support throughout, his extensive advice, and his patience. His tutelage has for ever changed the way I look at science, possibly for the better.

I thank Bernard Hoflack, Teymuras Kurzchalia and Gerhard Rödel for being part of my thesis advisory committee, and Bernard Hoflack as well as Lukas Huber for kindly agreeing to review this thesis.

Heartfelt thanks go to all the members of the Simons lab I had the pleasure working with, most notably for scientific collaboration (Masanori and Aki), alleviating cynicism in the wake of experimental disaster (Joachim and Lucie), philosophising (Robin and Tobias), sleepless nights (VIP17), shared agony (Doris), as well as help, silliness and shared chocolate (everybody).

Sebastian, Monika, Jochen, Imke, Kim and Ingmar are acknowledged for making Predoc life at the MPI bearable. I am sure we will fondly remember our time at the institute once we are grown-ups at last.

Finally, I am grateful to Anne, my parents, Teresa and all the others who kept reminding me, with moderate success, that there is a world outside the lab.